

AFRL-SN-RS-TR-1998-31
Final Technical Report
April 1998



DOUBLE SIDEBAND SUPPRESSED CARRIER OPTICAL MODULATOR

Tracor AES

Ronald T. Logan Jr, R. Dale Bynum, Dilip Paul, Steve Bonocore, and Jerry Wood

19980603 046

APPROVED FOR PUBLIC RELEASE; DISTRIBUTION UNLIMITED.

**AIR FORCE RESEARCH LABORATORY
SENSORS DIRECTORATE
ROME RESEARCH SITE
ROME, NEW YORK**

DTIC QUALITY INSPECTED 1

This report has been reviewed by the Air Force Research Laboratory, Information Directorate, Public Affairs Office (IFOIPA) and is releasable to the National Technical Information Service (NTIS). At NTIS it will be releasable to the general public, including foreign nations.

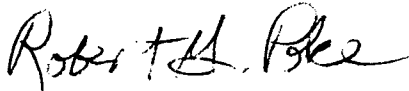
AFRL-SN-RS-TR-1998-31 has been reviewed and is approved for publication.

APPROVED:



JAMES R. HUNTER
Project Engineer

FOR THE DIRECTOR:



ROBERT G. POLCE, Acting Chief
Rome Operations Office
Sensors Directorate

If your address has changed or if you wish to be removed from the Air Force Research Laboratory Rome Research Site mailing list, or if the addressee is no longer employed by your organization, please notify AFRL/SNDR, 25 Electronic Parkway, Rome, NY 13441-4515. This will assist us in maintaining a current mailing list.

Do not return copies of this report unless contractual obligations or notices on a specific document require that it be returned.

REPORT DOCUMENTATION PAGE			Form Approved OMB No. 0704-0188	
<small>Public reporting burden for this collection of information is estimated to average 1 hour per response, including the time for reviewing instructions, searching existing data sources, gathering and maintaining the data needed, and completing and reviewing the collection of information. Send comments regarding this burden estimate or any other aspect of this collection of information, including suggestions for reducing this burden, to Washington Headquarters Services, Directorate for Information Operations and Reports, 1215 Jefferson Davis Highway, Suite 1204, Arlington, VA 22202-4302, and to the Office of Management and Budget, Paperwork Reduction Project (0704-0188), Washington, DC 20503.</small>				
1. AGENCY USE ONLY (Leave blank)		2. REPORT DATE April 1998	3. REPORT TYPE AND DATES COVERED Final Sep 94 - Sep 96	
4. TITLE AND SUBTITLE DOUBLE SIDEBAND SUPPRESSED CARRIER OPTICAL MODULATOR			5. FUNDING NUMBERS C - F30602-94-C-0277 PE - 63726F PR - 2863 TA - 92 WU - 68	
6. AUTHOR(S) Ronald T. Logan Jr., R. Dale Bynum (UTP) Dilip Paul, Steve Bonocore, Jerry Wood (Tracor)				
7. PERFORMING ORGANIZATION NAME(S) AND ADDRESS(ES) Prime Contractor: Subcontractor: Tracor AES (Formerly AEL) Uniphase Telecommunications Products 305 Richardson Road Transmission Systems Division Lansdale PA 19446-1485 500 Horizon Drive Chalfont PA 18914			8. PERFORMING ORGANIZATION REPORT NUMBER N/A	
9. SPONSORING/MONITORING AGENCY NAME(S) AND ADDRESS(ES) Air Force Research Laboratory/SNDR 25 Electronic Parkway Rome NY 13441-4515			10. SPONSORING/MONITORING AGENCY REPORT NUMBER AFRL-SN-RS-TR-1998-31	
11. SUPPLEMENTARY NOTES Air Force Research Laboratory Project Engineer: James R. Hunter/SNDR/(315) 330-7045				
12a. DISTRIBUTION AVAILABILITY STATEMENT Approved for public release; distribution unlimited.			12b. DISTRIBUTION CODE	
13. ABSTRACT (Maximum 200 words) The development of a novel single-chip integrated optic double sideband suppressed carrier (DSSC) modulator on lithium niobate substrate for operation at 1300 and 1550 nm wavelengths is described in this report. This chip contains two Mach-Zehnder (m-z) and two phase modulator sections which are computer controlled for operation at the third-order intermodulation distortion point minimum. To assess insertion potential into microwave/millimeter wave (mW/mmW) systems, systems level performance characteristics of the DSSC has been investigated. Performance measures included but were not limited to measurement of IMD, harmonics, noise figure (NF), and phase drift. This data was used to determine the intercept point, spurious free dynamic range (SFDR), etc. To some extent environmental and operational effects were also studied. Additional investigation was conducted to look into alternative biasing schemes to improve or optimize performance of the DSSC. Experiments were performed to validate optimization and are reported here.				
14. SUBJECT TERMS RF Photonics Links, Optical Modulator, Optical Links, Mach-Zehnder Modulator			15. NUMBER OF PAGES 144	
			16. PRICE CODE	
17. SECURITY CLASSIFICATION OF REPORT UNCLASSIFIED	18. SECURITY CLASSIFICATION OF THIS PAGE UNCLASSIFIED	19. SECURITY CLASSIFICATION OF ABSTRACT UNCLASSIFIED	20. LIMITATION OF ABSTRACT UL	

Table of Contents

Page

1.	Executive Summary	3
2.	Foreward	4
3.	Motivation	5
4.	Analysis	6
5.	Experimental Results	17
6.	Control Loop	25
7.	Discussion of Results	28
8.	References	30
A	Appendix A - RF S11 and S21 response of modulators.	31
B	Appendix B - DSSC Optical Link Demonstration & Test Results	38
C	Appendix C - DSSC Performance Simulation	104
D	Appendix D - Summary and Recommendation	105
E	Appendix E - DSSC Modulator Performance Enhancement Simulation	106

SUMMARY

The Double Sideband Suppressed Carrier (DSSC) optical modulator contract was awarded to Tracor AES (formerly AEL) to validate a new technique of increasing dynamic range of a fiber optic link. The technique combined predistortion of the detected signal to cancel third order spurious signals with more signal current (relative to the current produced by optical carrier) on the photodetector to achieve increased dynamic range.

Initial performance of the contract work was performed at Tracor. Due to a turn over in personnel, a subcontract was issued to UTP in Lansdale to complete the validation of the DSSC optical modulator.

The first section of this final report is a copy of the final report prepared by UTP under subcontract to Tracor (SFT57001G). The theory of operation, performance predictions, and summarized test results are included in their report.

The balance of the data taken on the DSSC contract is contained in appendices. This data contains more detailed test data, information on hardware set-ups, the software operation, and additional analysis on a technique that can further extend the dynamic range of fiber optic links. Appendix A contains the interface to the DSSC hardware and operator instructions. Appendix B contains the DSSC test configurations and the test results. Appendix C contains the simulated performance overview. Appendix D summarizes Tracor's recommendations. Appendix E contains the detailed simulation of the DSSC performance compared to a modified modulator configuration.

Each major section of the report; the UTP report and the appendices, contain a summary of the material contained in it.

1. Executive Summary

This Report describes theoretical and experimental investigations performed by Uniphase Telecommunications Products (UTP) on a double-sideband suppressed-carrier (DSSC) waveguide modulator [1]. The DSSC modulator structure exhibits enhanced sub-octave linearity compared to the standard Mach-Zehnder modulator, and has operating points where either second-order or third-order distortion suppression may be achieved. By contrast, a standard Mach-Zehnder modulator only exhibits a second-order distortion suppression point.

In the initial phase of the program, four devices were fabricated at 1300 nm wavelength to validate the concept of optical carrier suppression. After good agreement between theoretical and experimental results was obtained with the 1300 nm devices, UTP fabricated and tested two more devices at 1550 nm. Investigations of the 1550 nm devices also incorporated an erbium-doped fiber amplifier (EDFA).

Experimental results of harmonic content versus bias point obtained at both 1300 nm and 1550 nm are in good agreement with theoretical predictions. At the third-order distortion suppression point, the measured harmonic content at 1300 nm is consistent with a sub-octave spurious-free dynamic range of $125 \text{ dB-Hz}^{2/3}$ at a DC photocurrent of 0.5 mA.

The modulators investigated in this work were fabricated by UTP in LiNbO_3 using the annealed-proton-exchange (APE) optical waveguide process, and packaged with optical fiber-pigtails using UTP's standard commercial high-volume process, thereby validating the practicality of volume production of these devices. Six low-loss fiber-pigtailed modulators were fabricated (four devices at 1300 nm, 2 devices at 1550 nm). The considerations leading to the enhanced linearity are not specific to LiNbO_3 , and similar transfer characteristics are expected with other material systems incorporating the DSSC geometry.

2. Foreward

This Report is divided into five main sections: Section 3 entitled "Motivation," discusses the motivation for the DSSC design in the context of the performance and limitations of previously existing waveguide Mach-Zehnder optical modulators. Section 4 entitled "Analysis" presents results of theoretical analysis and calculated predictions of the DSSC performance in terms of link loss, harmonic content, noise figure, second-order and third-order intercept points, and spurious-free dynamic range. Section 5 entitled "Experimental Results" contains experimental data collected on the DSSC modulator. Section 6 describes the automatic control loop developed to maintain the modulator bias point at the third-order suppression point. Finally, Section 7 contains a discussion of the results and general conclusions. Section 8 lists bibliographic references. Appendix A lists RF frequency response and return loss data for the DSSC modulator devices.

3. Motivation

Fiber-optic transmission of radio-frequency (RF) analog signals with high dynamic range is desired for many applications, including antenna-remoting and phased-array radar feeds. For the most demanding RF and microwave applications, a system comprised of a high-power laser that is intensity-modulated using an external Mach-Zehnder optical waveguide modulator has been shown to achieve the greatest transmission distances with the highest bandwidth, carrier-to-noise ratio, and dynamic range [2,3]. Although the RF bandwidth of externally-modulated fiber-optic systems is comparable to, or even exceeds that of many electronic transmission systems, there is still considerable improvement desired in noise figure and dynamic range to make them suitable for many applications.

High-power diode-pumped Nd:YAG lasers are already commercially available with intensity noise at the shot-noise limit, and the intensity noise of high-power DFB laser diodes is typically within 10 dB of the shot noise limit. Therefore, immediate improvements in externally-modulated fiber optic systems are most likely to result from efforts to improve the linearity and sensitivity of modulators and photodetectors. For electro-optic modulators, the sensitivity is fundamentally limited by the electro-optic coefficient of the modulator material, and the linearity is limited by the voltage-to-optical power transfer characteristic of the device.

In most applications using Mach-Zehnder waveguide modulators, the dynamic range is limited by the third-order distortion of the interferometric sinusoidal voltage-to-intensity transfer characteristic. In systems operating over more than one octave of frequency, the Mach-Zehnder modulator is biased at the midpoint of the transfer characteristic to achieve suppression of the second-order distortion products. In sub-octave bandwidth systems, the second-order distortion products fall out of band and thus are not important, but the third-order intermodulation distortion limits the spurious-free dynamic range in the signal bandwidth. Various optical techniques have been proposed to extend the spurious-free dynamic range of externally modulated fiber-optic links, including low-biasing of the Mach-Zehnder modulator [4], optical carrier filtering [5], and cascaded modulators [6].

Low-biasing [4] and carrier-filtering [5] are very similar in that both techniques reduce the optical power in the carrier while maintaining the sideband power to achieve enhanced spurious-free dynamic range at the expense of increased optical loss and second-order distortion. With cascaded modulators [6], third-order distortion terms can be minimized by adjustment of the bias voltages of the modulators and the coupling ratio of the RF input signal between the modulator sections. However, this technique suffers from the increased complexity of the control system required to maintain the modulator sections at the optimum bias point, and the need for multiple RF signal inputs with proper phase relationship.

The DSSC device works on the same basic principle of external optical carrier filtering [5], in that the optical carrier is suppressed to maximize the ratio of modulation sideband-to-carrier power. However, the DSSC device eliminates the need for an external optical filter, which in practice can be difficult to implement and control. In the DSSC modulator, the carrier suppression is achieved entirely on the integrated optical chip, by splitting off a portion of the input electric field and recombining it at the output of a Mach-Zehnder modulator with appropriate amplitude and phase (see Figure 1 block diagram of DSSC chip layout). By selectively cancelling the optical carrier, the optical modulation index is effectively enhanced. Then, by employing an optical amplifier, a high-power, high-modulation-index signal is obtained which results in an optical link with less RF insertion loss. An undesirable effect of carrier suppression is generation of harmonic distortion. Therefore, the present research program has been directed toward determining the tradeoffs between carrier suppression and harmonic distortion in a general sense, to identify the optimum operating points for the DSSC modulator.

4. Analysis

A fiber-optic link incorporating the DSSC modulator, shown in Figure 1, was analyzed to determine the following performance parameters as a function of the DC bias point of the RF modulator section:

- 1). Link loss
- 2). Noise figure
- 3). Second and third-order intercept
- 4). 1 dB compression point
- 5). Spur-free dynamic range

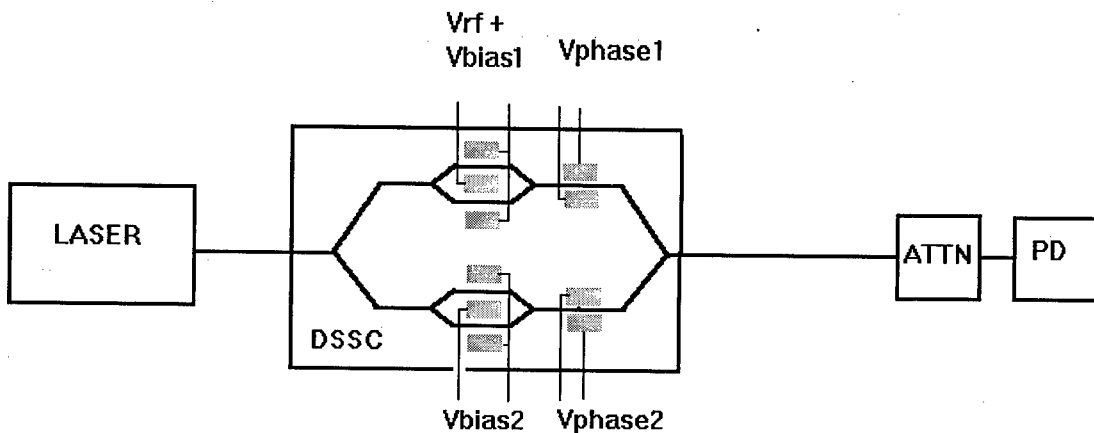


Figure 1. Block diagram of fiber-optic link incorporating DSSC modulator as analyzed.

For this analysis, the modulator section in the carrier suppression arm, V_{bias2} , was biased for maximum transmission. The voltages V_{phase1} and V_{phase2} are assumed to be adjusted to achieve a phase shift of 180 degrees between the two arms. For these conditions, the DC transfer characteristic for optical power versus bias point of the RF modulator section, V_{bias1} , is shown in Figure 2. The introduction of the anti-phase electric field from the carrier suppression arm at the output of the RF Mach-Zehnder causes the transfer function to be asymmetric, compared to a standard Mach Zehnder modulator. This asymmetry can be exploited to realize enhanced dynamic range. The vertical lines indicate the bias points at which the second-order and third-order distortion terms are minimized.

The second-order distortions are minimized when the modulator is biased at the point where the transfer characteristic has its highest degree of symmetry, indicated as a vertical line at 4.19 radians in Figure 2. This also corresponds approximately to the DC half-power bias point. At this point, the modulator behaves very much like a standard Mach-Zehnder modulator. The third-order terms are minimized at a bias of 4.96 radians, where the transfer characteristic most closely approximates a quadratic function. This bias point does not occur in the standard Mach-Zehnder modulator.

The parameters of the link used in the calculations are as indicated in Table 1.

V_{pi}	8 V
Optical Excess Insertion Loss (at maximum transmission)	6 dB
Input Impedance	50 ohms
Input Optical Power	20 mW
Laser RIN	-160 dB/Hz
Wavelength	1550 nm
Photodiode Responsivity	0.9 A/W
RF input power	- 12 dBm
modulation depth	3 %

Table 1. Optical link parameters.

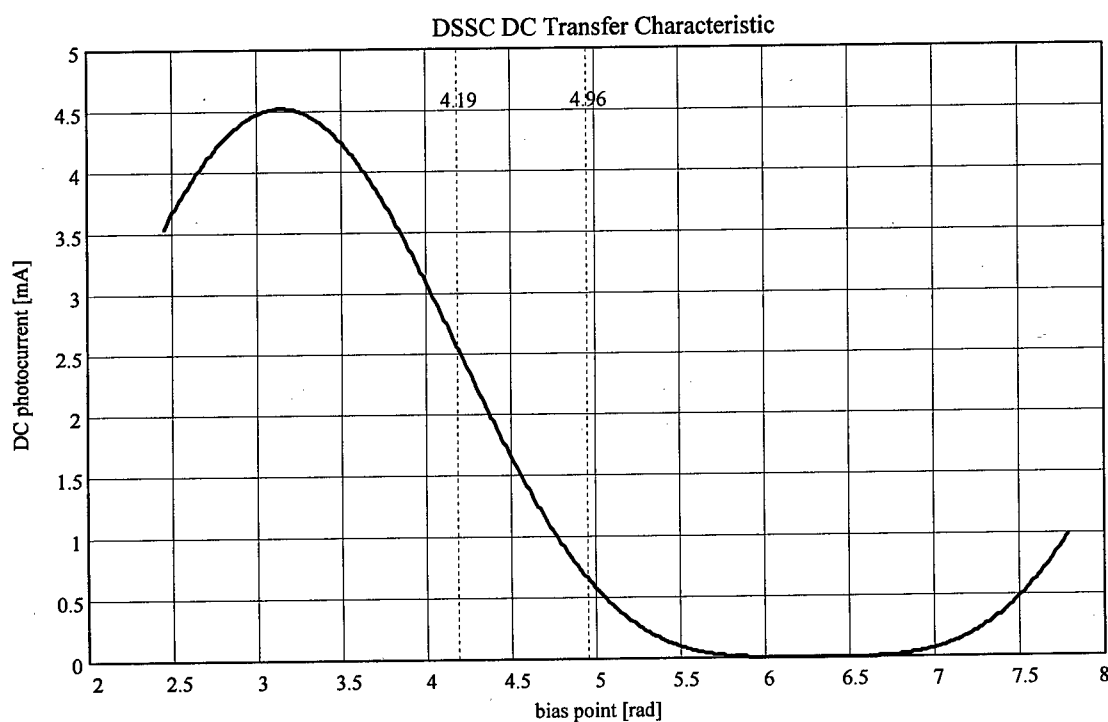


Figure 2. DC optical output power vs. DC bias V_{bias1} of RF modulator section for 20 mW constant optical input power to DSSC.

The calculated RF output power versus bias point of the RF section is shown in Figure 3. The point at which second-order distortion terms are minimized occurs at a bias of 4.19 radians. This bias point is useful for wideband systems in which the modulation signal may span more than one octave of frequency. The third-order distortion performance of the DSSC modulator at this bias point is similar to that of a standard Mach-Zehnder modulator. The point at which the third-order distortion terms are minimized occurs at 4.96 radians. This bias point is useful for narrowband systems spanning less than one octave, since the second-order distortion terms are not minimized at this point.

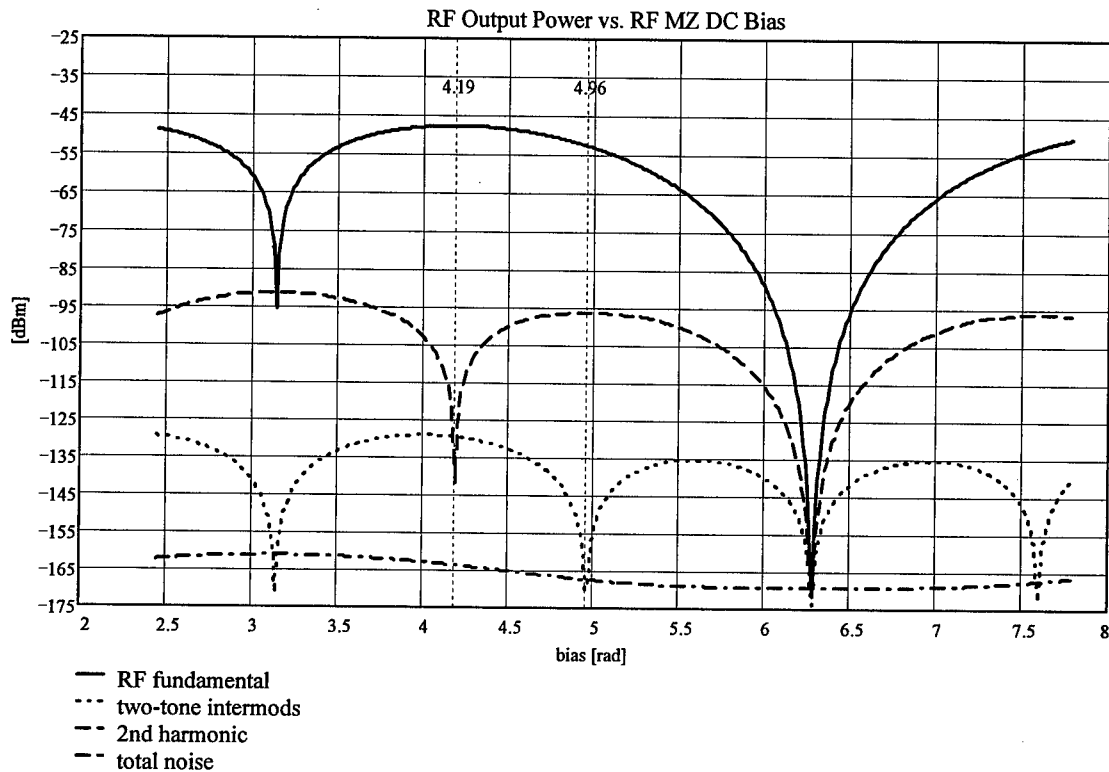


Figure 3. RF power vs. DC bias of RF modulator section for constant optical input power to DSSC modulator.

The RF gain of the DSSC link was computed as the ratio in dB of output signal RF power to input signal RF power. This is shown in Figure 4. For a fixed-level of laser input power to the modulator, the RF gain is reduced by approximately 6 dB at the third-order distortion minimum, compared to the second-order distortion minimum. However, the DC optical power at the third-order distortion null is also reduced by approximately 6 dB compared to the second-order null. Therefore, if more optical power is added to keep the DC link **optical output power** constant as the bias point of the RF Mach-Zehnder is varied, then the effective RF link gain is increased at the third-order null, as shown in Figure 5. This is similar to the case of low-biasing a standard Mach-Zehnder modulator [1]. However, the DSSC modulator has the added feature of greatly reduced third-order distortion, due to its modified transfer function.

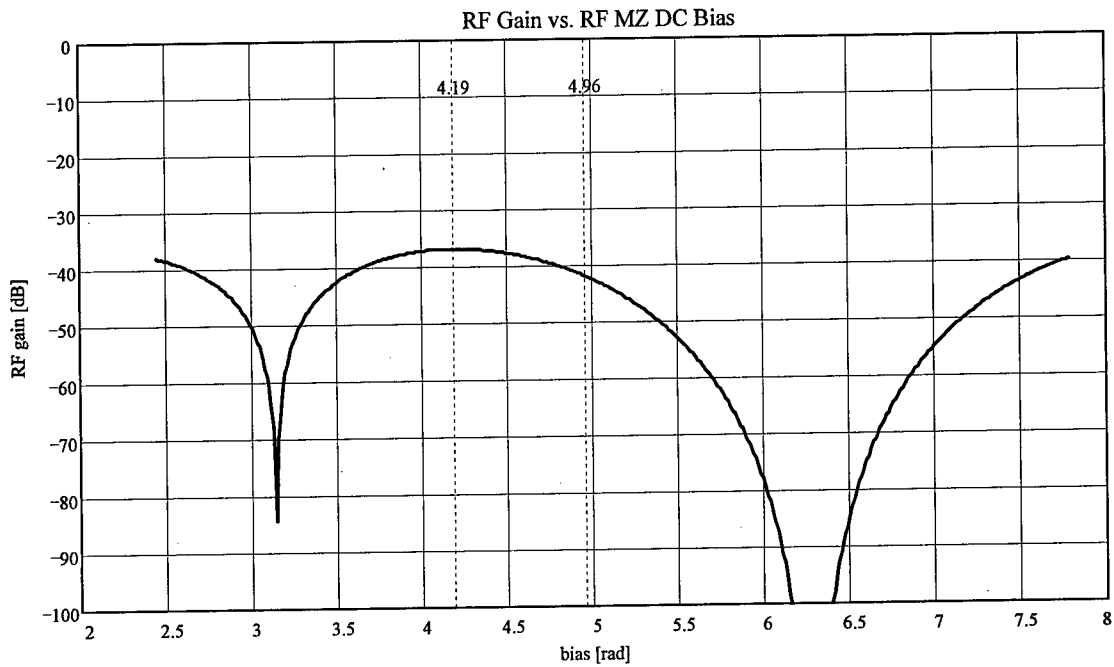


Figure 4. RF gain vs. DC bias of RF modulator section for constant optical input power to DSSC modulator.

From Figure 5 it can be seen that the RF gain of the DSSC link at the third-order null point is increased by approximately 12 dB for the case of constant optical output power compared to constant optical input power. Also, the gain is increased by about 6.8 dB compared to the wideband bias point. The additional RF gain comes at the expense of an additional 6 dB of optical power. However, the DC photocurrent is not increased. Therefore, when the output power is kept constant, we can view the increase in RF gain as an effective **decrease** in the modulator V_{pi} by a factor of 2 when going from the second-order null point to the third-order null point. It is emphasized that this effective 2-fold decrease in V_{pi} comes at the expense of a 4-fold increase in optical power.

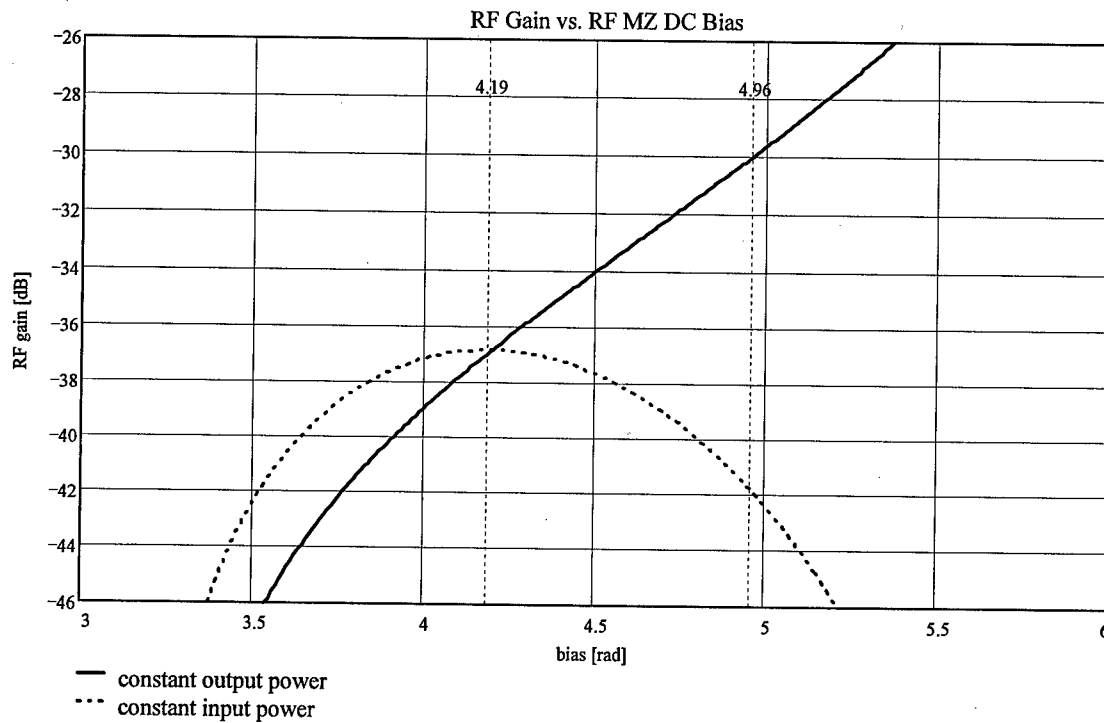


Figure 5. RF gain vs. DC bias of RF modulator section for constant optical output power from DSSC modulator.

The RF output noise sources for the DSSC link were computed, and are plotted in Figure 6 vs. bias of the RF modulator section. These calculations assume only the noise contribution due to the laser diode. The noise due to the EDFA will add to this value, but the exact amount of added noise will be highly dependent on the characteristics of the particular EDFA, the modulation depth, and the input optical power. At present, no good analytic treatment of the noise of the saturated EDFA exists, so it is necessary to measure the actual noise contribution for a particular EDFA vs. optical input power.

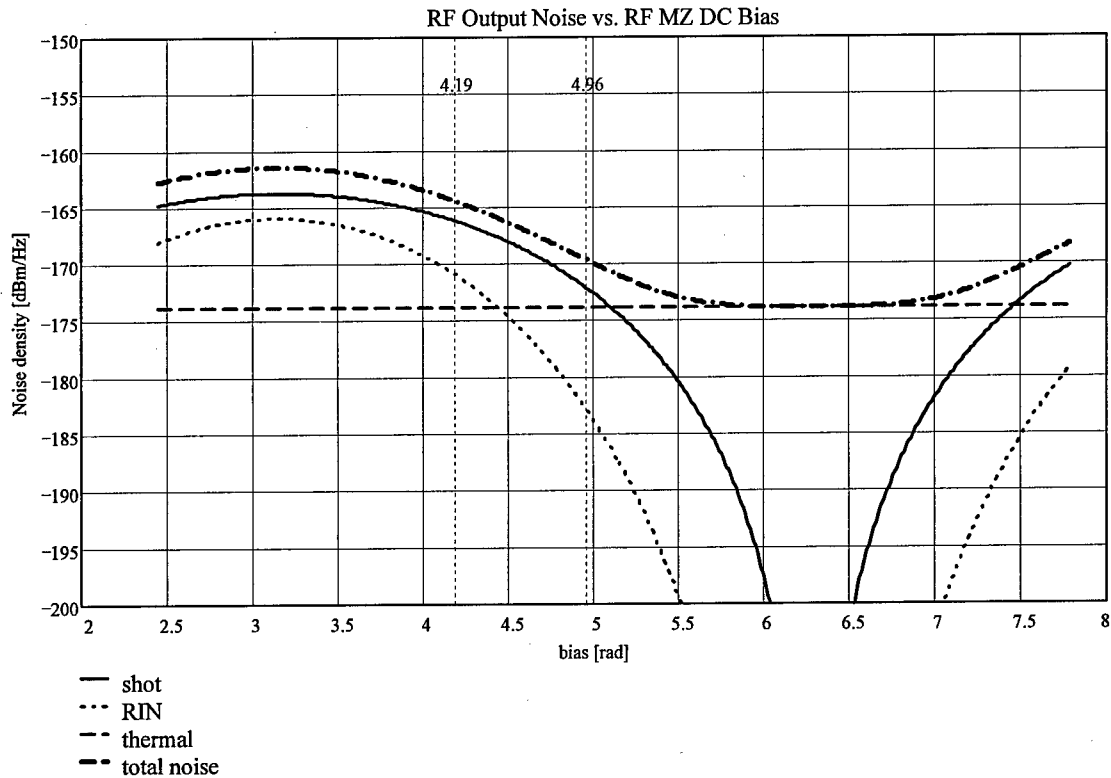


Figure 6. RF output noise sources vs. DC bias of RF modulator section for constant optical input power to DSSC modulator (no EDFA).

The computed noise figure of the DSSC link is shown in Figure 7 for the case of constant input optical power. Although the RF gain is lower at the third-order null, the noise figure does not degrade appreciably when moving from the second-order null to the third-order null, since the output noise is also lower. Therefore, the computed RF noise figure is approximately 47 dB for both cases. For the case where the optical output power is maintained at a constant level vs. bias point, the RF output noise will also be constant for all bias points. Since the RF gain is increased by 6.8 dB when moving from the second-order null to the third-order null, but the optical power and output noise are unchanged, the RF noise figure will be reduced by 6.8 dB when moving from the second-order null to the third-order null for the case of constant optical output power.

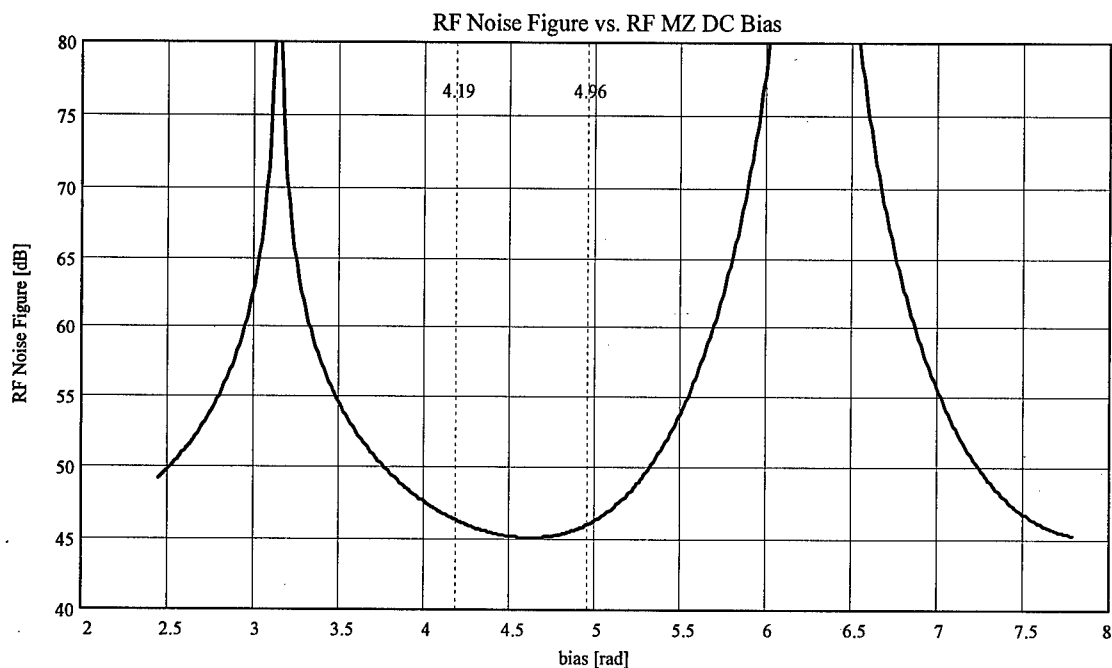


Figure 7. RF noise figure vs. DC bias of RF modulator section for constant optical input power to DSSC modulator.

The input second-order and third-order intercept points vs. bias on the RF Mach-Zehnder section are plotted in Figure 8. The intercept points are the same for the cases of both constant optical input power and constant optical output power. This is because the link gain and output intercept points exactly cancel each other.

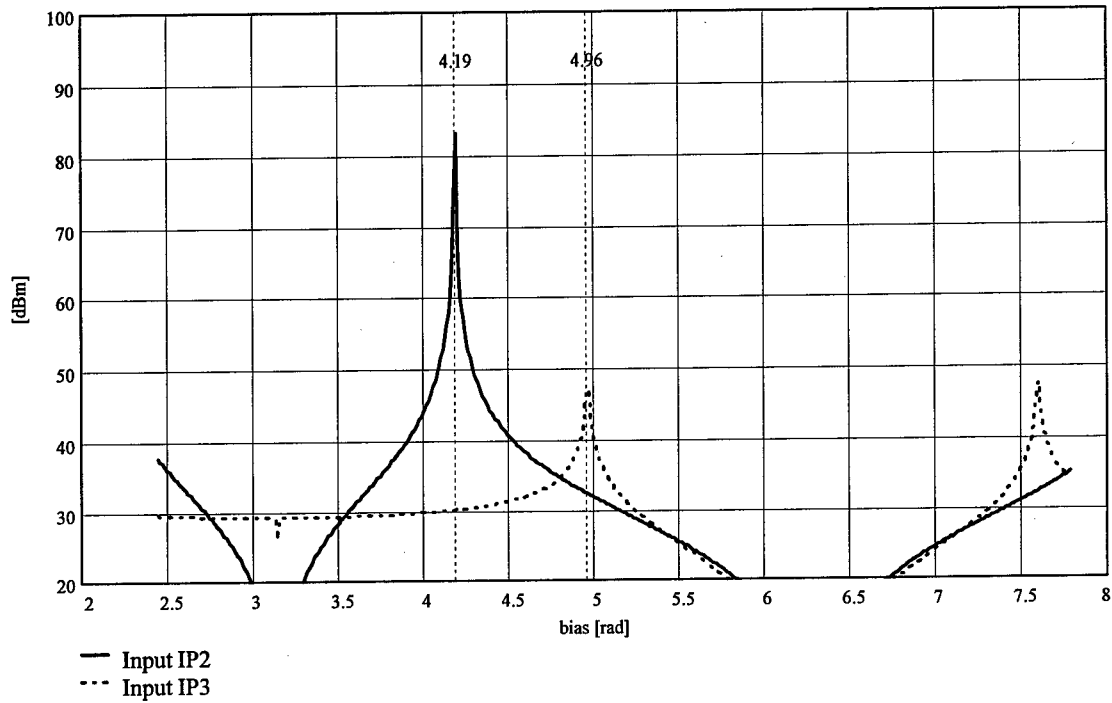


Figure 8. Input 2nd-order and 3rd-order intercept points vs. DC bias of RF modulator section for DSSC modulator.

The input 1 dB compression point is plotted in Figure 9 for both constant optical input power and constant optical output power. The 1 dB compression point is estimated as being 10 dB lower than the input third-order intercept point.

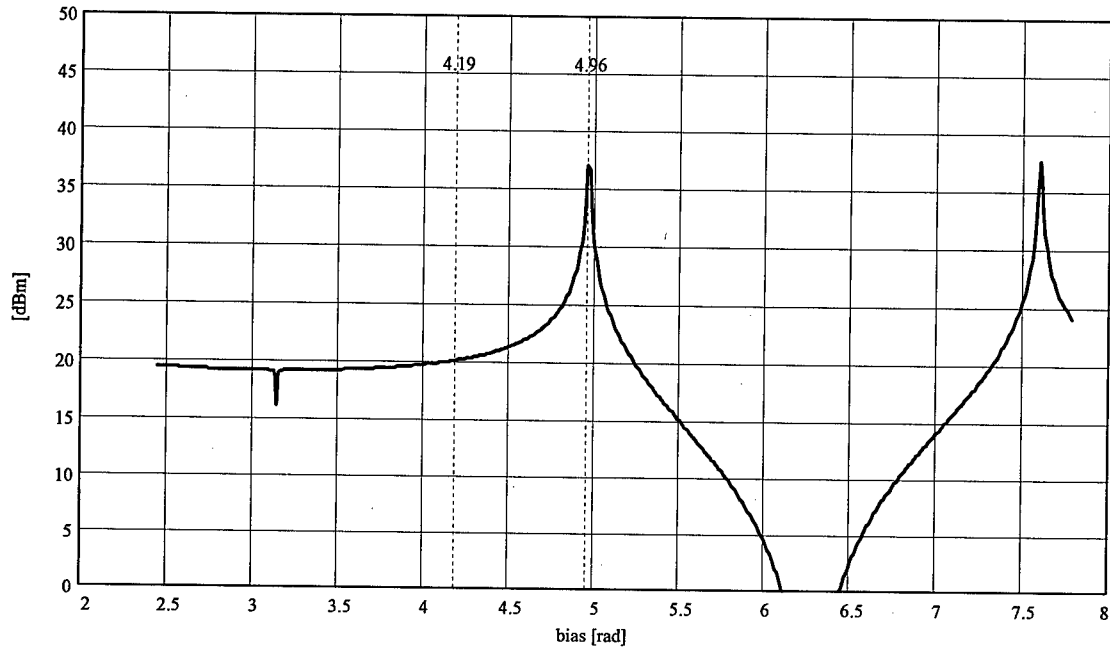


Figure 9. Input 1 dB compression point vs. DC bias of RF modulator section for both constant optical input power and constant optical output power.

Finally, the spurious-free dynamic range (SFDR) is plotted in Figures 10a and 10b for both constant optical input power and constant optical output power. The 1550 nm case is plotted in Figure 10a, while the 1300 nm case with the 200 mW Nd:YAG laser is plotted in Figure 10b. The value of SFDR at the second-order null is equal to the value obtained using a standard Mach-Zehnder modulator with the same photocurrent. The noise figure for the 1300 nm case is lower, since the Nd:YAG laser is shot noise limited, whereas the DFB has excess RIN in addition to shot noise. As will be seen in the next section, the predicted value of SFDR at the third-order null for the 1300 nm case is within 1 dB of the measured value shown in Figure 20. Thus, good agreement exists between the theoretical predictions and experimental values for the DSSC modulator.

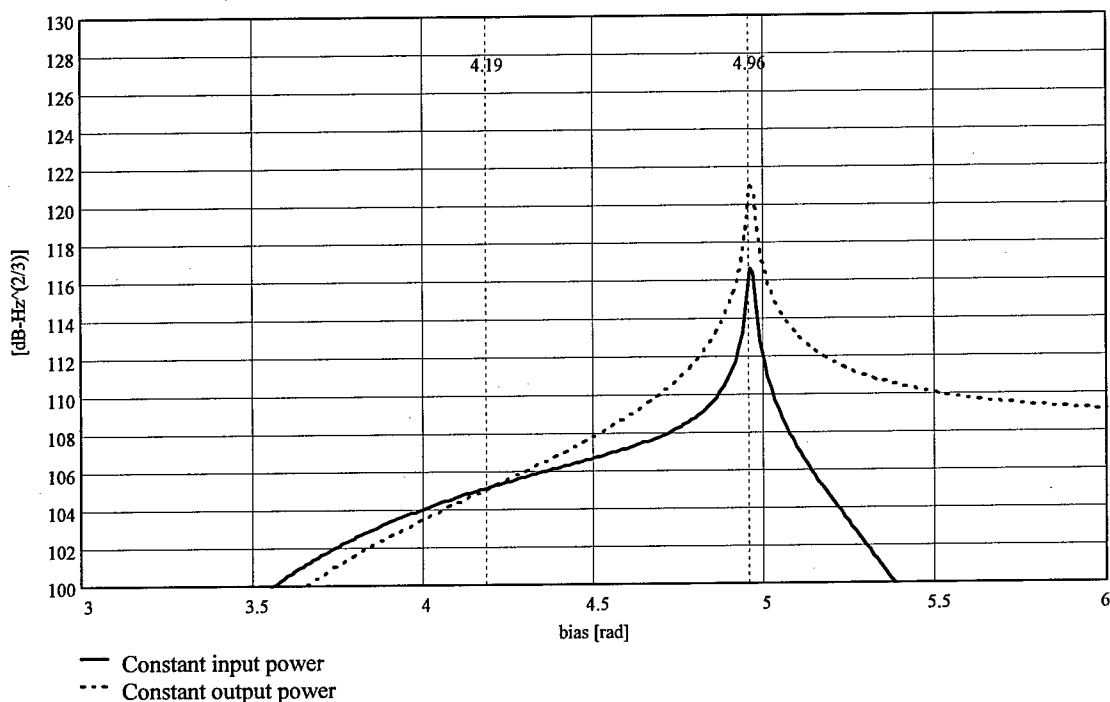


Figure 10a. 1550 nm (no EDFA) spurious-free dynamic range vs. DC bias of RF modulator section for both constant optical input power and constant optical output power.

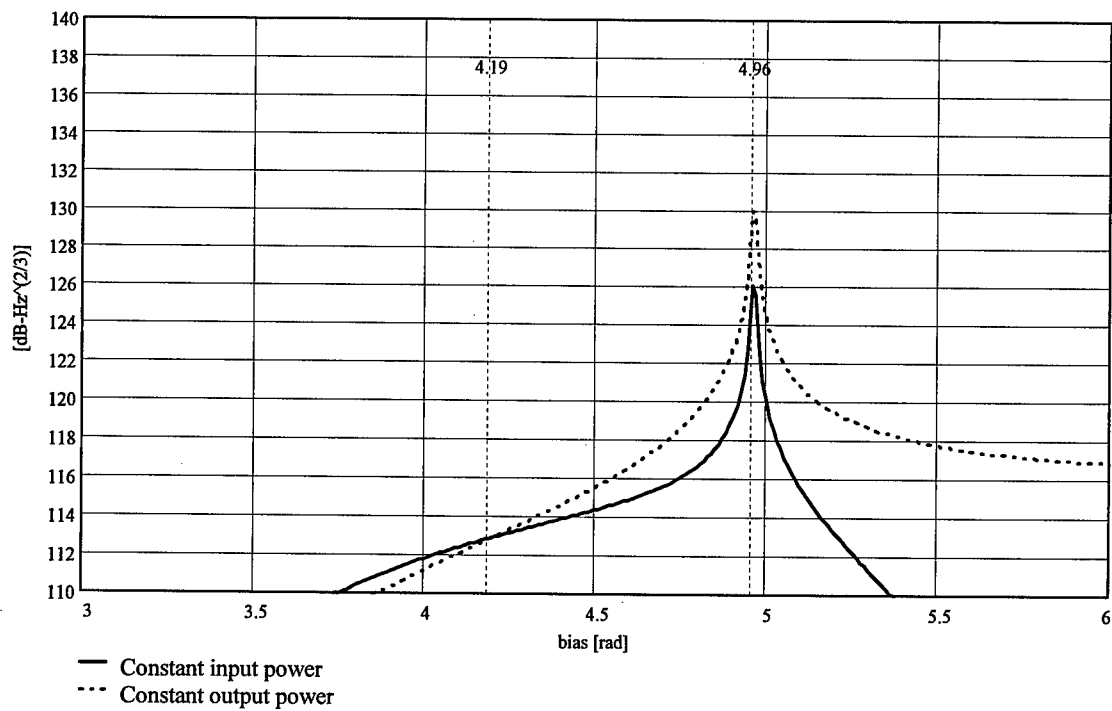


Figure 10b. 1300 nm calculated spurious-free dynamic range vs. DC bias of RF modulator section for both constant optical input power (200 mW) and constant optical output power.

5. Experimental Results

All DSSC modulator devices (2 GHz, 6 GHz, and 18 GHz) were characterized for frequency response, RF return loss, insertion loss, and V_{pi}. The predicted harmonic content from the analysis versus bias voltage is in good agreement with measured results, as shown in Figure 11. This indicates that the differential phase balance of the RF Mach-Zehnder section achieved on the devices is adequate for the DSSC application (i.e., there is apparently no measurable incidental phase modulation of the optical carrier by the RF Mach-Zehnder modulator section on any of the initial devices). Therefore, it appears that the initial devices worked as expected, and no substantial changes to the waveguide or electrode structure are required.

A computer-controlled test station was constructed to facilitate the device testing using A/D and D/A boards in an IBM PC compatible computer running LabVIEW instrument control software to control the bias electrodes of the modulator, and GPIB control of a spectrum analyzer to collect the RF and harmonic amplitudes versus the bias points. Experimental results for all of the devices of RF fundamental and harmonics vs. DC bias of the RF Mach-Zehnder section are shown in Figures 11 through 19. The value "a" refers to the relative carrier suppression amplitude (i.e., a=1 implies equal amplitude in upper and lower arms of the DSSC, as shown in Figure 1.)

The spurious-free dynamic range (SFDR) was calculated from the theory, and is in good agreement with measured results in both wideband (second-order distortion suppressed) and narrowband (third-order distortion suppressed) modes. In wideband mode, the SFDR is 104 dB-Hz^{2/3} at a DC photocurrent of 1 mA, which is equal to the SFDR of a standard Mach-Zehnder modulator. This assumes 50-50 current divider between internal photodiode load and external circuit load. At the third-order distortion suppression point, the SFDR is approximately 124 dB-Hz^{2/3} at a DC photocurrent of 1 mA. These results are shown in Figure 20.

Parameter	1187	1188	1189	1190	3082	3083
Wavelength [nm]	1319	1319	1319	1319	1550	1550
Insertion Loss O1 [dB]	5.5	4.94	5.79	5.2	4.7	5.5
Insertion Loss O2 [dB]	5.6	4.94	5.72	6.0	4.7	5.4
Extinction Ratio MZ1 [dB]	43.2	35.8	33.5	32.3	30.3	27.3
Extinction Ratio MZ2 [dB]	43.2	35.6	30.7	31.1	33.7	27.5
V _{pi} of PM1 [V]	6.34	5.6	6.0	5.8	5.1	5.0
V _{pi} of PM2 [V]	5.47	6.4	6.8	6.4	5.2	5.3
V _{pi} of Vb1 [V]	5.47	5.5	5.8	5.8	5.2	5.3
V _{pi} of Vb2 [V]	5.84	5.4	5.8	6.0	5.1	5.3
V _{pi} of RF @100 Mhz [V]	6.5	6.6	22.2	18.6	5.1	5.0

Table 2. Measured DC parameters of DSSC modulators.

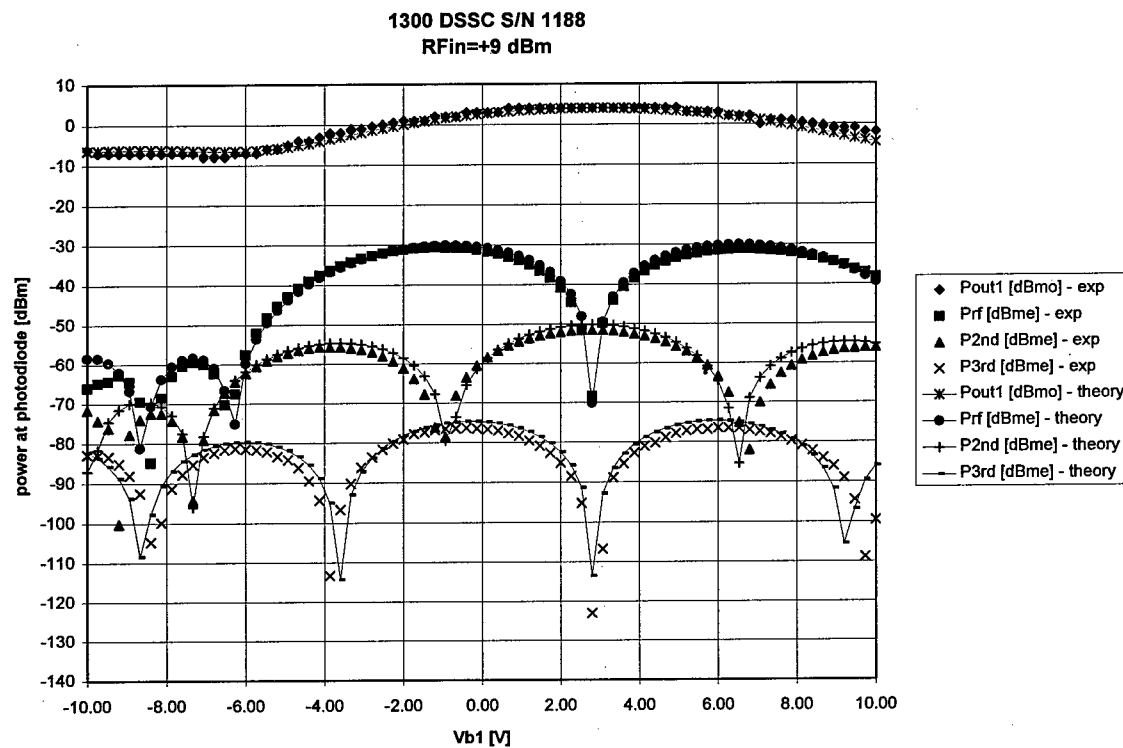


Figure 11. DSSC 1188 response verses Vb1 bias voltage, including theory, $a = 0.8$.

(S1188_9.XLS)

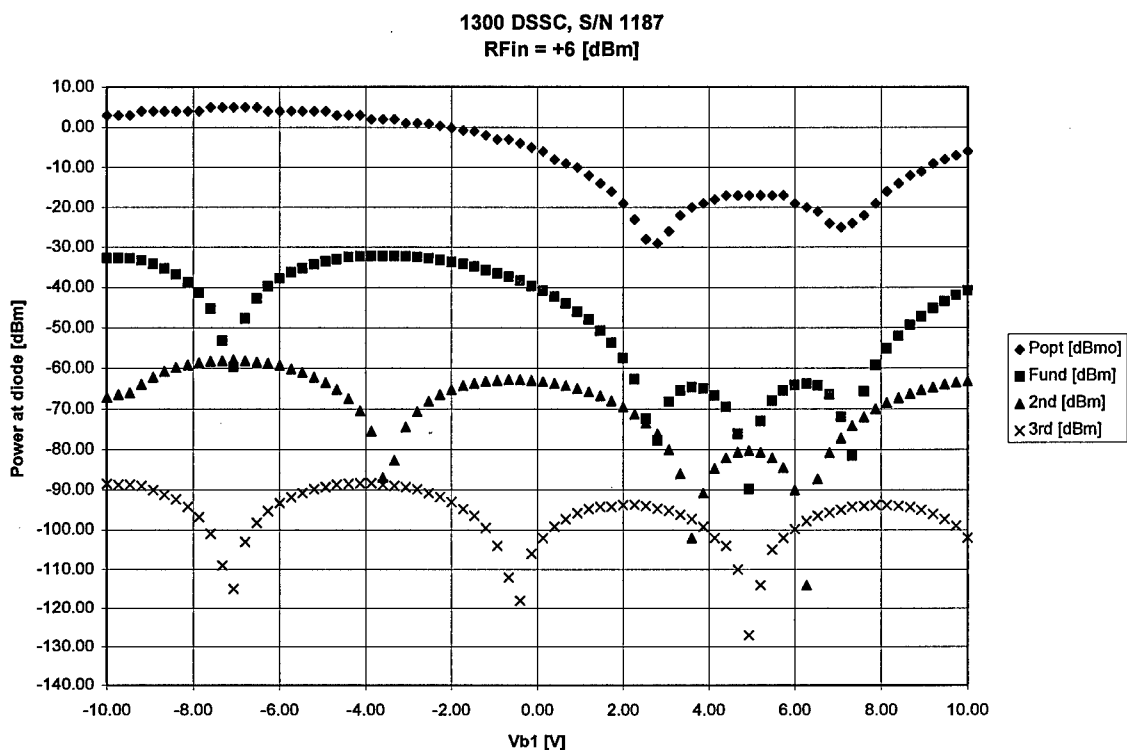


Figure 12. DSSC 1187 response versus Vb1 bias voltage, $a = 0.8$. (RF6DBMF.XLS)

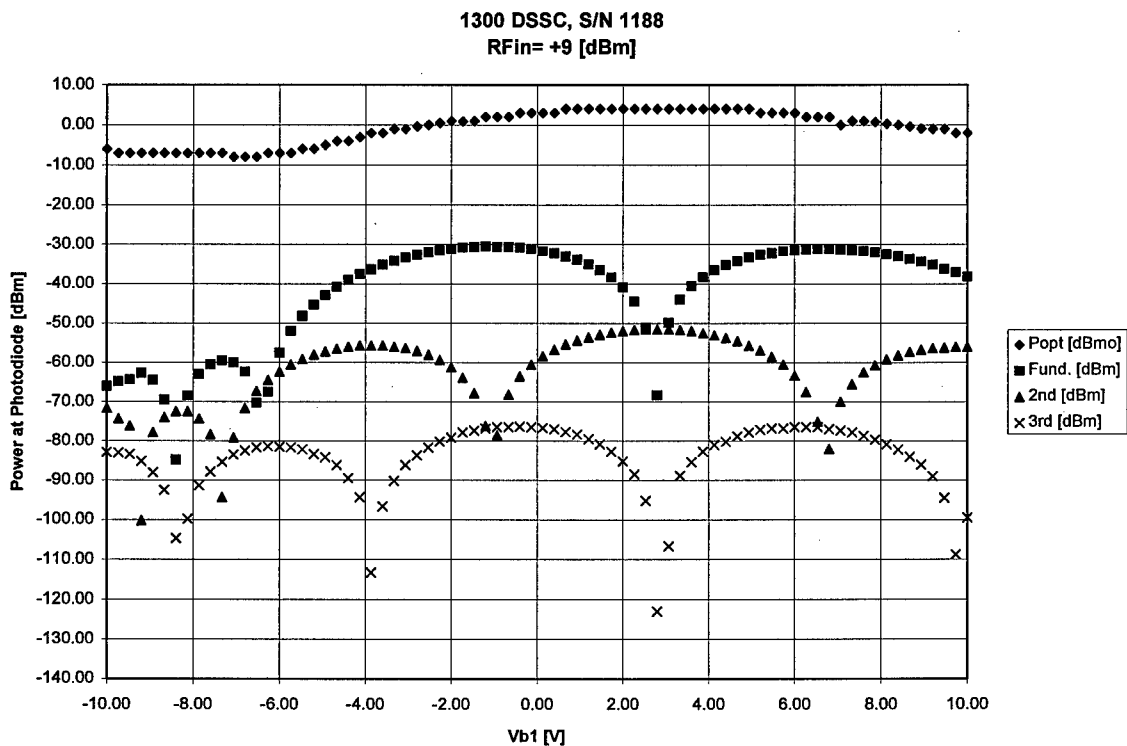


Figure 13. DSSC 1188 response versus Vb1 bias voltage, $a = 0.8$. (60M9DB.XLS)

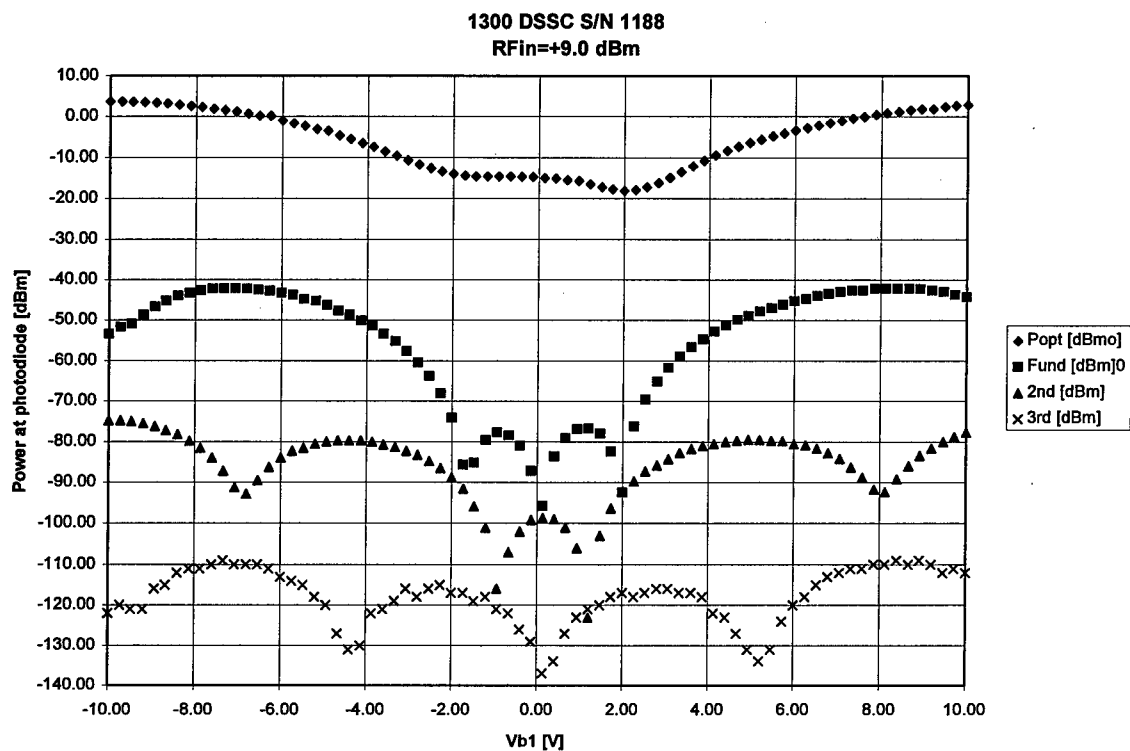


Figure 14. DSSC 1189 response verses bias voltage, $a = 0.8$. (1189_9.XLS)

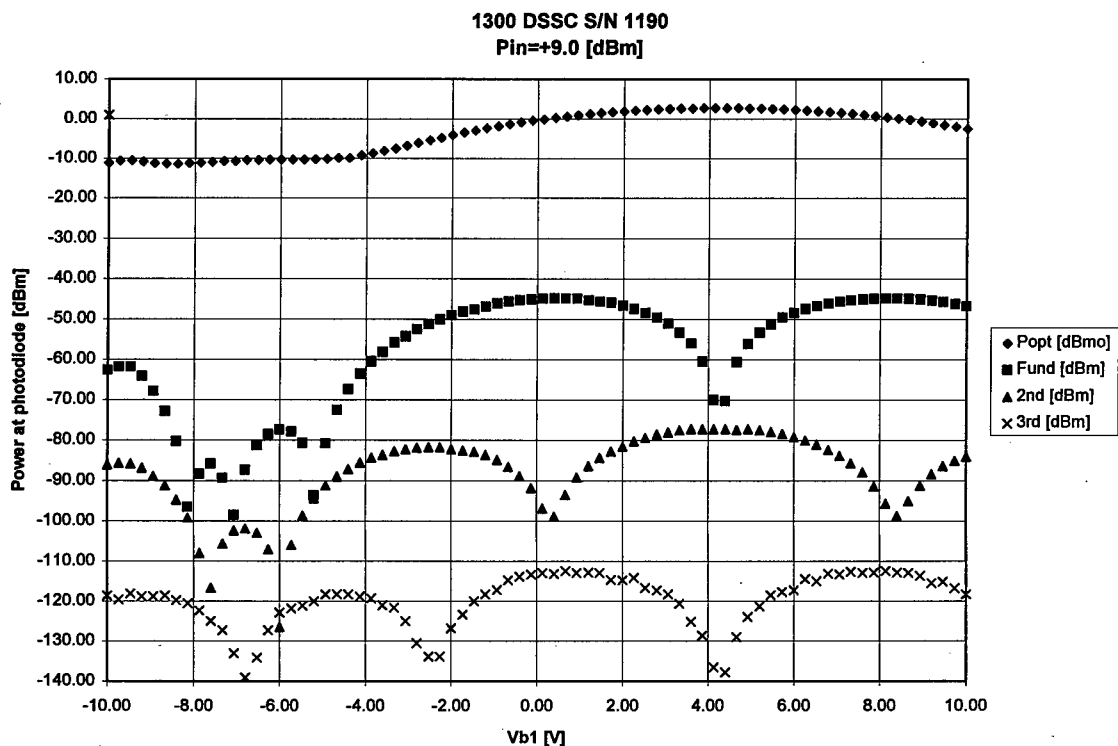


Figure 15. DSSC 1190 response verses Vb1 bias voltage, $a = 0.8$. (1190_9.XLS)

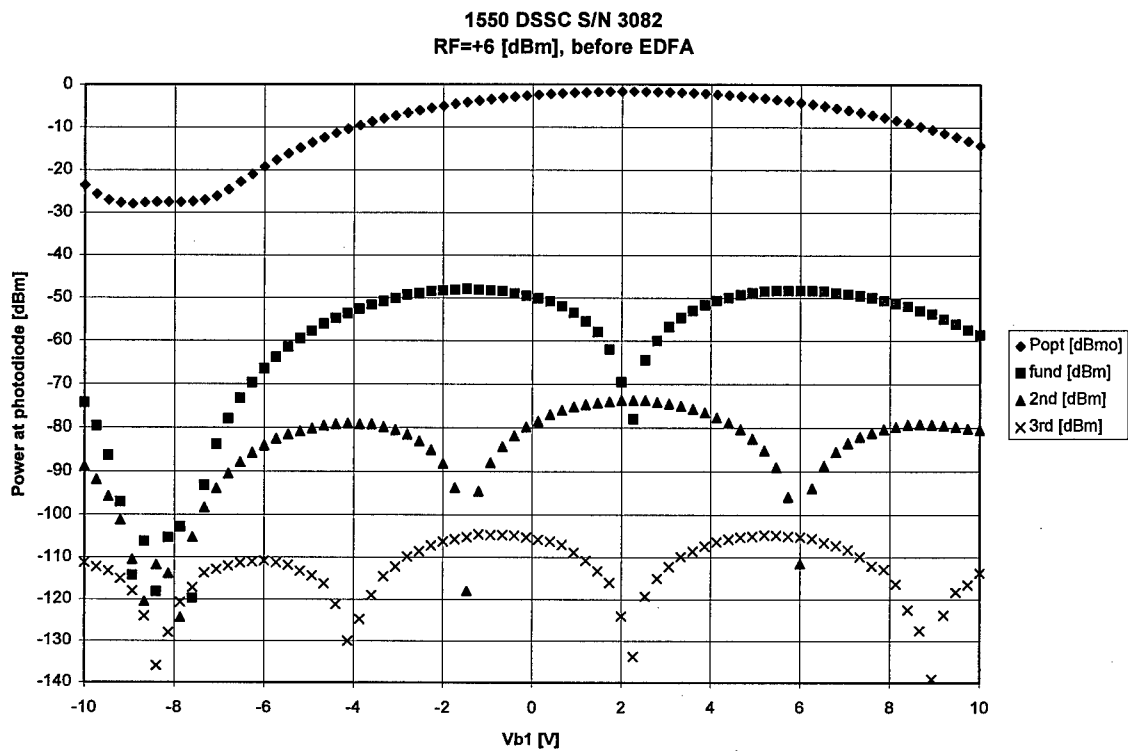


Figure 16. DSSC 3082 response versus Vb1 bias voltage, a = 1. (3082-6D.XLS)

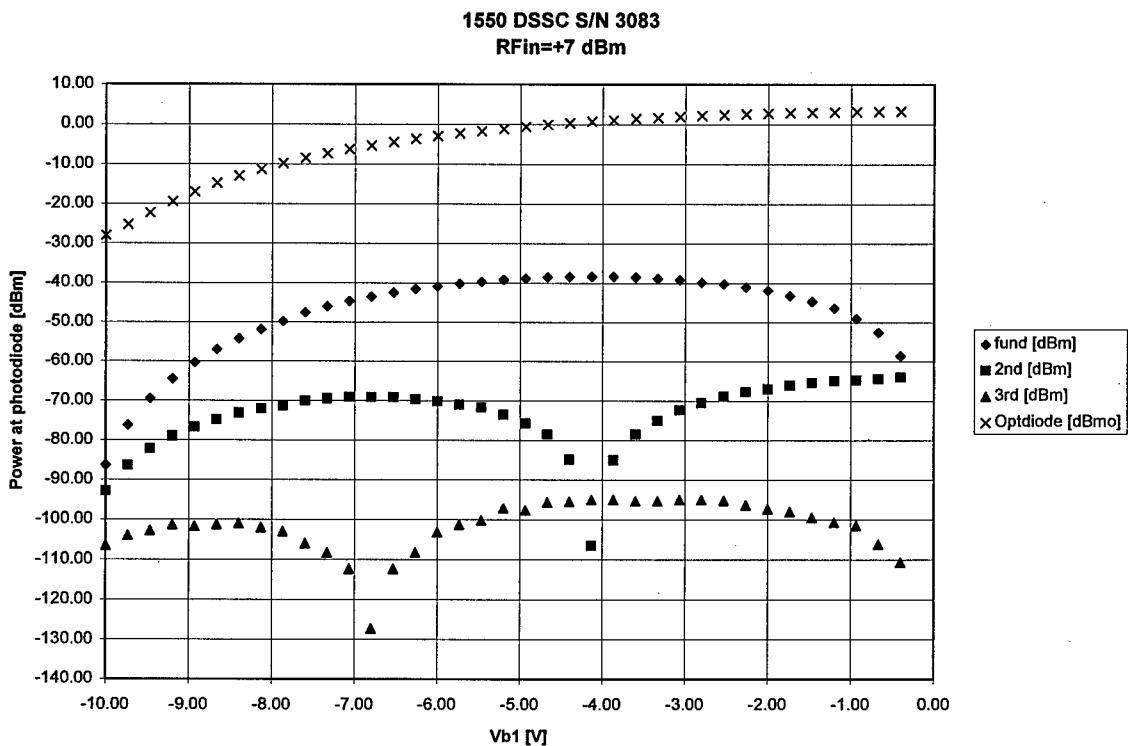


Figure 17. DSSC 3083 response versus Vb1 bias voltage, prior to EDFA, a = 1. (G1-A.XLS)

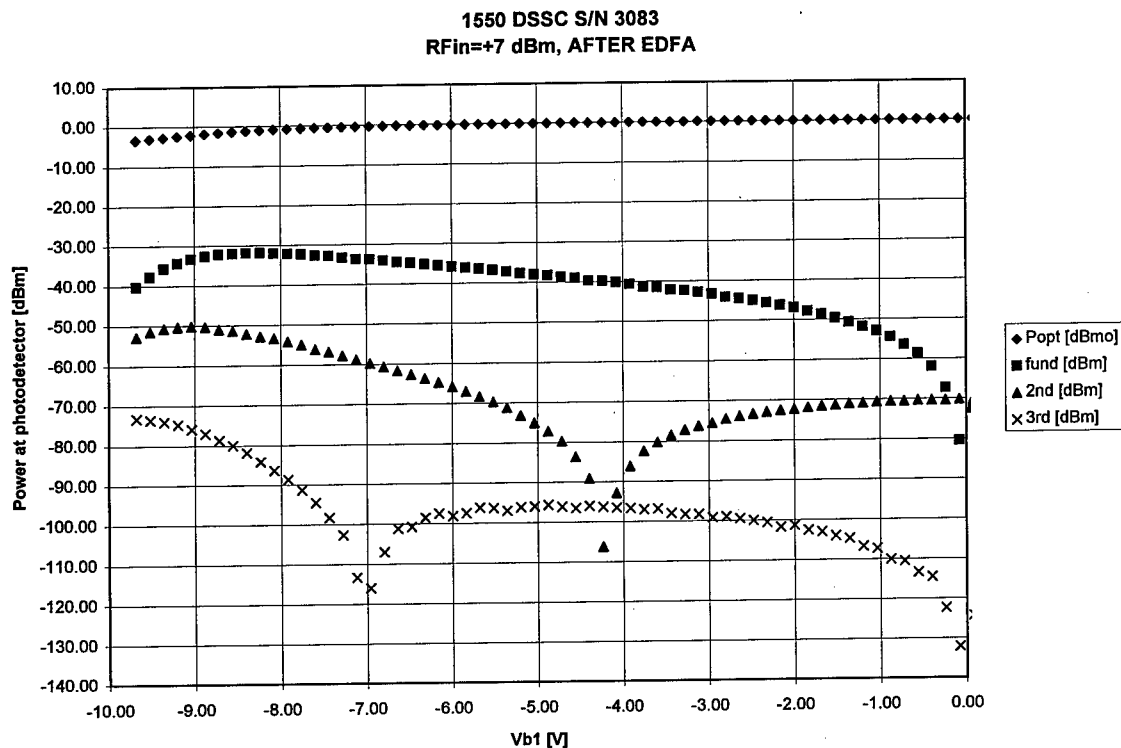


Figure 18. DSSC 3083 response versus Vb1 bias voltage, after EDFA, a = 1. (G1-B.XLS)

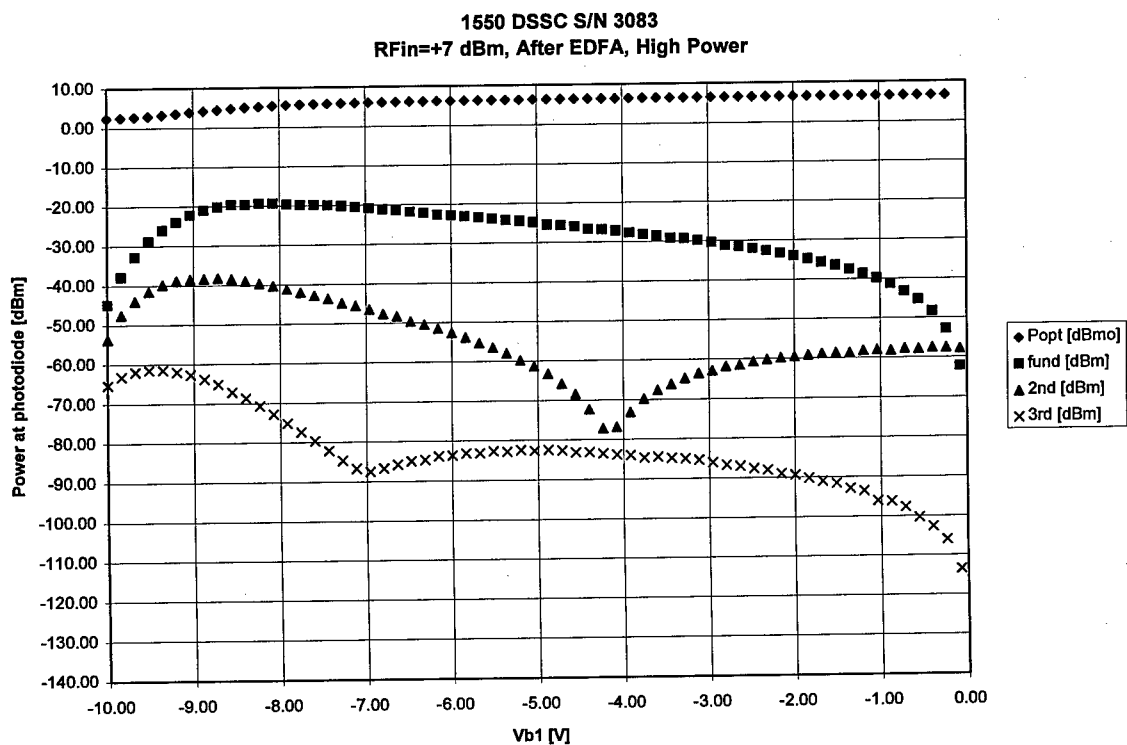


Figure 19. DSSC 3083 response versus Vb1 bias voltage, after EDFA, with high photodiode current, a = 1. (G1-C.XLS)

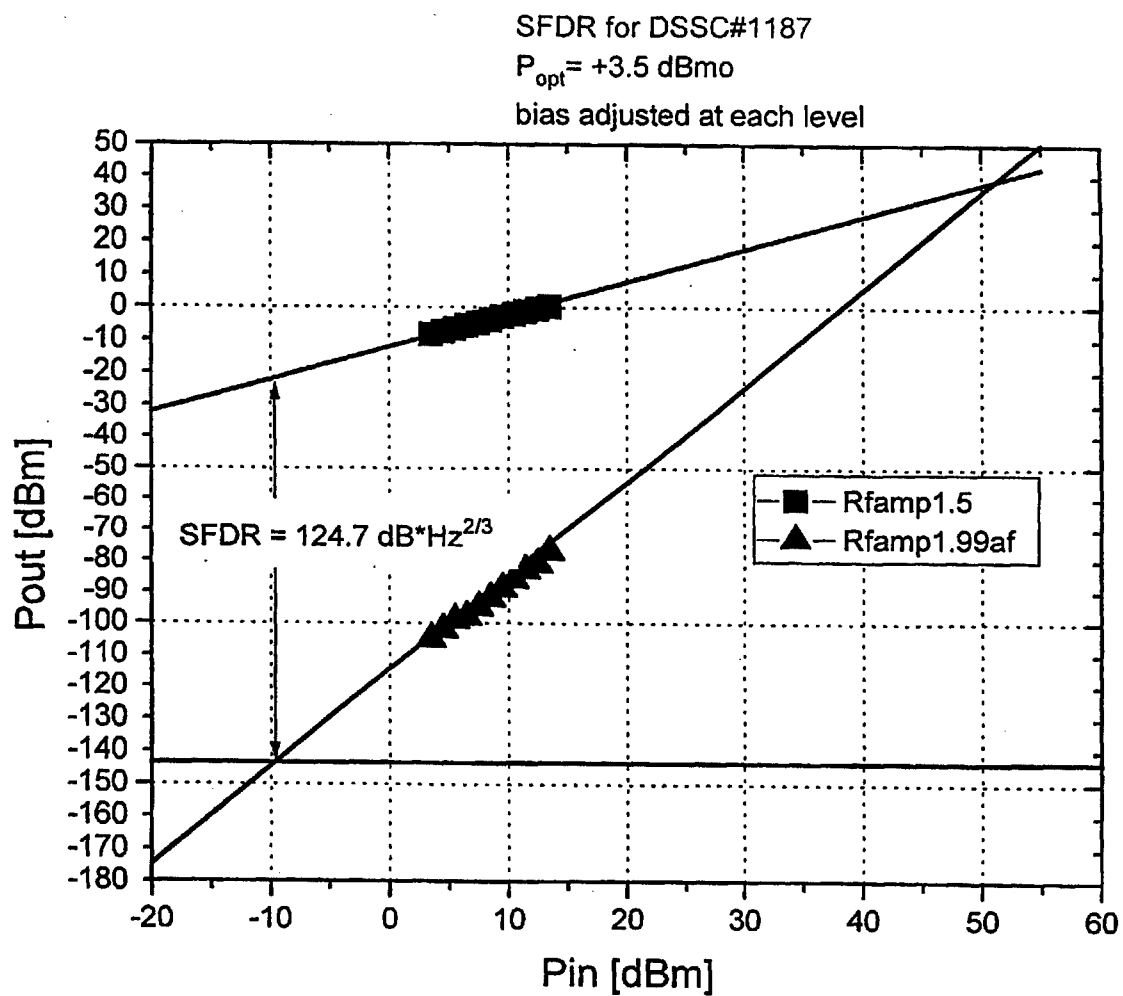


Figure 20. Measured Spurious-Free Dynamic Range (SFDR) of 1300 nm DSSC link, 200 mw optical input power.

6. Control Loop

To realize the maximum SFDR, a control loop is necessary to maintain the DSSC bias at either the second-order or the third-order suppression point, due to the slow bias-point drift versus temperature and optical input power level characteristic of lithium niobate interferometric modulators. The second-order suppression can be accomplished in the same way as with a standard Mach-Zehnder, with a control loop that adjusts the DC bias so as to minimize the second harmonic of a test signal applied to the DSSC. To operate at the third-order suppression point, the circuit illustrated in Figure 21 was built, in which an out-of-band two-tone test signal is applied to the DSSC, and an error signal is derived from the third-order intermodulation sideband amplitude. A computer control algorithm senses this error signal and adjusts the modulator bias to minimize the error signal.

Referring to Figure 21, the third-order bias control system operates as follows: An out-of-band two-tone pilot signal with 10.7 MHz separation at 872 MHz and 882.7 MHz is first generated. Both tones are synthesized coherently from a common 10.7 MHz crystal oscillator reference. The two-tone pilot signal is then combined with the RF input signal to be transmitted and applied to the DSSC RF input. In this case, the input signal is at baseband frequencies up to 435 MHz. The pilot signal frequency must be twice the bandwidth of the baseband RF input, to prevent intermodulation products from falling into the signal band. As the bias point of the modulator drifts from the optimum third-order suppression point, the intermodulation products generated at 10.7 MHz to either side of the two-tone pilot signals increase. To close the loop, a portion of the modulated optical output power of the DSSC is photodetected, filtered, and mixed with the 872 MHz tone, which downconverts one of the intermodulation sidebands to a baseband frequency of 21.4 MHz. The amplitude of this 21.4 MHz signal is minimized when the bias of the modulator is properly adjusted for third-order suppression. To achieve the required sensitivity, the 21.4 MHz signal is subsequently filtered, amplified, and synchronously detected with the doubled 10.7 MHz reference to produce a DC voltage which is proportional to the bias-error. This DC level is sampled by an IBM PC compatible computer running a control program that adjusts the DSSC bias voltage to minimize the error signal.

A 1300 nm device was temperature cycled to quantify the control system performance in terms of harmonic content vs. DSSC temperature. The results of these tests are shown in Figure 22.

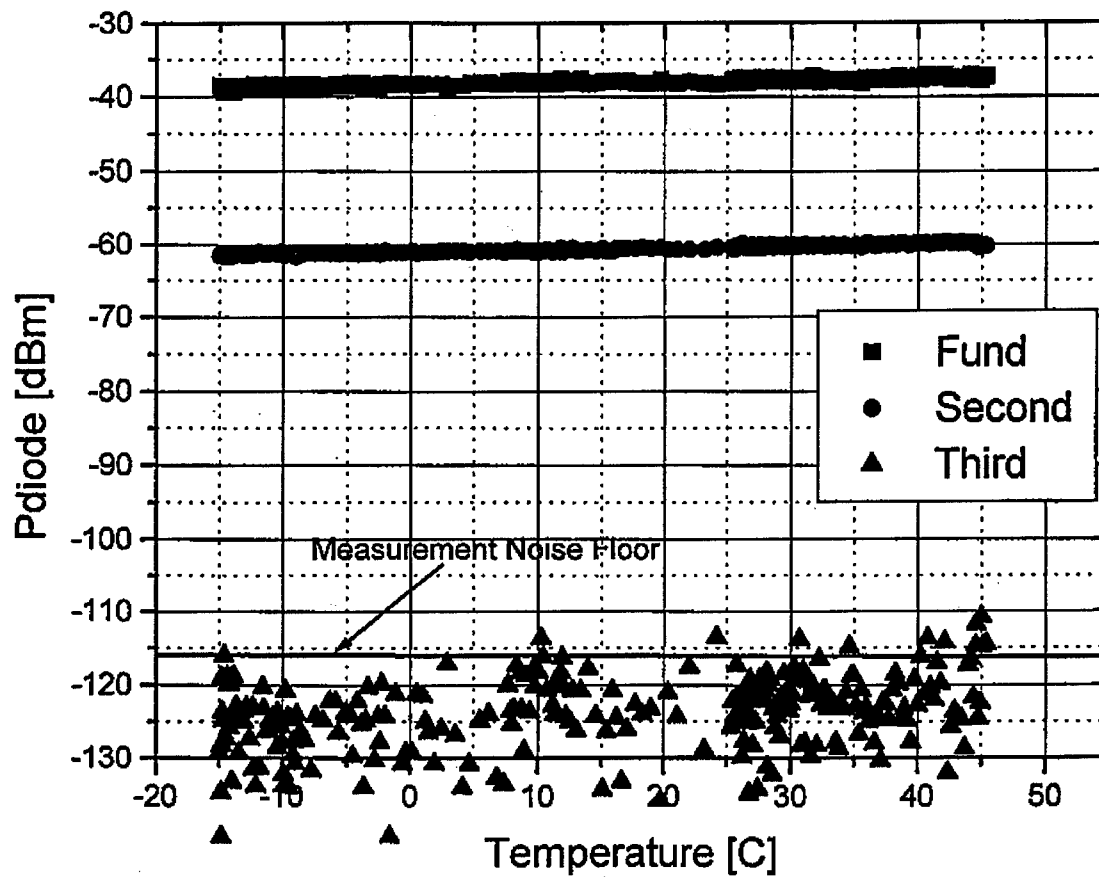


Figure 22. Harmonic power levels verses temperature of DSSC modulator with bias control loop operating.

7. Discussion of Results

This Report has described results of theoretical and experimental investigations performed by UTP on the DSSC waveguide optical modulator. It was shown that fiber-optic links constructed with the DSSC modulator can exhibit enhanced RF gain and reduced levels of third-order intermodulation distortion compared to links employing a standard Mach-Zehnder modulator. The experimental results are in good agreement with the theoretical predictions. In this section, the results and their system impacts are discussed.

The DSSC modulator concept was originally proposed [1] to circumvent a primary limitation to RF fiber-optic link losses: photodiode saturation. It was envisioned that the DSSC modulator would enable low-loss fiber-optic transmission of RF signals by virtue of the reduced optical carrier power compared to the sideband power, so that photodiode saturation due to high carrier power could be avoided. When combined with an optical amplifier, it was proposed that the RF sidebands could be amplified at the output of the DSSC modulator in the optical domain, while minimizing the optical carrier power on the photodiode, and thereby achieve lower RF link losses.

In the course of this research program, reduced RF link losses through carrier suppression were demonstrated theoretically and experimentally. In Figure 5, the RF gain versus bias on the RF Mach-Zehnder section (V_{b1}) is plotted for the cases of both constant optical input power and constant optical output power. From this plot, it can be seen that the RF gain at the third-order distortion minimum point is calculated to increase by approximately 12 dB when the optical power on the photodiode is held constant as the bias point V_{b1} is varied. In the calculation of Figure 5, the optical output power was held constant at the level obtained at the second-order distortion null. Constant optical output power can be achieved in practice by placing an EDFA operating in saturation between the output of the DSSC and the photodiode input.

In Figure 17, the RF power versus V_{b1} without an EDFA is plotted for DSSC S/N 3083. In this experiment the optical output power at the second-order null is approximately +1 dBm. From this plot, the RF link gain is seen to be approximately -50 dB at the third-order null near $V_{b1} = -6.8$ V, at an optical output power of -5 dBm. In Figure 18, the response of DSSC device S/N 3083 is plotted with an EDFA inserted between the DSSC and the photodiode. Since the EDFA output power level is approximately +14 dBm, an optical attenuator is used to reduce the EDFA output power to a level of 0 dBm at the third-order null point. In this case, the RF gain at the third-order distortion null is measured to be approximately -40 dB. If the optical output power is normalized to be +1 dBm to compare with the output power level at the second-order null point, then the gain is actually -38 dB. Therefore, approximately 12 dB improvement in RF link loss was observed when using the DSSC in conjunction with an optical amplifier, in good agreement with the theoretical prediction of 12 dB improvement from Figure 5.

Even larger amounts of link gain improvement are possible by operating at bias points other than the third-order distortion null. For example, comparing Figures 17 and 18, a 27 dB improvement in link gain is observed when using the EDFA at a bias point V_{b1} of approximately -8.5 V. However, the absolute value of the link gain with EDFA at this operating point is -35 dB. Although a 27 dB improvement in link gain is impressive, the absolute value of the link gain not significantly improved over the value obtained at the third-order null point of -38 dB. This bias point corresponds to operation of the device closer to complete carrier suppression. Since operating points in this region exhibit a substantially higher level of third-order distortion than would typically be acceptable in most systems, they were not investigated further.

Also, the amount of second- or third-harmonic suppression was not appreciably degraded by the introduction of the optical amplifier. In the experiments of Figures 17 and 18, the second-harmonic suppression at the third-order null was approximately 14 dB in both cases. The third-harmonic suppression was in excess of 80 dB in both cases.

When operating the photodiode at higher optical power, as shown in Figure 19, the link losses can be reduced even further. In Figure 19, at the third-order null point near $V_{b1} = -7$ V, the link gain is -28 dB, with an optical output power of approximately +6 dBm. This is a 10 dB improvement in link gain compared to the case of Figure 18. The optical power increase at the third-order null between these two experiments is 5 dB, so the RF gain scales 2 dB for each 1 dB of optical power, as expected. The approximately 12 dB degradation in third-order distortion suppression observed at in Figure 19 is probably due the photodiode beginning to saturate at this high input power level.

Although lower link losses can be achieved through the introduction of carrier suppression, the improvement in link gain is accompanied by an increase in second-harmonic distortion compared to the standard Mach-Zehnder modulator at quadrature bias. This is what might be expected intuitively, since it is well-known that in the limit of complete carrier suppression in the Mach-Zehnder modulator, a very strong RF second-harmonic is generated upon photodetection. In fact, the "null-biasing" technique has been employed to use the Mach-Zehnder link as a frequency-doubler, and to generate tunable optical local oscillator signals for use in photonic mixing systems.

The bulk of the present research effort was directed toward identifying the operating points at which the harmonic distortion is minimized in the DSSC. In Figure 3, the calculated RF power versus bias point of the RF modulator section is plotted. When carrier suppression is complete, which occurs near 6.25 radians in this plot, the RF fundamental power is also completely suppressed. This is confirmed experimentally in Figures 11 through 16. However, it can be seen that a point exists at 4.96 radians where the third-order intermodulation distortion is strongly suppressed. This type of suppression does not occur in the standard Mach-Zehnder modulator.

The DSSC achieves enhanced linearity via the introduction of a controlled amount of unmodulated optical carrier at the output of a standard balanced Mach-Zehnder modulator. This introduces an asymmetry into the voltage-to-optical power transfer characteristic compared to the standard Mach-Zehnder, so that an operating point exists where third-order distortion terms are minimized. When operated at this point, the DSSC has significantly enhanced linear dynamic range compared to the standard Mach-Zehnder modulator. This extended dynamic range is achieved when the DSSC is biased at a point where the third-order term in its polynomial expansion is minimized. However, at this operating point, the second-order distortion is not minimized. Therefore, this operating point is limited to sub-octave applications. (In a sub-octave application, second-harmonics will fall out of band.)

The spurious-free dynamic range of the DSSC at 1300 nm was calculated as shown in Figure 10b to be approximately $126 \text{ dB-Hz}^{(2/3)}$. This was confirmed experimentally as shown in Figure 20, in which the spurious-free dynamic range was measured to be $124.7 \text{ dB-Hz}^{(2/3)}$. This value was inferred from measurements of the third-order intermodulation products and the computed shot-noise level due to the Nd:YAG laser. This level of dynamic range is only achievable in a sub-octave bandwidth, as discussed previously.

8. References

1. E. Gertel and K. Pedrotti, "Optical logarithmic convertor," Proceedings of the 4th Biennial Department of Defense Fiber Optics and Photonics Conference, McClean, VA, March 1994, p. 283.
2. C.H. Cox III, G.E. Betts, and L.M. Johnson, "An analytic and experimental comparison of direct and external modulation in analog fiber optic links," IEEE Trans. Microwave Theory Tech., Vol. 38, pp. 501-509, May 1990.
3. X. S. Yao, G. F. Lutes, R. T. Logan Jr., L. Maleki, "Field Demonstration of X-Band Photonic Antenna Remoting in the Deep Space Network," JPL/NASA Telecommunications and Data Acquisition Progress Report, 42-117, Jan.-Mar. 1994, p. 29.
4. M.R. Farwell, W.S.C. Chang, and D.R. Huber, "Increased linear dynamic range by low biasing the Mach-Zehnder modulator," IEEE Photon. Tech. Lett., Vol. 5, No. 7, pp. 792-795, July 1993.
5. M.J. LaGasse, W. Charzenko, M.C. Hamilton, S. Thaniyavarn, "Optical carrier filtering for high-dynamic Ku-band fiber optic links," SPIE Conference of Optical Technology for Microwave Applications VII, (conference # 2560), San Diego, CA, 11-12 July 1995.
6. G.E. Betts, "Linearized modulator for suboctave-bandpass optical analog links," IEEE Trans. Microwave Theory Tech., Vol. 42, No. 12, pp. 2642-2649, December 1994.

Appendix A

Swept Frequency Response Data for DSSC modulator devices.

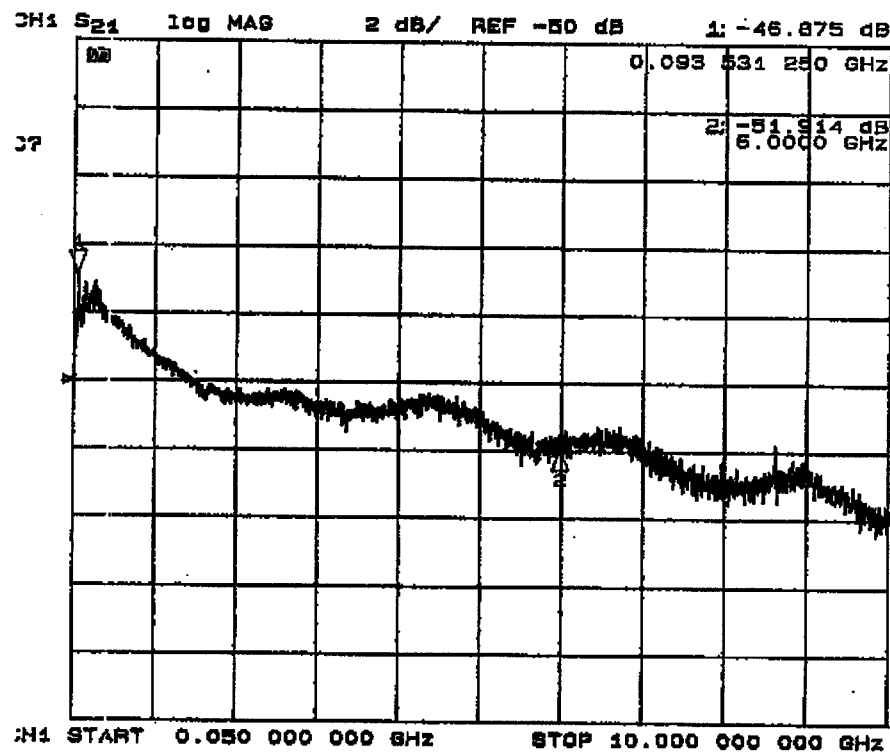
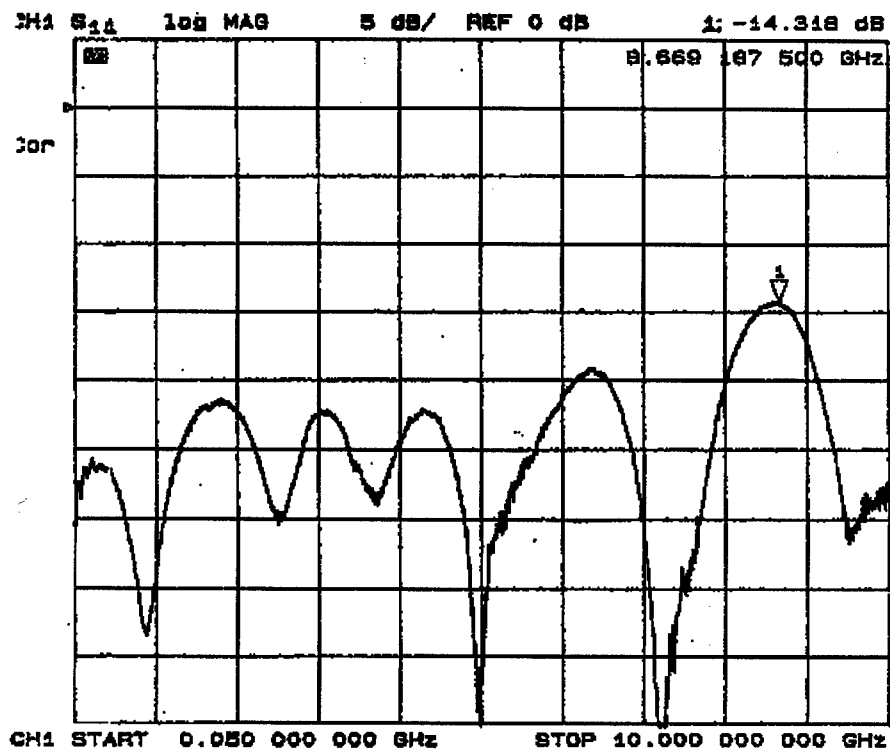


Figure A-1. RF return loss and through loss verses frequency for modulator number 1187.

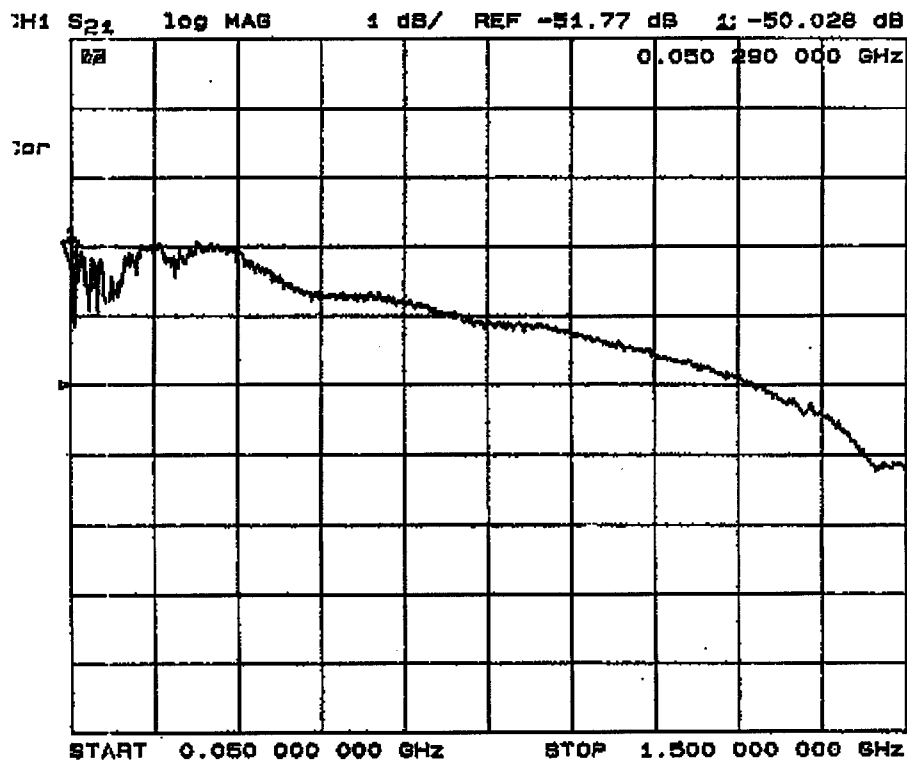
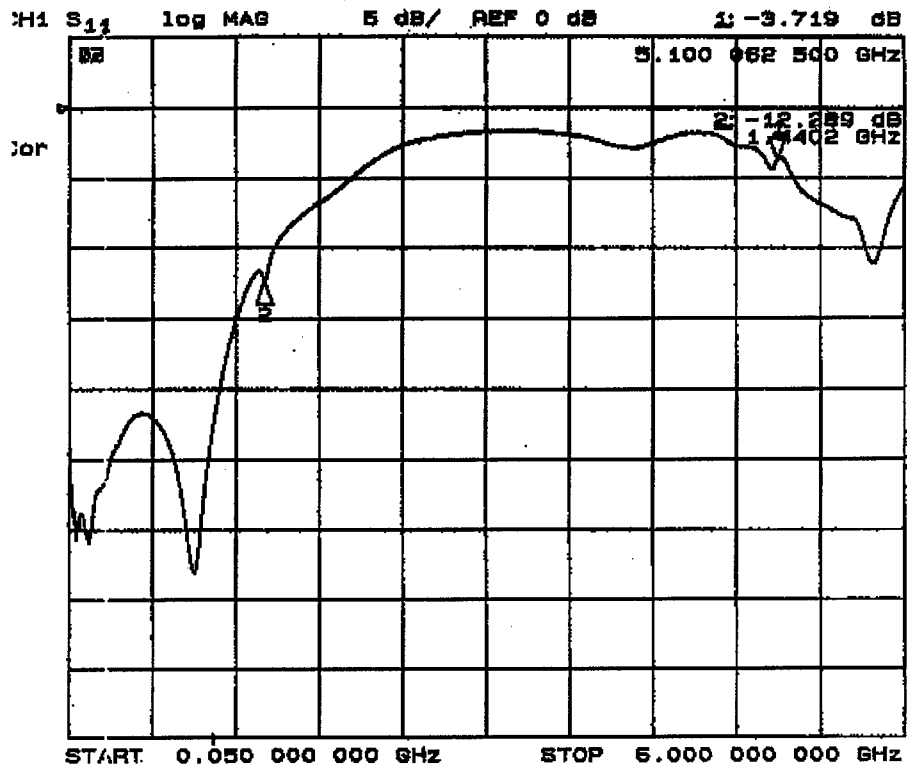


Figure A-2. RF return loss and through loss verses frequency for modulator number 1188.

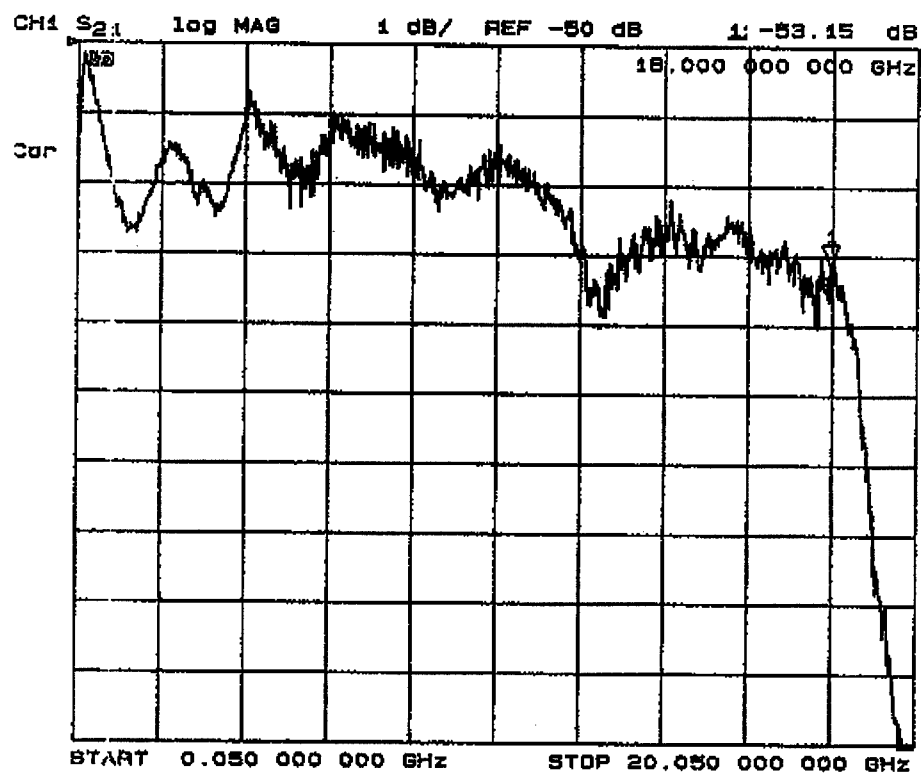
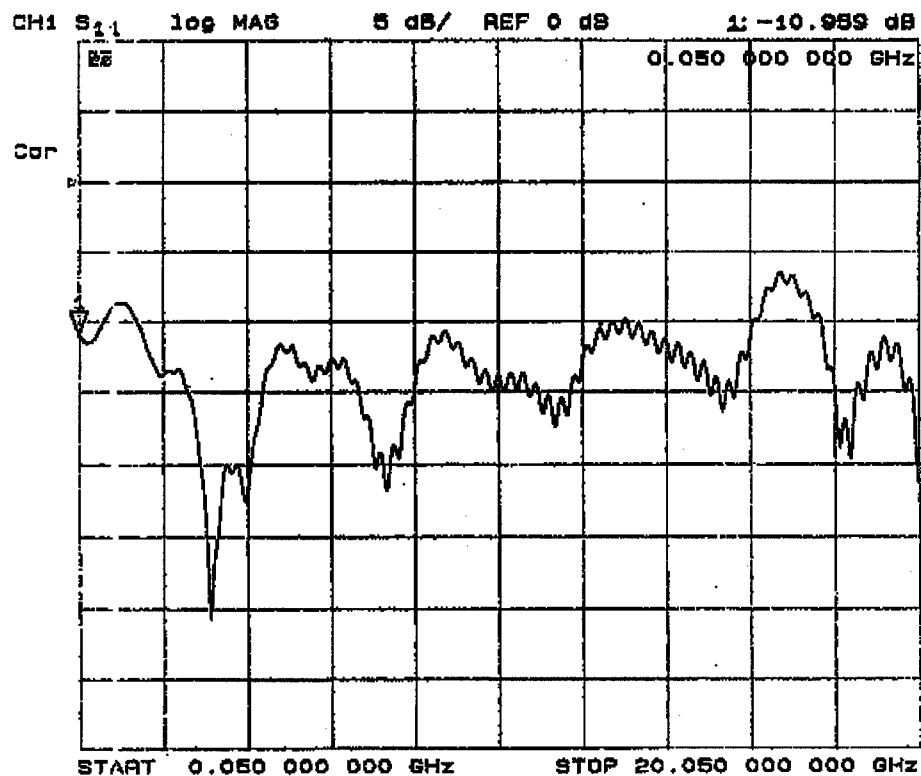


Figure A-3. RF return loss and through loss verses frequency for modulator number 1189.

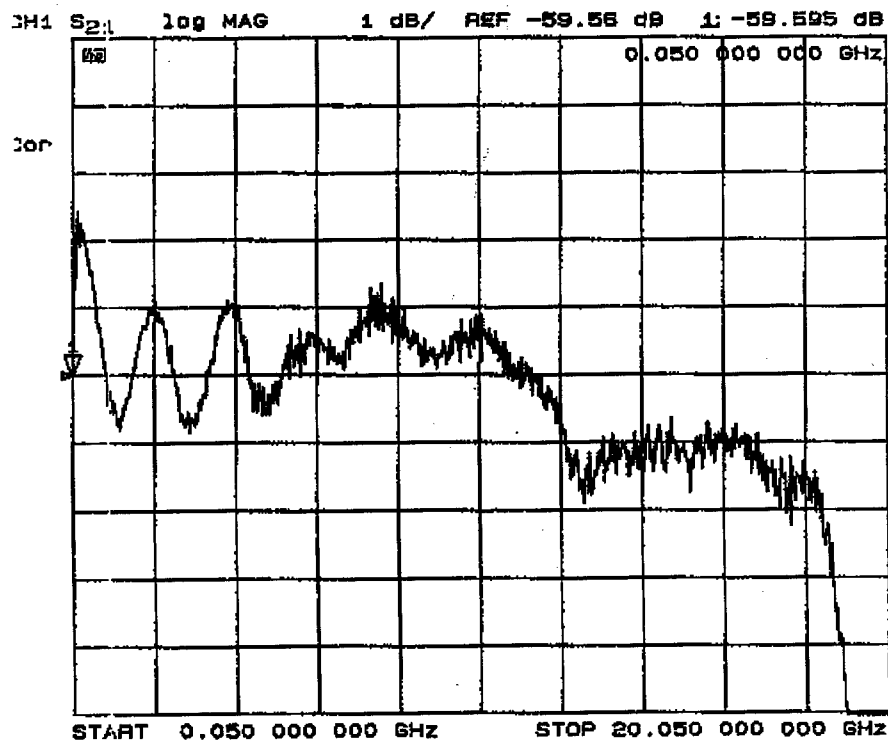
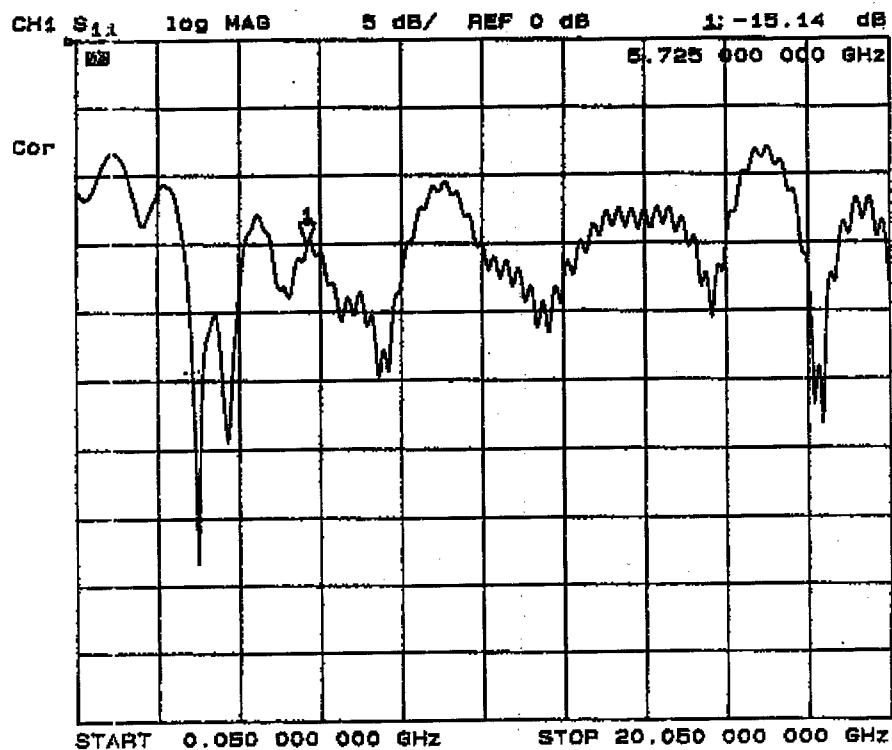


Figure A-4. RF return loss and through loss verses frequency for modulator number 1190.

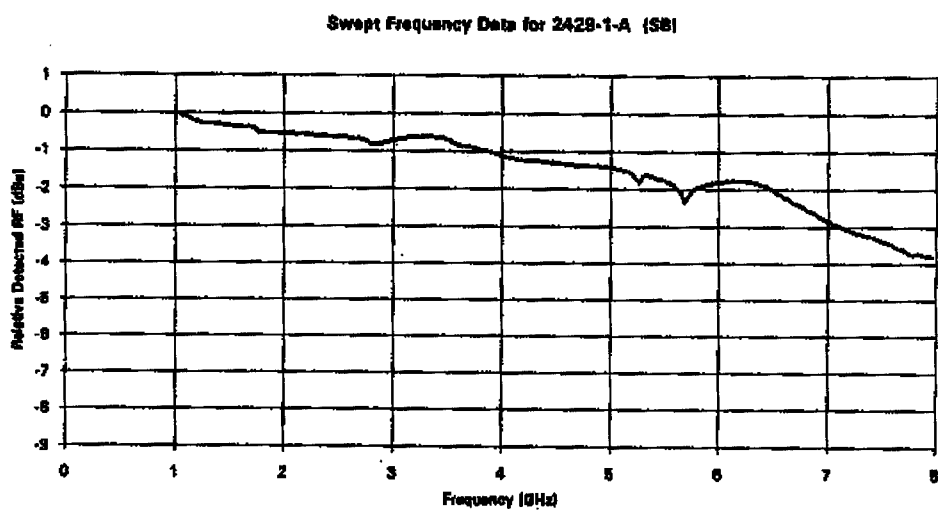
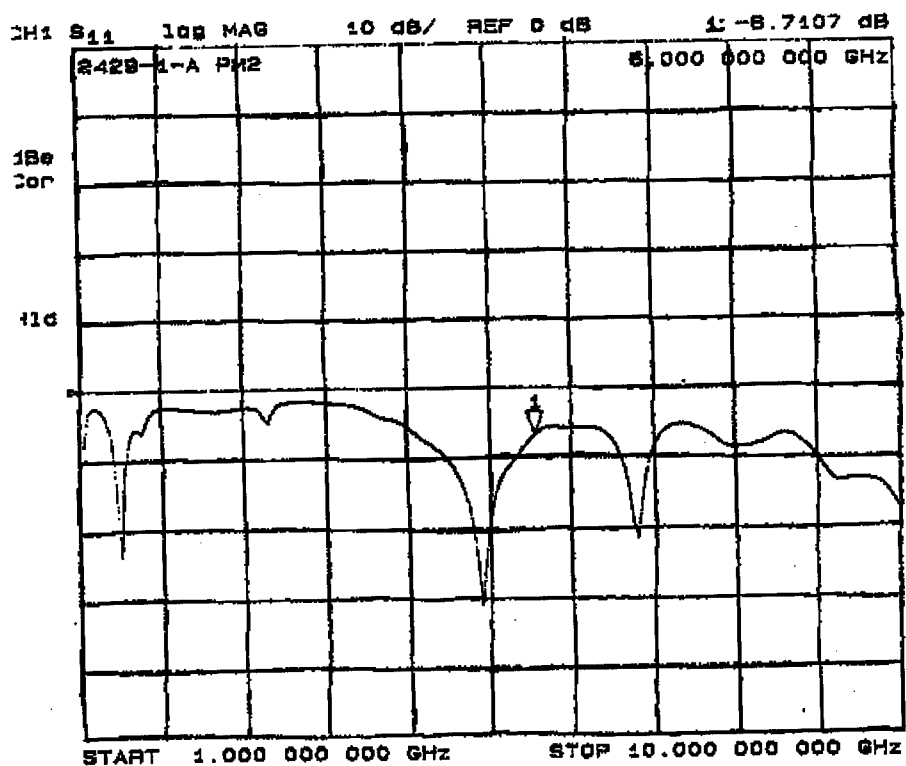
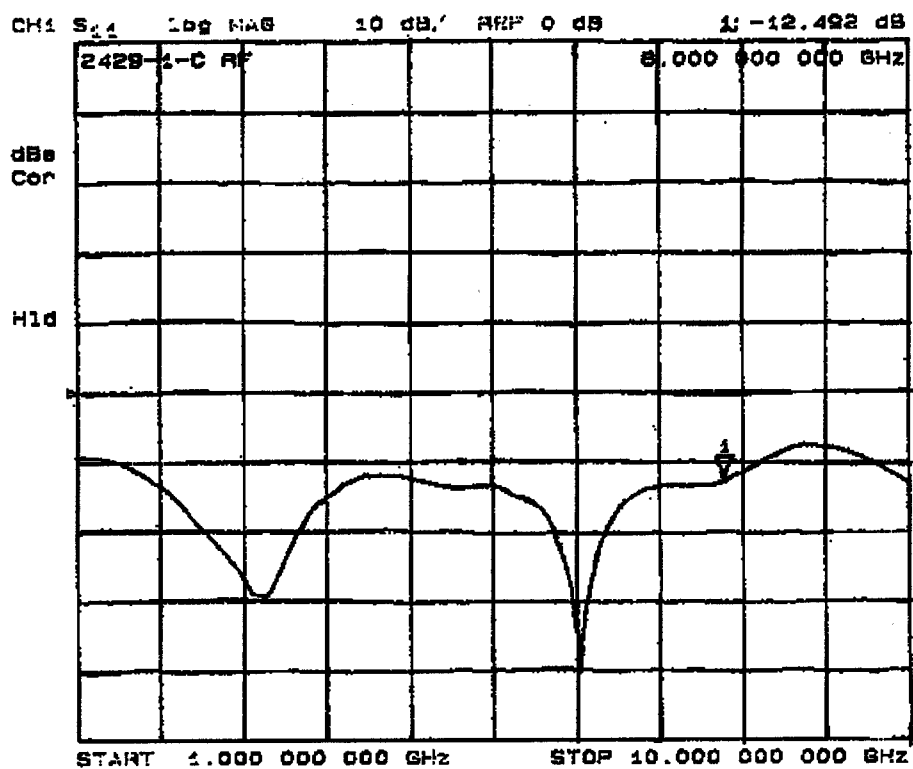


Figure A-5. RF return loss and through loss verses frequency for modulator number 3082.



Swept Frequency Data for 242B-1-C (SB)

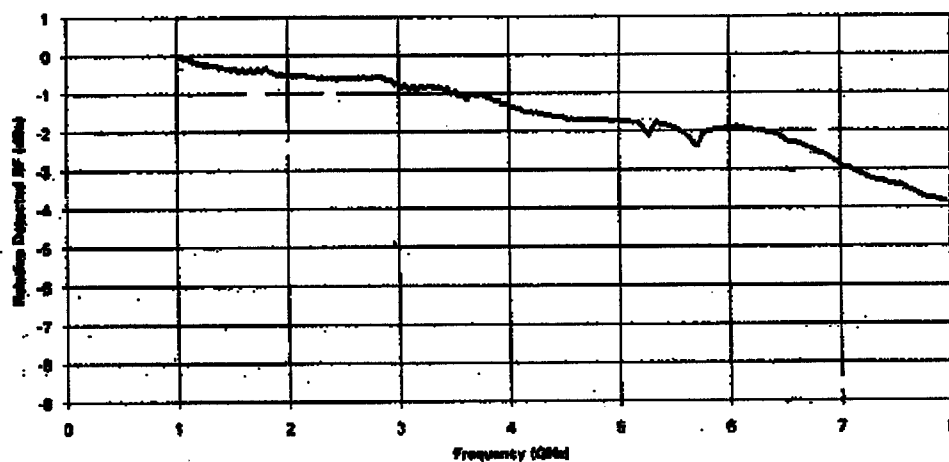


Figure A-6. RF return loss and through loss verses frequency for modulator number 3083.

DSSC Optical Link: Demonstration & Test Results

Final Scientific and Technical Report
(Contract #)

Prepared for:

USAF
Rome Laboratory
Rome, NY 13441-4515
Attn. Mr. Brian Hendrickson
Mr. James Hunter (TPOC)

December, 10, 1996

Tracor-AEL
AEL Industries, Inc.
Systems Engineering Division
305 Richardson Road, Lansdale, PA 19446-1485

DSSC Optical Link Demonstration/Test Results

Synopsis

Several specific performance tests per schedule (Figures B-1-0-1 and B-1-0-2) were conducted for the DSSC Optical Link. These measurements were made in addition to those presented in the UTP-supplied Final Report (draft) submitted previously to Rome Laboratory by AEL, Inc. This table lists the categories and purpose of the experiments and the link characteristics thus analyzed. Experiment/test configuration for each of these tests conducted at AEL are also provided. The test results have been summarized in the following sections and conclusions on the usefulness of the DSSC modulator in high dynamic range optical link applications drawn. In addition to providing new data on the experiments listed in Figure B-1-0-2, this report is prepared to supplement the UTP-supplied Final Report (draft). Therefore, detailed instructions to operate the DSSC controller and to successfully conduct the required DSSC link performance demonstration are important features of this report.

The report contains the following sections:

- A. DSSC Interface and Operating Instructions
- B. DSSC Demo/Performance Testing
- C. DSSC Performance Simulation
- D. Summary and Recommendation
- E. Appendix
 - I: Nortel EDFA Operating Manual
 - II: DSSC Computer Control: Labview Instructions
 - III: DSSC Modulator Performance Enhancement Simulations

List of Figures and Tables

Figure A-1-1.	DSSC Hardware.
Figure A-1-2a.	Picture of the DSSC Hardware and Test Setup (for Noise Figure, Phase-stability, and Multicarrier IM) at AEL.
Figure A-1-2b.	Picture: DSSC Hardware and Phase Noise Test Setup at AEL.
Figure A-1-3.	Computer Interface to DSSC Hardware: D/A and A/D Terminal Boards with Interconnection Diagram.
Figure A-1-4.	Power Distribution Scheme for the DSSC Hardware (Rear Panel).
Figure A-1-5.	DSSC Hardware Interconnection (Rear Panel).
Figure A-1-6.	Schematic of the DSSC Biasing Circuit.
Figure A-1-7.	DSSC Modulator Hardware Layout: Transmit Channel and Accessories.
Figure A-1-8.	Picture of the DSSC Modulator Hardware Layout: Transmitter and Receiver Units.
Figure B-1-0-1.	DSSC Modulator Test Plan (Proposed).
Figure B-1-0-2.	DSSC Modulator Test Plan (Demonstration/Expt. Conducted).
Figure B-1-0-3.	DSSC Modulator Test Equipment List.
Figure B-2-0-1.	Two-tone IM Test Configuration: DSSC Link with EDFA.
Figure B-2-0-2.	Noise Figure Test Configuration.
Figure B-2-0-3.	Phase-Noise Test Setup and Accessories at AEL.
Figure B-2-0-4.	AEL Phase-Noise Test Setup: Automated Configuration Control.
Figure B-2-0-5.	Phase Stability Test Configuration.
Figure B-2-1-1.	Two-tone IMD Test Data Measured at C-band, 15-MHz Channel Spacing; DSSC Link w/o EDFA.
Figure B-2-1-2.	RF Output Signals Measured by the Spectrum Analyzer: Carriers, Harmonics, and IMs (for three tones set at 2.7, 2.715, and 2.73 GHz with 15 MHz spacing).
Figure B-2-1-3a.	Reduction of the third-order IM by DSSC Bias Control at S-band [Third-order IM, 2f3-f1 @ 2.76 GHz].
Figure B-2-1-3b.	Reduction of the third-order IM by DSSC Bias Control at S-band [Third-order IM 2f1-f3 @ 2.67 GHz].
Figure B-2-1-4a.	Multicarrier IM Products of the DSSC Modulator: Three-tone Tests at S-band [DSSC Modulator w/o EDFA, three tones set @ ~ 2.7 GHz, 15-MHz apart; input optical power level- low (0.474 mW)].
Figure B-2-1-4b.	Multicarrier IM Products of the DSSC Modulator: Three-tone Tests at S-band [DSSC Modulator w/EDFA and Lasertron PD, three tones set @ ~ 2.7 GHz, 15-MHz apart; input optical power level- medium (0.95 mW)].

Figure B-2-1-4c.	Multicarrier IM Products of the DSSC Modulator: Three-tone Tests at S-band [DSSC Modulator w/EDFA and Lasertron PD, three tones set @ ~ 2.7 GHz, 15-MHz apart; input optical power level- high (1.9 mW)].
Figure B-2-1-5.	Dynamic Range (DR) Estimation from the Measured IM Data of an Analog Link.
Figure B-2-1-6a.	Performance Analysis of Externally Modulated Optically Preamplified Direct Detection Link: Optical Hardware Configuration.
Figure B-2-1-6b.	Performance Analysis of Externally Modulated Optically Preamplified Direct Detection Analog Link: Effect of Link Loss on the Noise Figure for a fixed RIN @ -160 dB/Hz.
Figure B-2-1-6c.	Performance Analysis of Externally Modulated Optically Preamplified Direct Detection Analog Link: Effect of Laser RIN on the Noise Figure for a Fixed Link Gain/Loss @ -60 dB.
Figure B-2-1-7a.	DSSC/EDFA Link Operation at Various Input Optical Power Levels : Low Power.
Figure B-2-1-7b.	DSSC/EDFA Link Operation at Various Input Optical Power Levels : Medium Power.
Figure B-2-1-7c.	DSSC/EDFA Link Operation at Various Input Optical Power Levels : High Power.
Figure B-2-2-1.	DSSC Link Gain and Noise Figure Data Measured Using Lasertron PDs at Various Input Optical Power Levels.
Figure B-2-2-2.	DSSC Link Gain and Noise Figure Data Measured Using Ortel PDs at Various Input Optical Power Levels.
Figure B-2-2-3.	DSSC Link Performance at C-band: Noise Figure vs. RF Carrier Frequency (w/Lasertron PD).
Figure B-2-2-4.	DSSC Link Performance at C-band: Noise Figure vs. RF Carrier Frequency (w/Ortel PD).
Figure B-2-2-5.	DSSC Link Phase Noise Test data: Link with EDFA, Input Optical Power @ 0.95 mW.
Figure B-2-2-6.	DSSC Link Phase Noise Test Data: Link with EDFA, Input Optical Power @ 1.9 mW.
Figure B-2-2-7.	Phase Noise Test data: w/o DSSC Link.
Figure B-2-2-8.	DSSC Link Phase Noise Test Data: Link with EDFA, but w/o Pilot Tones Input Optical Power @ 3 mW.
Figure B-2-2-9.	Phase Noise Test Data: DSSC Link w/EDFA, Measured using HP Network Analyzer, 2.5 GHz RF Carrier.
Figure B-2-3-1.	Phase Stability Test Data of the DSSC Modulator Link.
Table A-1-1.	DSSC Interface Requirement.
Table A-1-2.	DSSC Bias Connectorization Scheme.
Table A-1-3.	DSSC DC Power Distribution Scheme: Color Code.
Table B-2-1-1.	DSSC Performance Characterization Using Optical Spectrum Analyzer.
Table B-2-1-2.	IM Performance of the DSSC Modulator Link.
Table B-2-2-1.	Comparison of Lasertron and Ortel PDs.
Table B-2-2-2.	Degradation of Ortel High-power PD.

A. DSSC Interface and Operating Instructions

A-1. Interfaces to DSSC Unit, Power Distribution Schematics, and Bias Control Circuits

This section provides the documentation for the various interfaces and the power distribution schemes related to the DSSC modulator hardware. The configurations are presented in a tabular format to identify the purpose/name of the port and signal levels. I/O of the computer to the A/D, D/A, and the HPIB interfaces to test equipment are shown. The operating instructions for the Nortel EDFA is included in **Section E, Appendix - I: Nortel EDFA Operating Manual**.

Figures A-1-1 and A-1-2 show the pictures of the DSSC hardware undergoing performance testing at AEL. Also included are the specialized test equipment used to evaluate the systems level performance of the DSSC optical link at high GHz frequencies. Computer I/O interfaces to the DSSC hardware is shown in Figure A-1-3 where the details of each interconnection are provided with the terminal boards clearly identified. The interface requirements and associated terminal boards are listed in Table A-1-1. The power distribution arrangement of the DSSC hardware is drawn in Figure A-1-4, completed with the bias connectorization schemes (see Table A-1-2), the color codes (see Table A-1-3) used for the various interconnections between the terminal boards (see Figure A-1-5). Physical interconnection of the DSSC hardware subunits (made in the rear panel) are identified in Figure A-1-5. As shown in these figures, the self-contained DSSC hardware consists of five major subunits:

- Optical transmitter/modulator,
- Optical receiver,
- Optical fiber amplifier (EDFA),
- Two-tone generator and DSSC bias control electronics, and
- DC power supplies and accessories

The bias control circuit shown in Figure A-1-6 is used to operate the DSSC modulator at the third-order null. In this circuit, two internally generated tones at 872 and 882.7 MHz provide the 10.7 and 21.4 MHz IF signals which are continuously monitored to maintain the operating bias points at the third-order null of the DSSC modulator chip. A description of the operating principle of the bias control circuit was submitted in a previous report. The bias stabilization is achieved automatically using Labview software. Also, such fully automated computer control can be by-passed for a manual mode of operation. The software developed allowed automatic collection as well as reduction of the test data for DSSC link performance evaluation (see **Section E, Appendix- II, Computer Control: Labview Instructions**, for the operating instructions of the software developed at AEL).

The transmit channel hardware (which includes a 1550-nm DFB laser and drive electronics, LiNbO_3 EO modulator chip with DC and RF bias and optical I/O ports, fiber pigtails, RF and optical connectors, etc.) is shown in Figure A-1-7. These optical components are assembled in the Laser/DSSC subunit. A similar subunit assembled for the optical receiver included a Lasertron PIN photodetector and biasing circuit. A pictorial presentation of the transmitter and receiver hardware layout within the respective chassis is given in Figure A-1-8.

Figure A-1-1. DSSC Hardware.

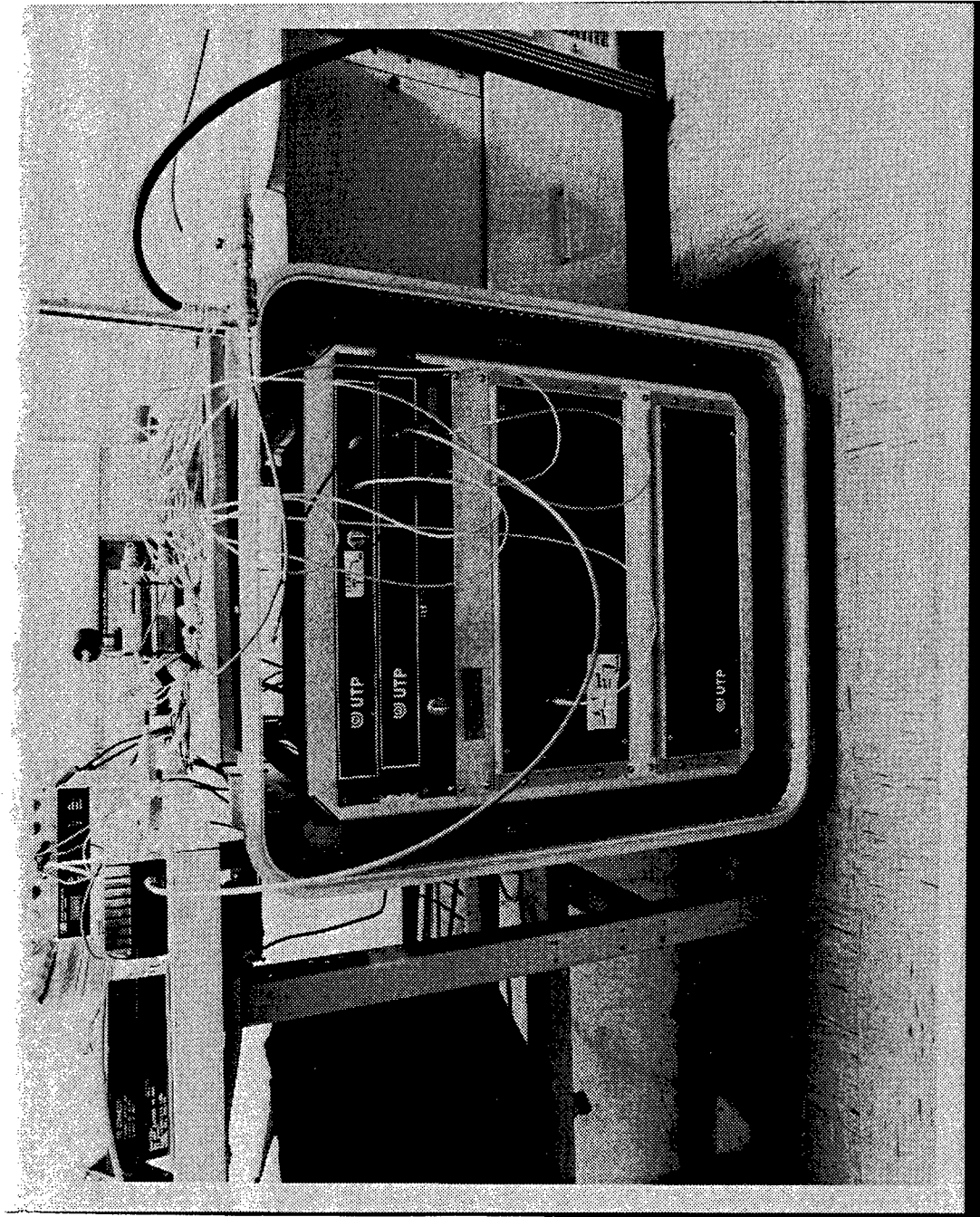


Figure A-1-2a. Picture of the DSSC Hardware and Test Setup (for Noise Figure, Phase-stability, and Multicarrier IM) at AEL.

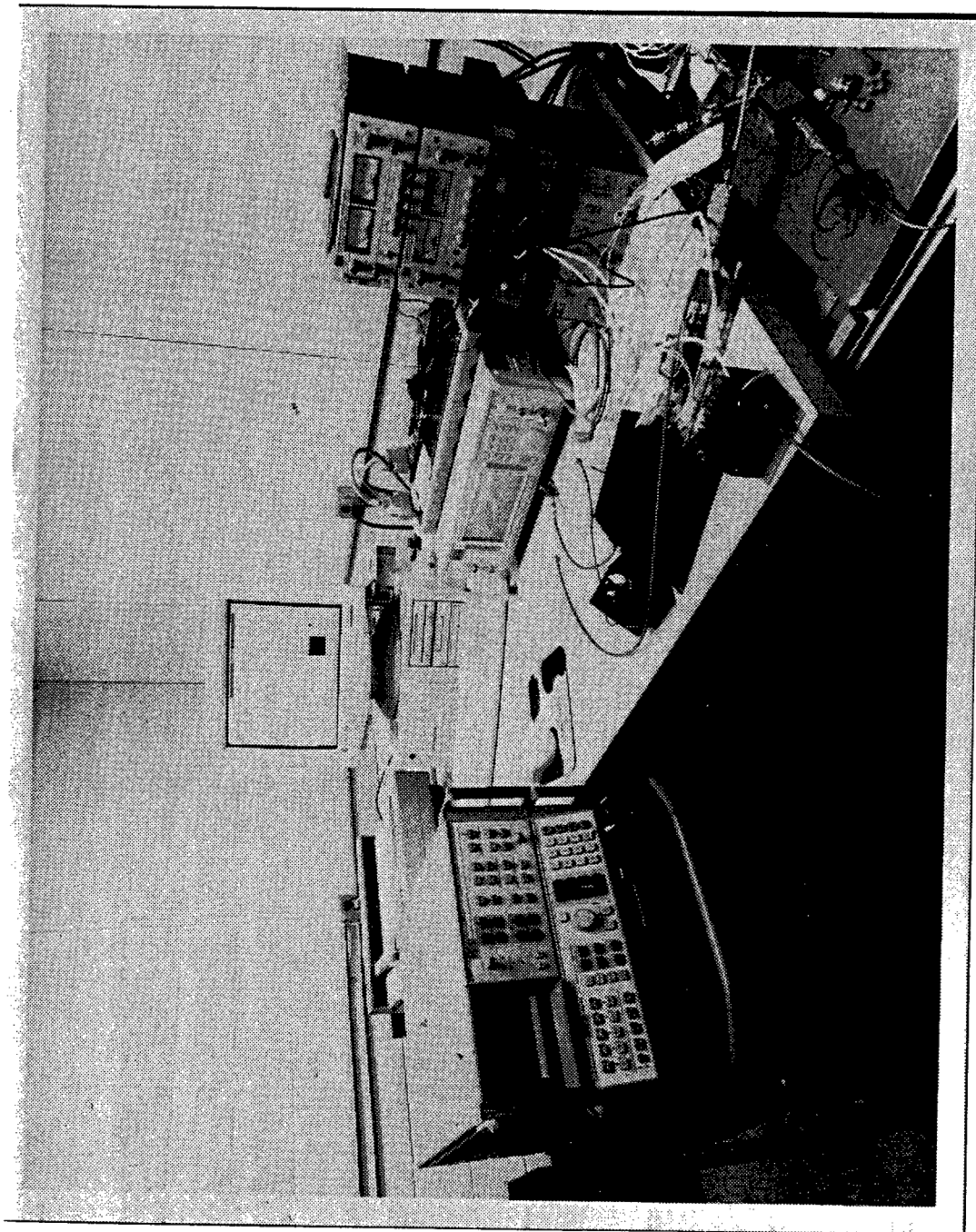


Figure A-1-2b. Picture of the DSSC Hardware and Phase Noise Test Setup at AEL.

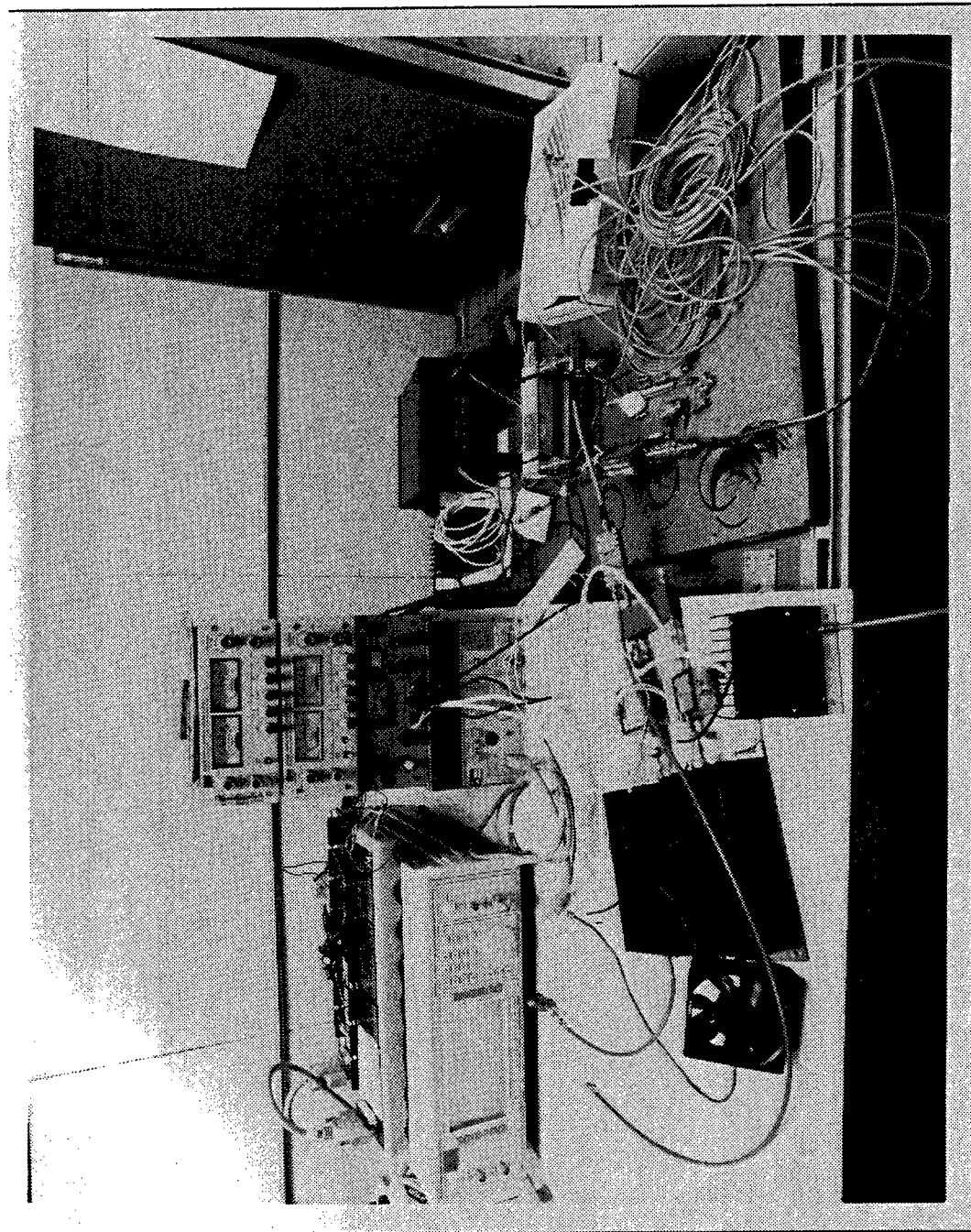


Figure A-1-3. Computer Interface to DSSC Hardware: D/A and A/D Terminal Boards with Interconnection Diagram.

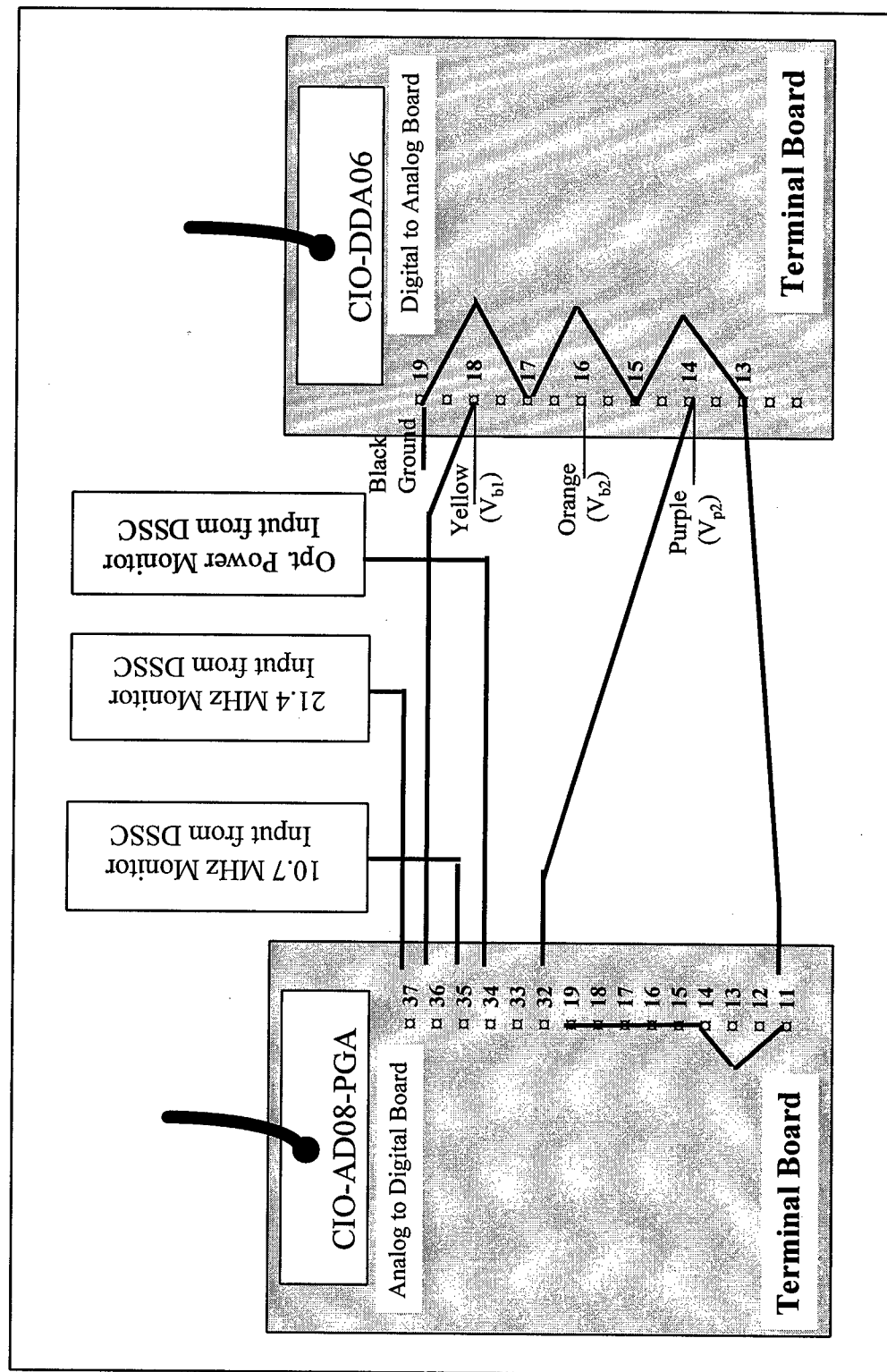


Table A-I-1. DSSC Interface Requirements.

The following hardware is required to run the DSSC software controls and interface the computer with the DSSC system:

- ◆ PC at least 486 processor with 66 MHz clock speed, 16MB RAM and at least 540 MB of hard drive available space. PC must have a trident VGA 256 color card to run Labview software. Note the software will not run with an accelerator card.
- ◆ GPIB board card is from National Instruments, Model PCIIA. This card controls the power meter and the spectrum analyzer. The card is mounted internal to the PC.
- ◆ Analog-to-Digital interface card, CIO-AD08-PGA, located in the DSSC computer is attached via a 37-pin interface cable to a terminal card
- ◆ Digital-to-Analog interface card, CIO-DDA06V6 (CIO-DDA06/12 ordered), located in the DSSC computer is attached via a 37-pin interface cable to the terminal card. This card takes a digital word provided by the LABVIEW program and converts it to an analog output voltage which is utilized to control the bias voltages on the modulators.
- ◆ Terminal card located external to the DSSC computer on the lab bench, Part # CIO-TERMINAL.
- ◆ Two 37-pin interface cables to connect the DSSC computer with the terminal card, Part # C37FFS-5.
- ◆ Lab View software (version 3.0)
- ◆ Software for A/D and D/A circuit cards use Universal software library and Universal Labview w/EXT purchased from Computer Boards, Inc.

Figure A-1-4. Power Distribution Scheme for the DSSC Hardware (Rear Panel).

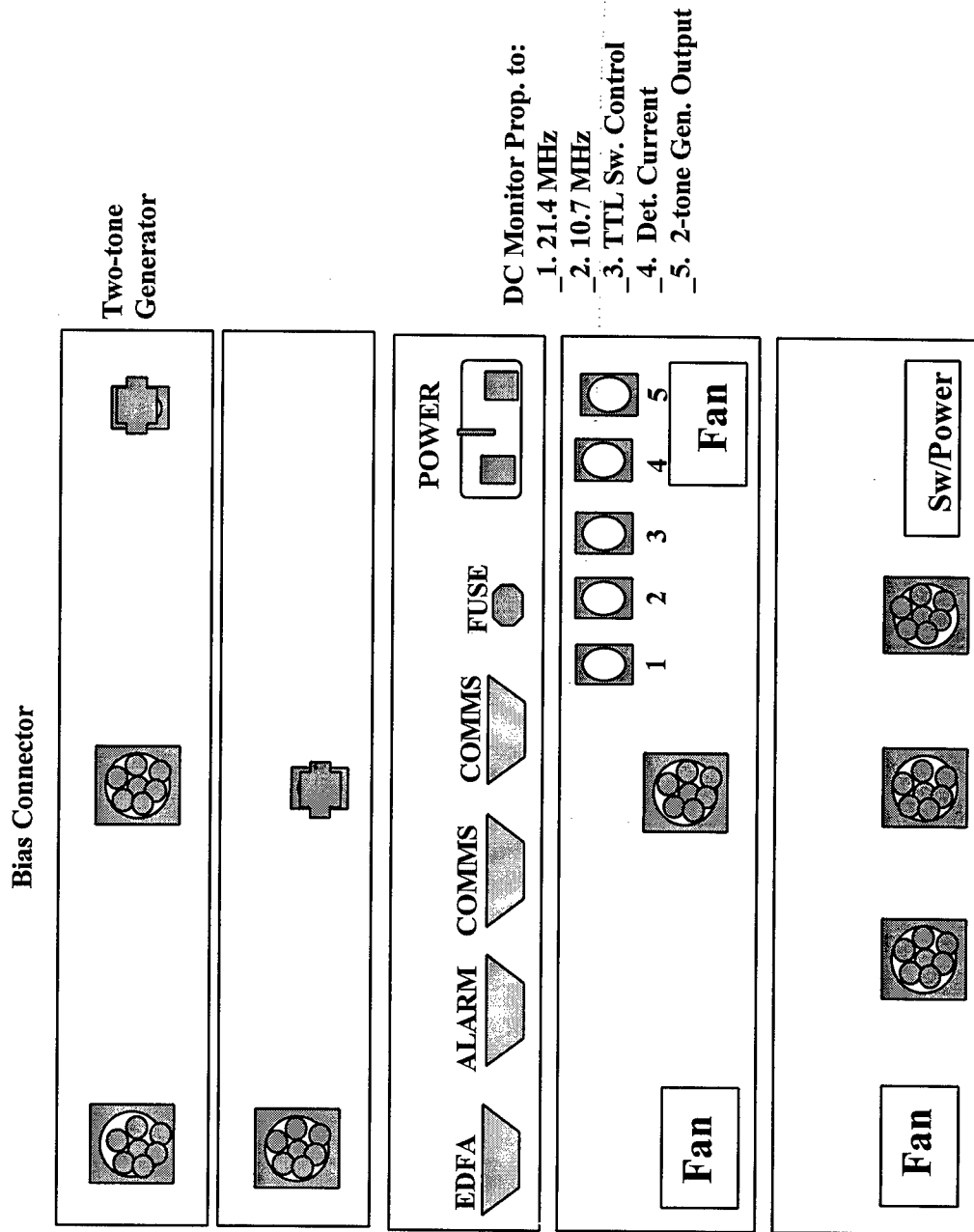


Table A-I-2. DSSC Bias Connectorization Scheme (for biasing DSSC, on rear of transmitter unit).

Mnemonic	Description	Color	Pin #
C1	DOC #1 -- Output	Brown	1
C2	DOC #2 -- Output	Red	2
B2	Vb2 -- Bias Voltage 2	Orange	3
B1	Vb1 -- Bias Voltage 1	Yellow	4
P2	Vp2 -- Phase Bias Voltage 2	Violet	5
Gnd.	Ground	Green	6

Table A-I-3. DSSC DC Power Distribution Scheme: Color Code.

Color	Voltage (V)
Yellow	+ 5
Blue	- 5
Red	+ 15
White	- 15
Violet	- 12
Orange	+ 24
Black	Ground
Green	Ground

Figure A-1-5. DSSC Hardware Interconnection (Rear Panel).

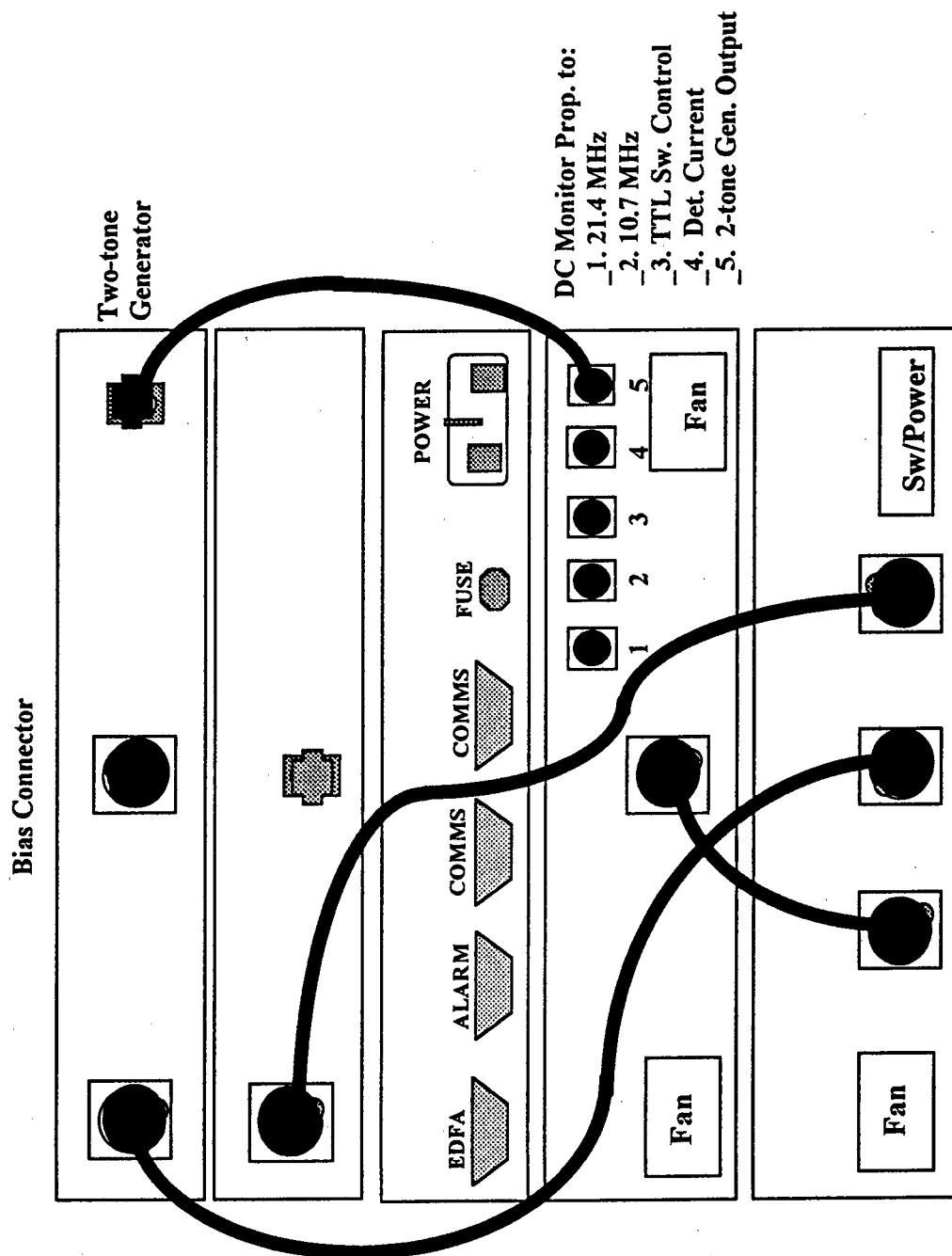


Figure A-1-7. DSSC Modulator Hardware Layout: Transmit Channel and Accessories.

DSSC Modulator Transmitter Unit

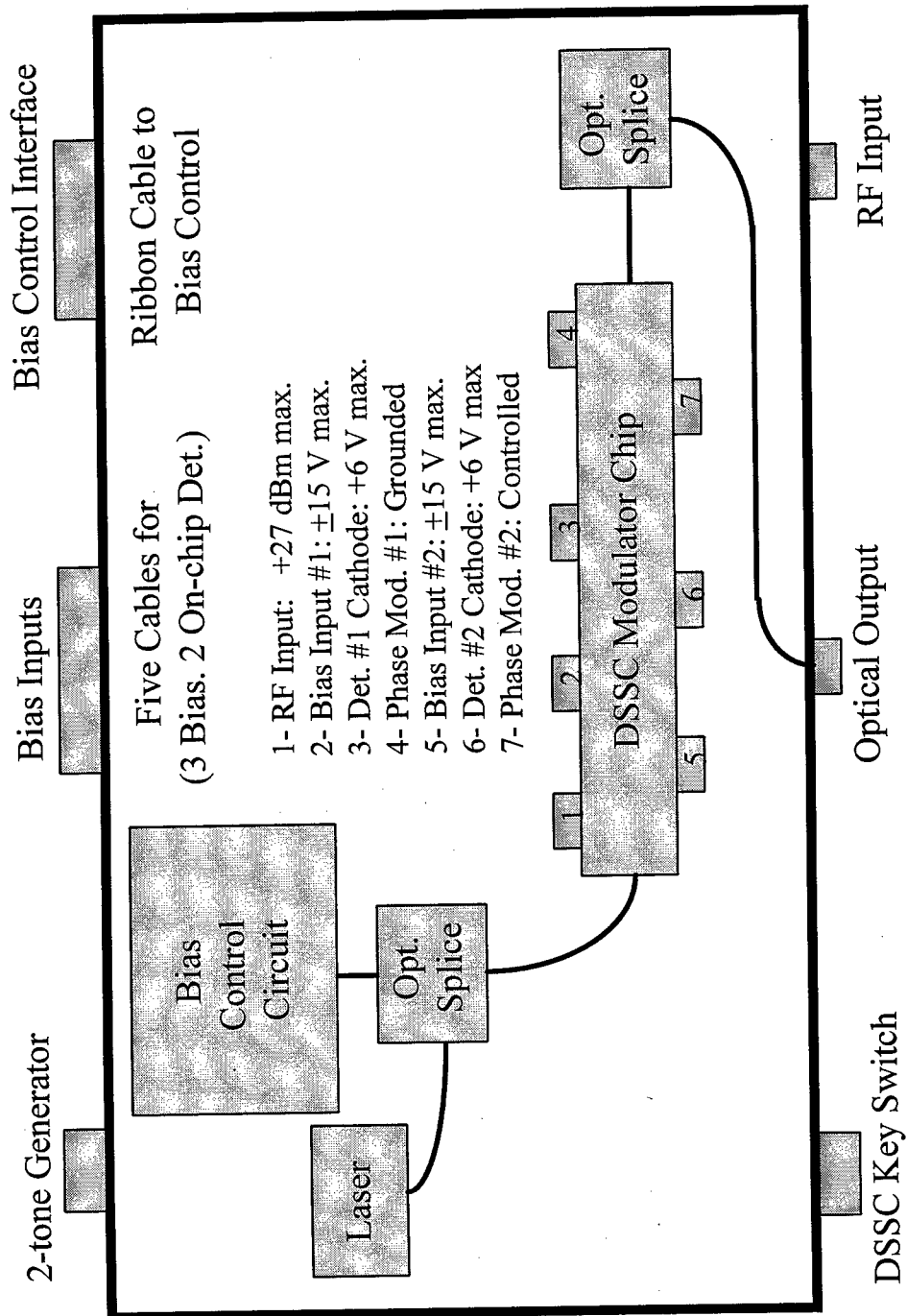
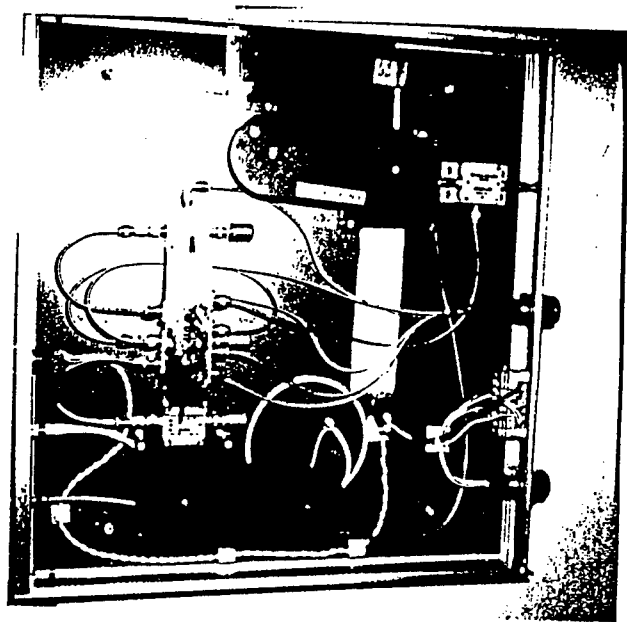
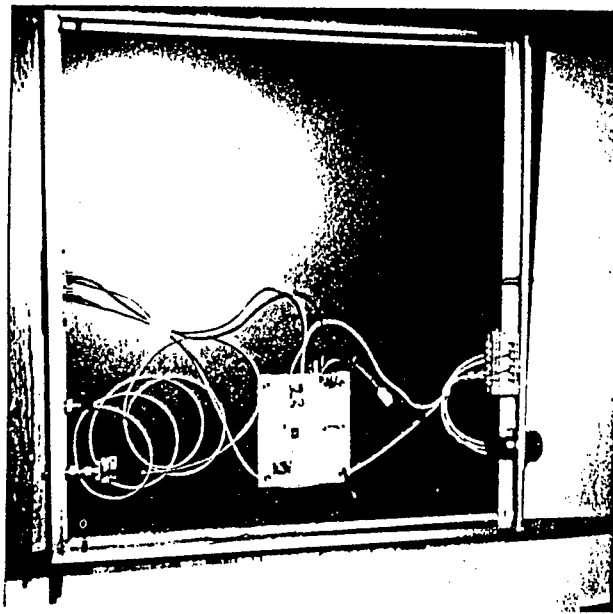


Figure A-1-8. Picture of the DSSC Modulator Hardware Layout: (a) Transmitter and (b) Receiver Units.



(A) DSSC Optical Modulator/Transmitter



(b) DSSC Optical Receiver

A-2. DSSC Link Operation Using Computer Control

This section provides a clear and concise documentation of the required procedure to control the DSSC biases using Labview software. The program and the subvi's developed are provided in diskettes. Also, detailed operating instructions for the DSSC link using Labview software is provided in **Section E, Appendix -II: DSSC Computer Control: Labview Instructions**. It should be noted that the DSSC modulator is a complex chip containing two Mach-Zehnder and two phase modulator sections, which requires biasing at the RF port as well as at the three other ports (V_{b1} , V_{b2} , and V_{p1} ; V_{p1} is set at zero volt). For third-order IMD minimization, these biases must be carefully controlled by using appropriate feedback/PLL circuits. An additional point to be made is that Lithium Niobate is known to be notoriously sensitive to charge build up and to thermal changes. These modulators operated without TEC tend to drift considerably at high RF drive condition. The DSSC chip developed under this program is not thermally stabilized; bias stabilization sensitivity is reliant totally on the capability of the feedback control circuit. Therefore, the DSSC bias control loop operated in *automatic control* mode was not very stable. We have often experienced considerable drift of the bias parameters (V_{b1} , V_{b2} , and V_{p2}) in a matter of half to an hour duration of the experiments. Surely, the third-order IMs are affected by this bias drift. However, there were a few occasions when the DSSC link behaved exceptionally well. In our tests at AEL, we only used the *automatic control* mode to establish the bias parameters *initially* and subsequently ran the DSSC unit in a *manual control* mode. This allowed maintaining the third-order IMDs within a reasonable limit (below -70-dBc).

In addition to controlling the operating bias points of the DSSC modulator chip at the third-order null, the Labview software developed is also capable of interfacing with various test equipment through GPIBs for data collection and reduction. It was therefore used to automatically run the optical transmission experiments and analyze the measured data for performance evaluation of the DSSC link. A full demonstration of the DSSC hardware included a presentation of the above performance, including bias stabilization for the third-order null and running the proposed experiments automatically.

B. DSSC Demo/Performance Testing

B-1.0 DSSC Test Plans

Specific experiments, test equipment and interface requirements are presented in this section. As noted in the attachments we planned to conduct tests on the linearity, spurious-free dynamic range (SFDR), noise figure, phase stability, phase noise, and thermal stability (see Figure B-1-0-1). As the DSSC modulator is integrated with the laser into the main unit, the logistic of conducting the thermal stability tests could not be supported. We have conducted all other tests as proposed (see Figure B-1-0-2). A list of test equipment used to perform these tests is provided in Figure B-1-0-3. We have also used AEL's sophisticated phase noise measurement set up to validate the low phase noise capability of externally modulated optical links powered by semiconductor lasers.

Figure B-1-0-1. DSSC Modulator Test Plan (Proposed).

Test Type	Opt. Power Level	Parameter RF Drive	Temp	Comment
*I/O Linearity	Fixed levels -Mid/High	Variable dr.	RT	*Nonlinearity due to -DSSC operation -PD saturation @ high power -Opt. amplifier
*TM, SFDR, NF -Two-tone -Multitone *Phase drift	Fixed levels -Low-High Mid	Variable dr. -Tones Variable	RT RT RT	*Functions of tones *lin. PD operation *Chirping of DSSC -RF dr. level, freq.
*Photorefrac. *Thermal stability	Variable Mid	Mid-High Mid-High	RT Variable	*Test to specificat. *Thermal cycling -Heat/cool rate -Holding time, -Atmosphere -No. of cycles

Figure B-1-0-2. DSSC Modulator Test Plan (Demonstration/Expt. Conducted).

- ◆ Setting up DSSC Modulator Control Loop and Stabilization Procedure
- ◆ Performance Test/Demo of 1550-nm DSSC Modulator Link at C-band with and without EDFA:
 - Two- and Three-tone IMDs
 - Linearity
 - SFDR
 - Noise Figure
 - Phase Noise
 - Phase Drift/Stability
 - Effect of High Incident Optical Power on Link Performance

Figure B-1-0-3. DSSC Modulator Test Equipment List.

- ◆ Performance tests conducted at C-band using test equipment:
 - RF Synthesizers (3)
 - Low-noise RF Amplifiers (3)
 - RF Isolators, Couplers, 90 Hybrids/Combiners, and Cables
 - Variable RF Attenuator (>30-dB range)
 - RF Power Meter
 - Variable Optical Attenuator (~ 20 to 30 dB)
 - Optical Couplers, Splitters (3)
 - Photodetector for Bias Control Loop
 - Fiber Patch Chords
 - RF Spectrum Analyzer
 - Noise Figure Test Set
 - RF Spectrum Analyzer
 - RF Network Analyzer
 - Optical Spectrum Analyzer

B-2.0 DSSC Test Configurations and Data

Multi-carrier tests were conducted to establish the SFDR of the DSSC link (see Figure B-2-0-1). In terms of channel spacing, the C-band carriers were spaced at small (10/15-MHz), medium (40 MHz), and large (100-MHz) intervals. Because of the RF couplers (~4.2-GHz) used in the DSSC hardware, the carriers were limited to 4.1-GHz. For the three tone tests, a third signal generator had to be used which was limited to 2.7 GHz. The three-tone tests were therefore conducted for carriers spaced 15-MHz apart at 2700, 2715, and 2730 MHz. These measurements were repeated as a function of optical power incident on the high frequency optical detector. Two detectors were used. One is a Lasertron photodetector, rated for 2-mW optical input power. Measurements at higher optical power levels were also conducted using Rome Laboratory-supplied ORTEL high power photodetector. The output of the EDFA was attenuated by a variable optical attenuator to appropriate levels. The ORTEL detector was rated for 10-15 mW power level. This detector was, however, more noisy, and ~17-dB less sensitive than the Lasertron device. Subsequently, we have noted a gradual degradation of the ORTEL detector performance. In our last measurements comparing the lasertron and ORTEL detectors, the sensitivity of the ORTEL detector was down by another 9 dB. Therefore, the advantages of using optical amplifier and high power photodetector to enhance the SFDR could not be clearly established. Later measurements on the DSSC were conducted using the built-in Lasertron detector.

Measurements of the DSSC link noise figure (NF), phase noise, and phase stability characteristics were performed with both unamplified and amplified optical signals. Specific test equipment and configurations of these experiments are shown in Figures B-2-0-2 (NF), B-2-0-3 and B-2-0-4 (phase noise), and B-2-0-5 (phase stability). The EDFA used for optical amplification was also tested in separate experiments.

The test data were analyzed and the SFDR estimated for the DSSC link operated under various test conditions. The results are presented in the following sections.

Figure B-2-0-1. Two-tone IM Test Configuration: DSSC Link with EDFA. Three-tone Testing, Requires a Third Tone.

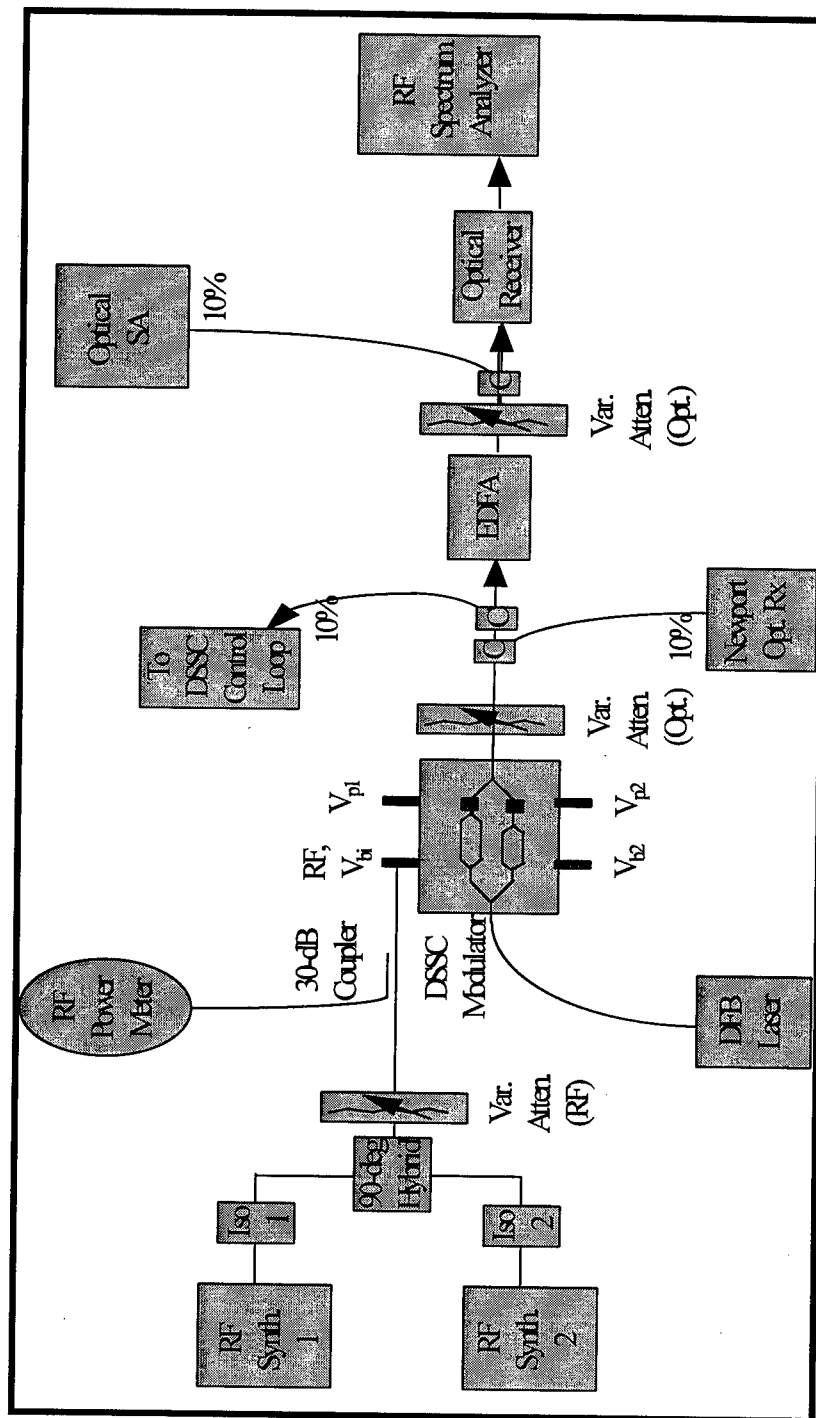


Figure B-2-0-2. Noise Figure Test Configuration.

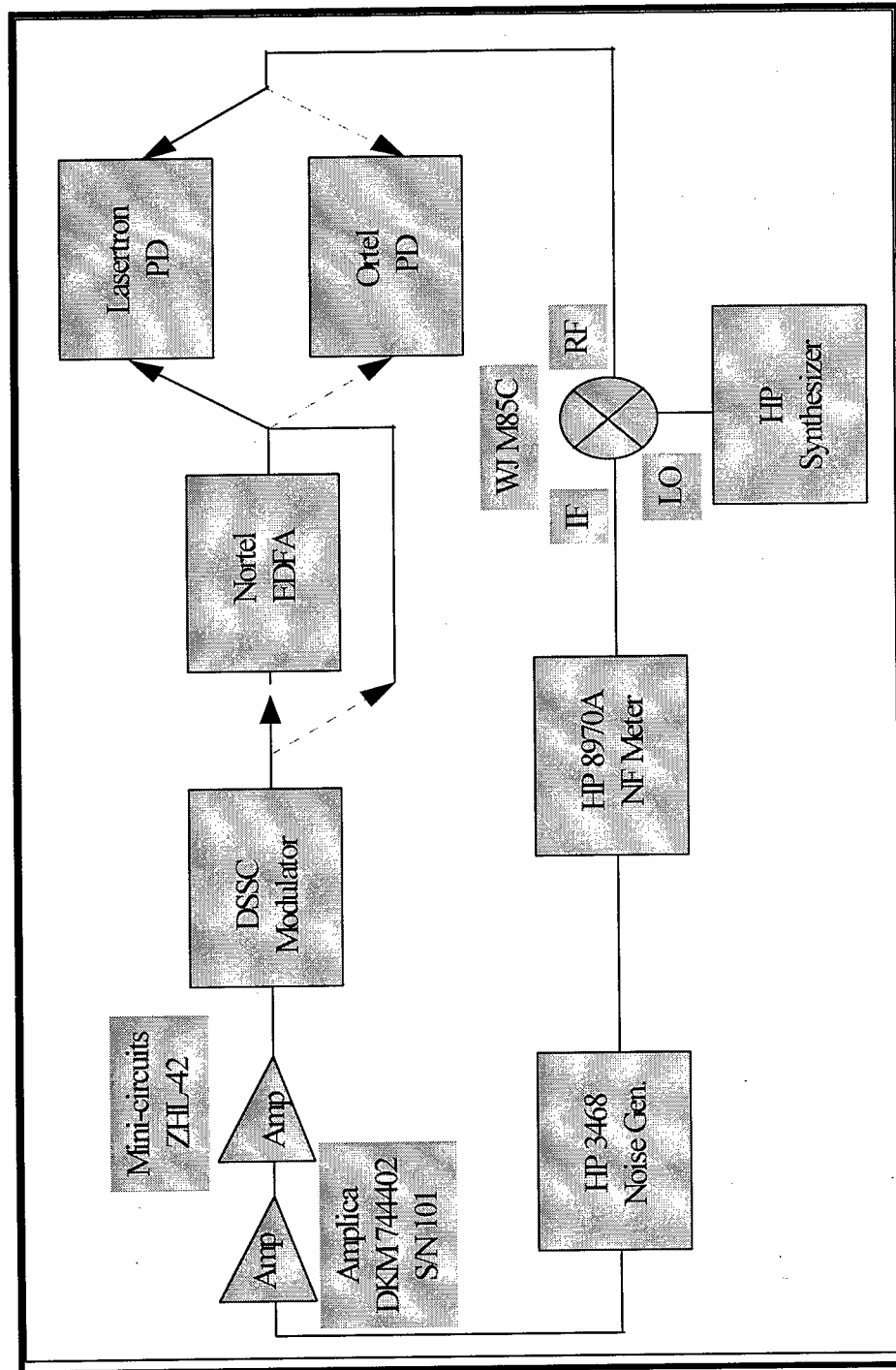


Figure B-2-0-3. Phase-Noise Test Setup and Accessories at AEL.

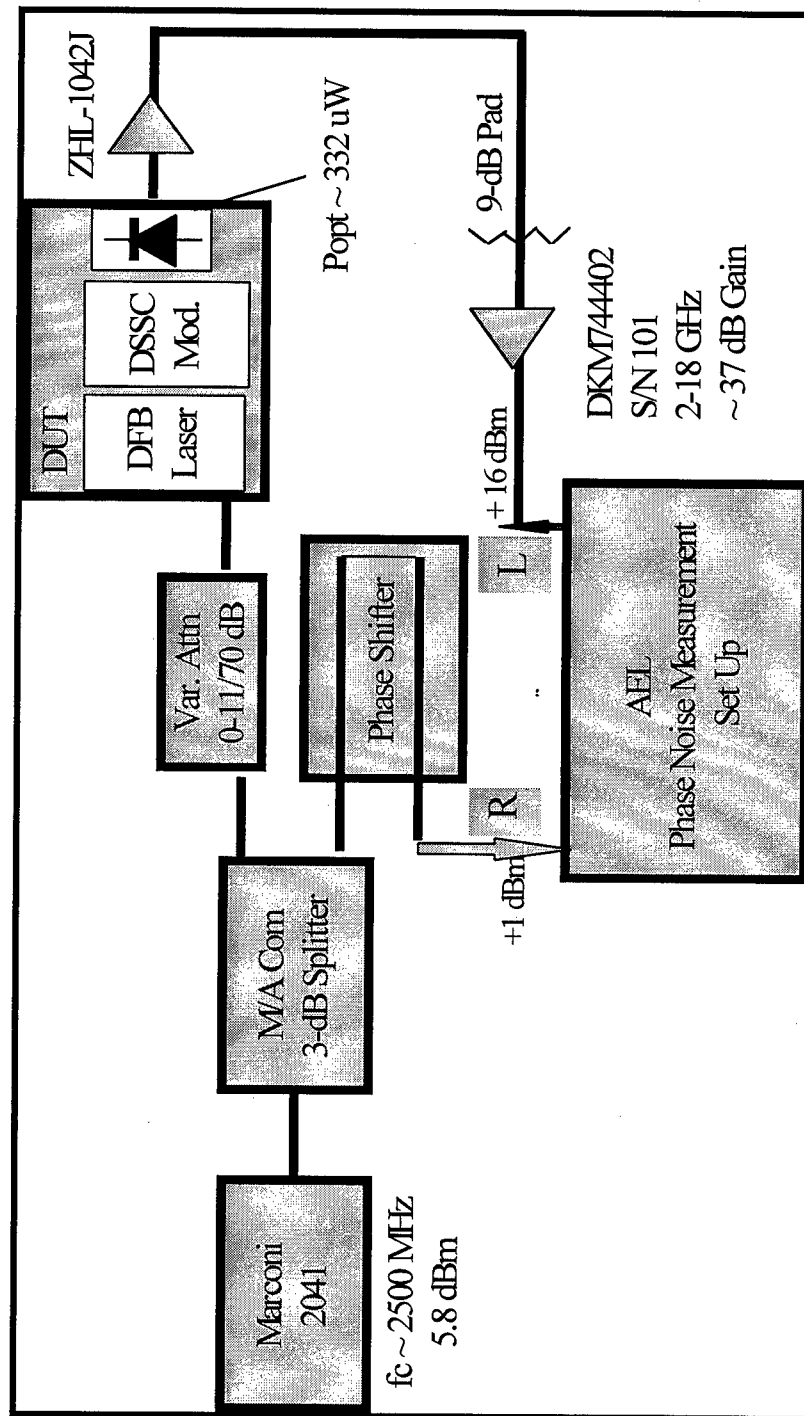
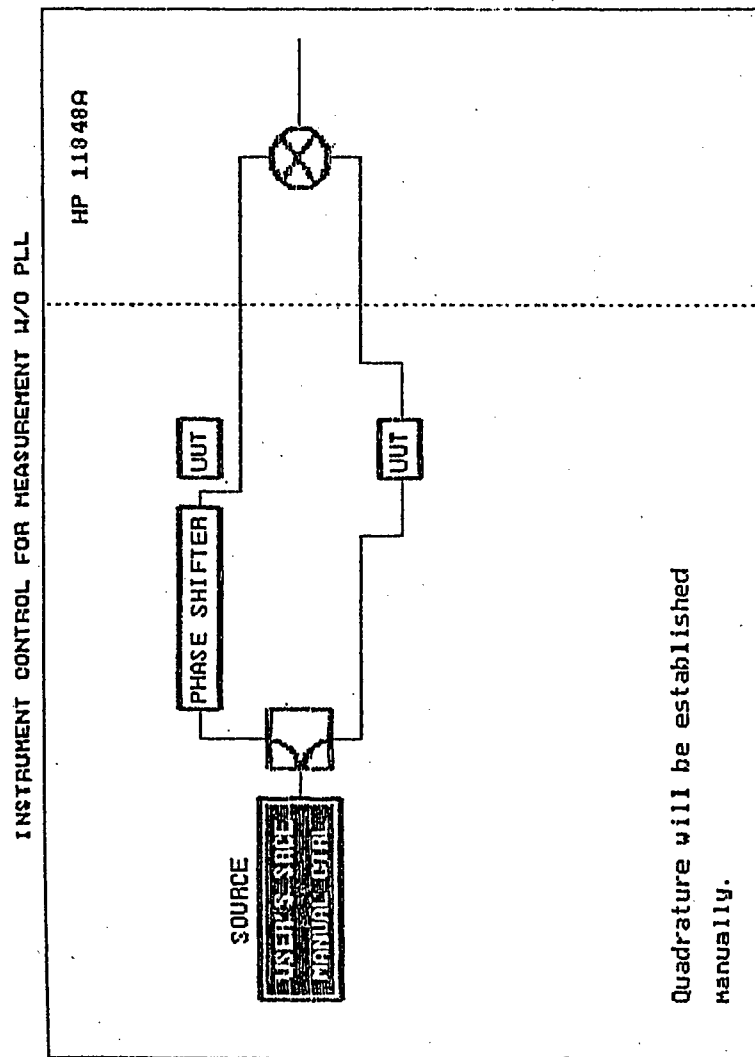
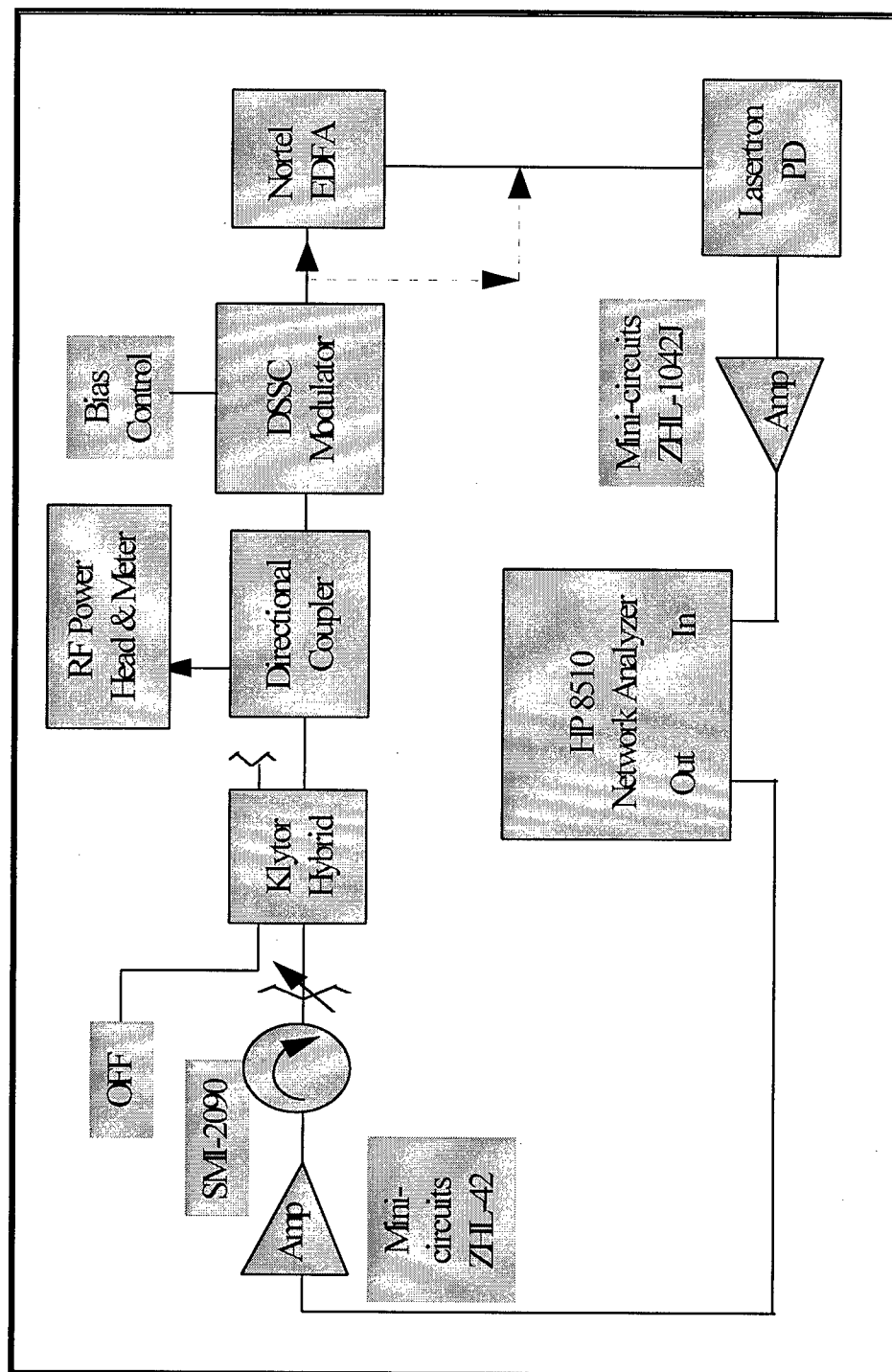


Figure B-2-0-4. AEL Phase-Noise Test Setup: Automated Configuration Control.



F1- System/Manual Control

Figure B-2-0-5. Phase Stability Test Configuration.



B-2.1 Multicarrier Performance

Systems related performance criteria such as transmission linearity, harmonics, intermodulation distortion (IMD), spur-free dynamic range (SFDR), input/output intercept points (IIP, OIP), etc. are determined by the nonlinearity of the components/subsystems constituting the link. Multicarrier transmission tests are specifically designed to address these characteristics. At AEL, we have focused on making these tests at high GHz frequencies compatible with the DSSC hardware. These measurements were done primarily at 2 to 4 GHz with a few tests at ~ 1 GHz. The schematic used for the multicarrier testing included low-noise, stable, clean synthesizers, RF power combiner and variable attenuator, isolators, power meter and sensor head, various optical patch cables, couplers, variable attenuator, power meters and spectrum analyzer (OSA) as well as RF spectrum analyzer. A series of tests were conducted using two and three carriers variously spaced at 10, 15, 40, and 100 MHz apart. The tests were conducted for both optically amplified (with EDFA after the DSSC modulator) as well as unamplified (w/o EDFA) links set at different optical detector power levels. Careful measurements were made of the input RF drive to the DSSC modulator and the corresponding output signals at the fundamental, and higher harmonics and IMDs (second and third order). Representative data are given in Figures B-2-1-1 through B-2-1-4. The measured data was analyzed to determine the link gain (loss), OIP3 (third-order intercept point), the noise output power, and finally, the SFDR (see figure B-2-1-5). An accurate estimation of the noise floor requires evaluation of the various noise components arising from thermal, shot, and laser RIN effects (see Figure B-2-1-6). The analysis used has considered parameters relevant to the DSSC hardware and the experimental conditions. An EDFA can be useful provided it is operated in saturation mode (otherwise, the noise will increase substantially). However, optical amplifier introduces an additional noise such as ASE to the link performance. Figure B-2-1-7 shows the optical spectra of the DSSC/EDFA link as measured in an Optical Spectrum Analyzer (OSA). A summary of the link performance is given in Table B-2-1-1.

For the DSSC link tested at AEL, we have typically 0.5 mA current on the photodetector and measured ~ 60 -dB link loss (includes the post detection amplifier gain used before the RF spectrum analyzer). The NF of the link is thus high, ~ 65 -75 dB. IM performance of the DSSC link is presented in Table B-2-1-2. The estimated SFDRs range between low-90s to 110 dB/Hz^{2/3}. We do observe enhanced performance with increased optical power incident on the photodetector; both the link gain is increased and the noise figure is reduced. The analytical results presented in this section highlights the impact of RIN noise and photodetector noise on the link performance. A compromise of achievable link loss and the laser RIN noise in combination with the incident optical power on the photodetector can yield a better performance.

The maximum SFDR achievable in a 1550-nm DFB laser/DSSC link was analyzed at AEL (detailed analysis and results are presented in a following section) to show that for a RIN of -165 dBm/Hz and 1 mA detector current on matched 50-ohm load, the SFDR is limited to 115 dB/Hz^{2/3}. Our best data thus far, as assessed from an exhaustive testing with close attention given to experimental and analytical details, is ~ 110 dB/Hz^{2/3}. In our experience with the DSSC modulator, we found it extremely hard to maintain a third-order null for any reasonable length of time (more than couple of hours). There are several underlying mechanisms such as temperature and bias dependent materials characteristics typical of lithium niobate ferroelectric material, device architecture and fabrication, and feed electrode arrangement to cause such nonlinearity.

Figure B-2-1-1. Two-tone IMD Test Data Measured at C-band, 15-MHz Channel Spacing; DSSC Link w/o EDFA.

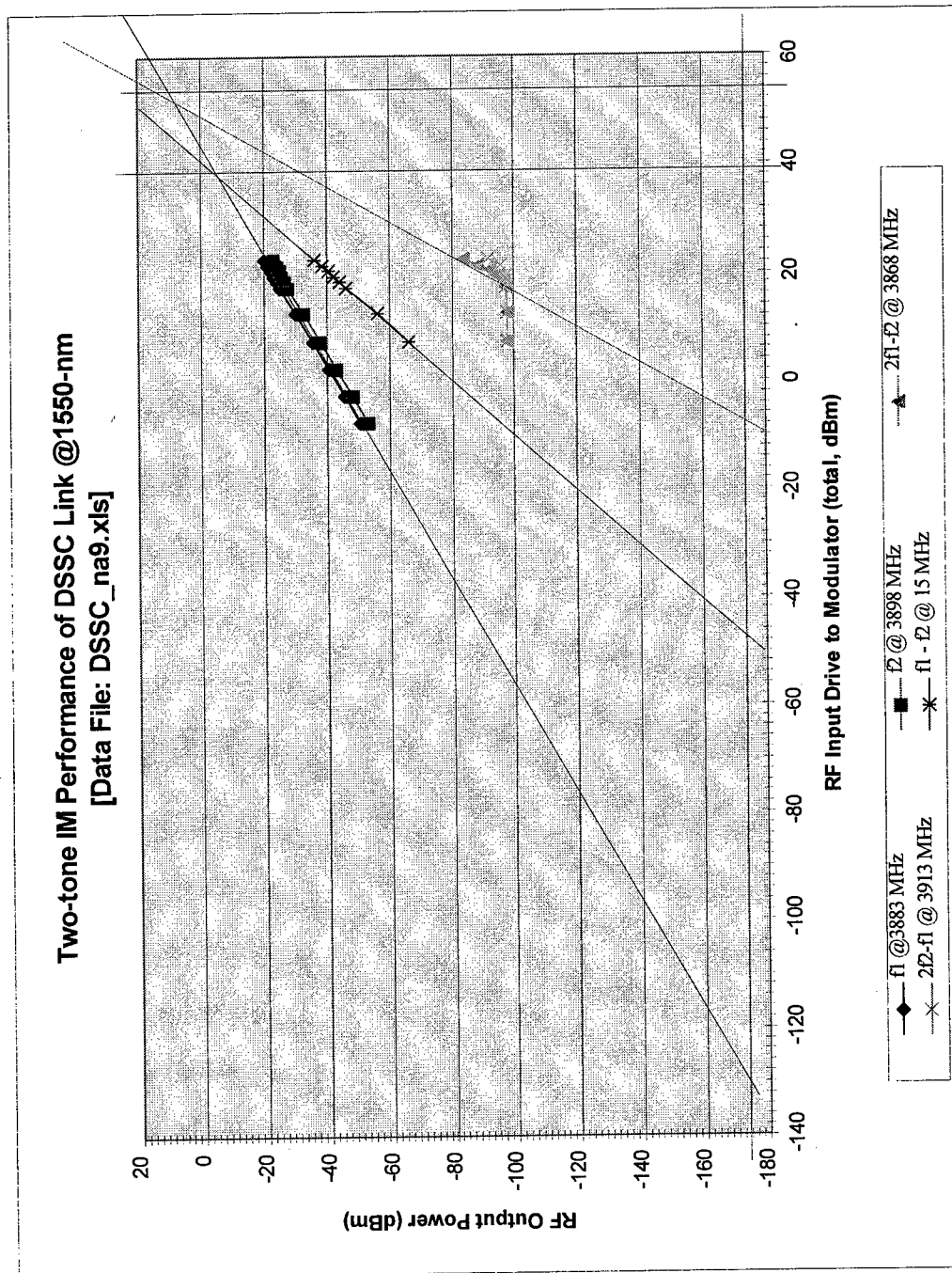


Figure B-2-1-2. RF Output Signals Measured by the Spectrum Analyzer [HP8563E]: Carriers, Harmonics, and IMs (for three tones set at 2.7, 2.715, and 2.73 GHz with 15 MHz spacing).

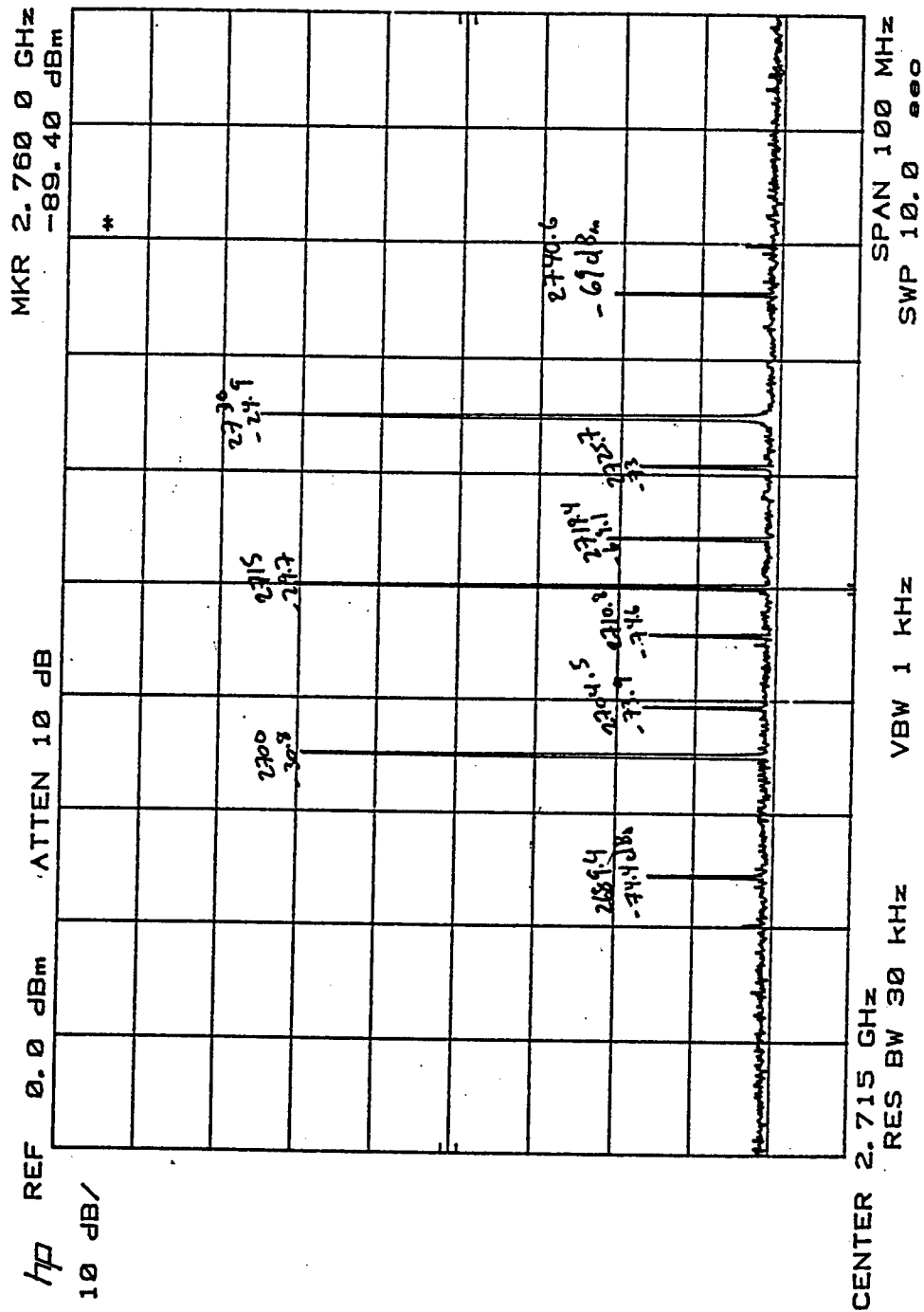


Figure B-2-1-3a. Reduction of the third-order IM by DSSC Bias Control at S-band [Third-order IM, 2f3-f1 @ 2.76 GHz].

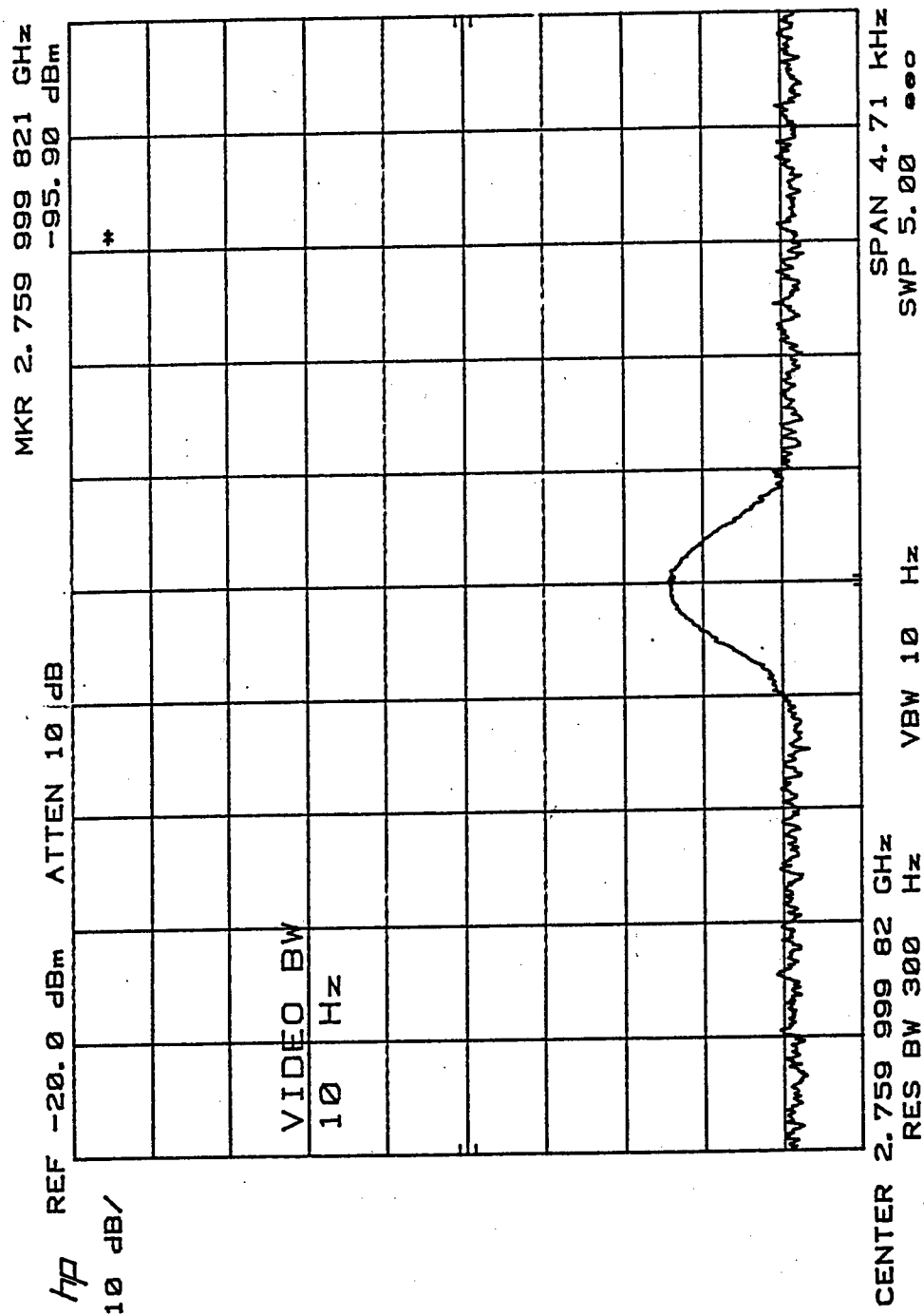


Figure B-2-1-4a. Multicarrier IM Products of the DSSC Modulator: Three-tone Tests at S-band [DSSC Modulator w/o EDFA, three tones set @ ~2.7 GHz, 15-MHz apart; input optical power level- low (0.474 mW)].

3 Tone IM Products with DSSC mod. and Lasertron PD(474 uW)

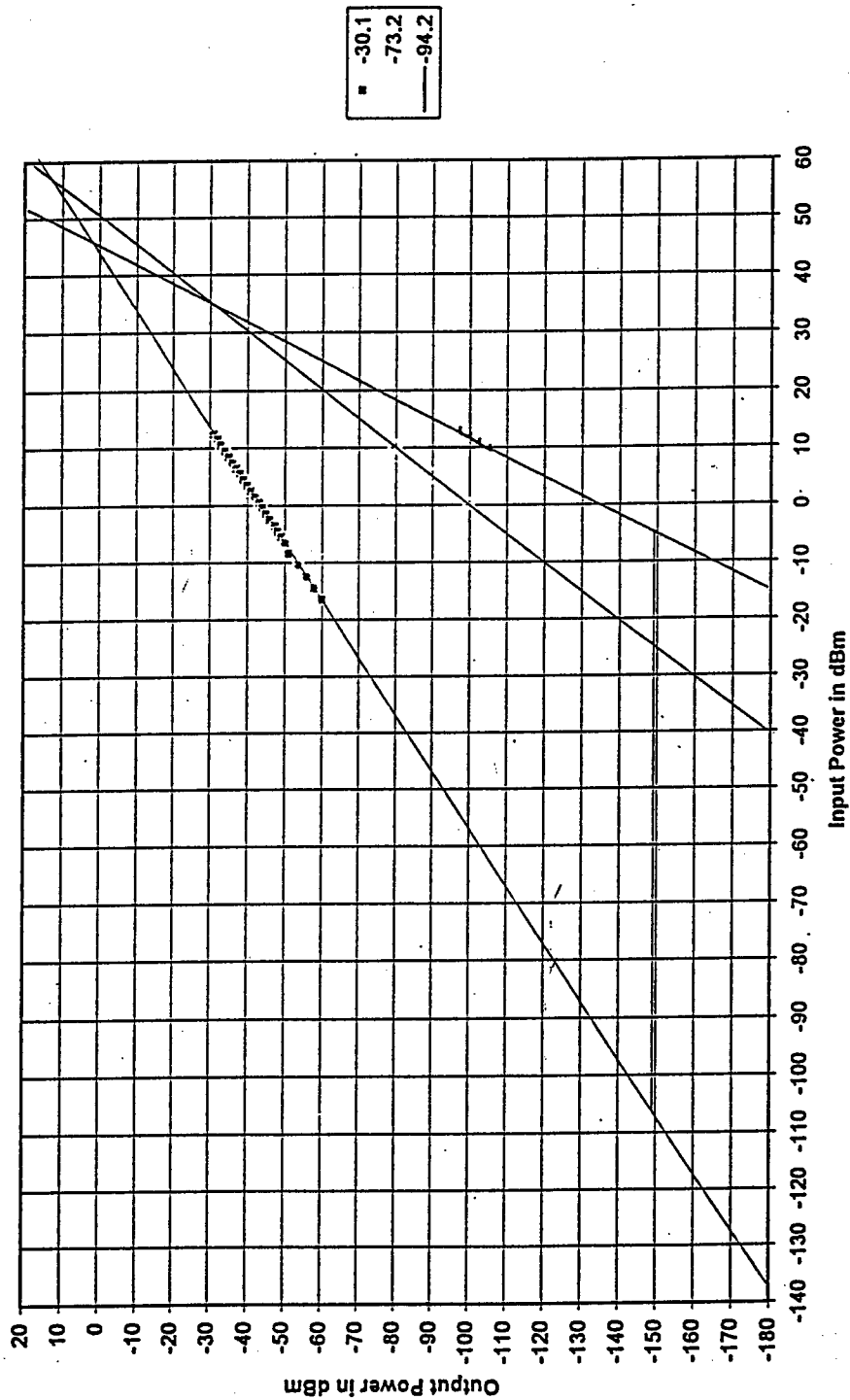


Figure B-2-1-4b. Multicarrier IM Products of the DSSC Modulator: Three-tone Tests at S-band [DSSC Modulator w/EDFA and Lasertron PD, three tones set @ ~ 2.7 GHz, 15-MHz apart; input optical power level- medium (0.95 mW)].

3 Tone IM Products w/ DSSC mod., w/EDFA, w/ Opt. Attn., and Lasertron PD (0.95 mW)

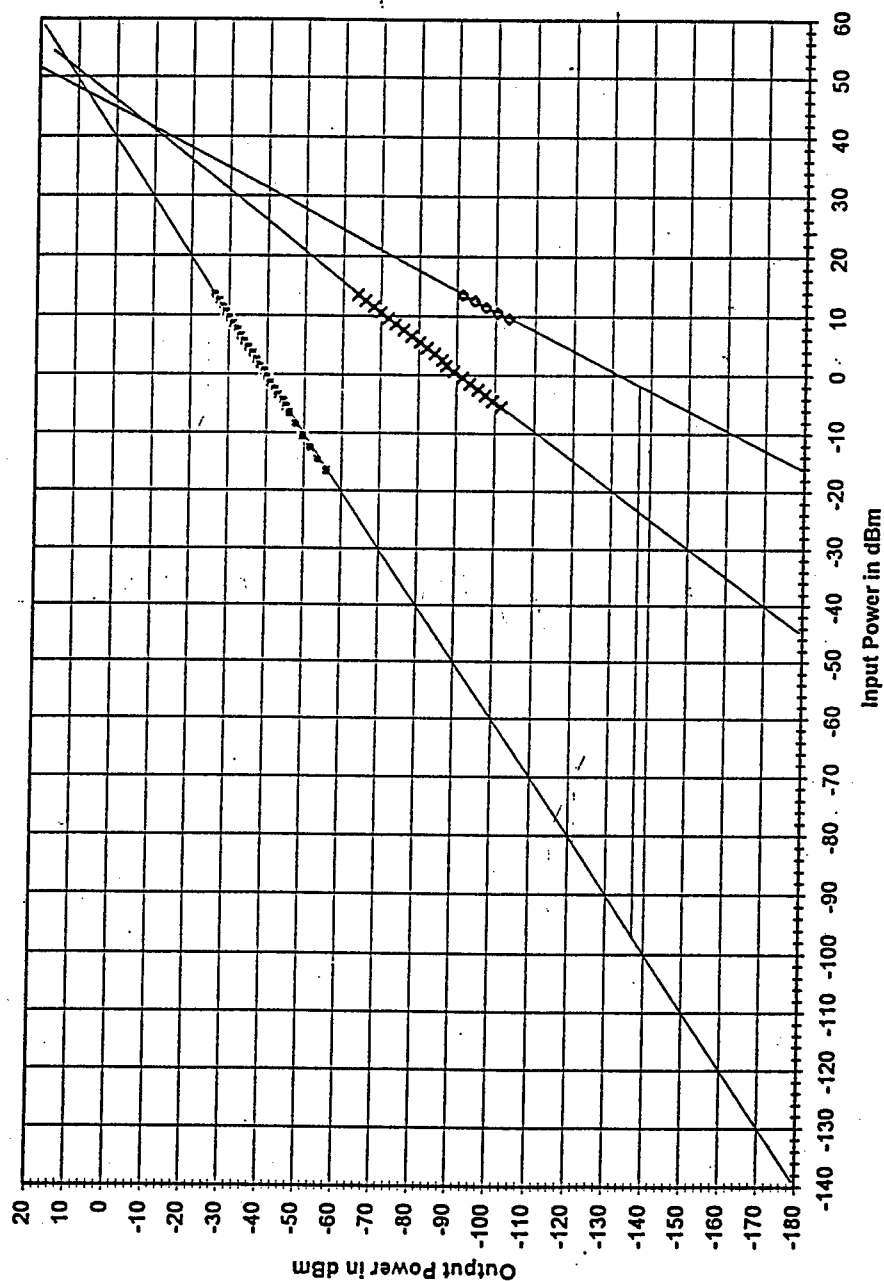


Figure B-2-1-4c. Multicarrier IM Products of the DSSC Modulator: Three-tone Tests at S-band [DSSC Modulator w/EDFA and Lasertron PD, three tones set @ ~ 2.7 GHz, 15-MHz apart; input optical power level- high (1.9 mW)].

3 Tone IM Products w/ DSSC mod., w/ EDFA, Opt. Attn., and Lasertron PD (1.9mw)

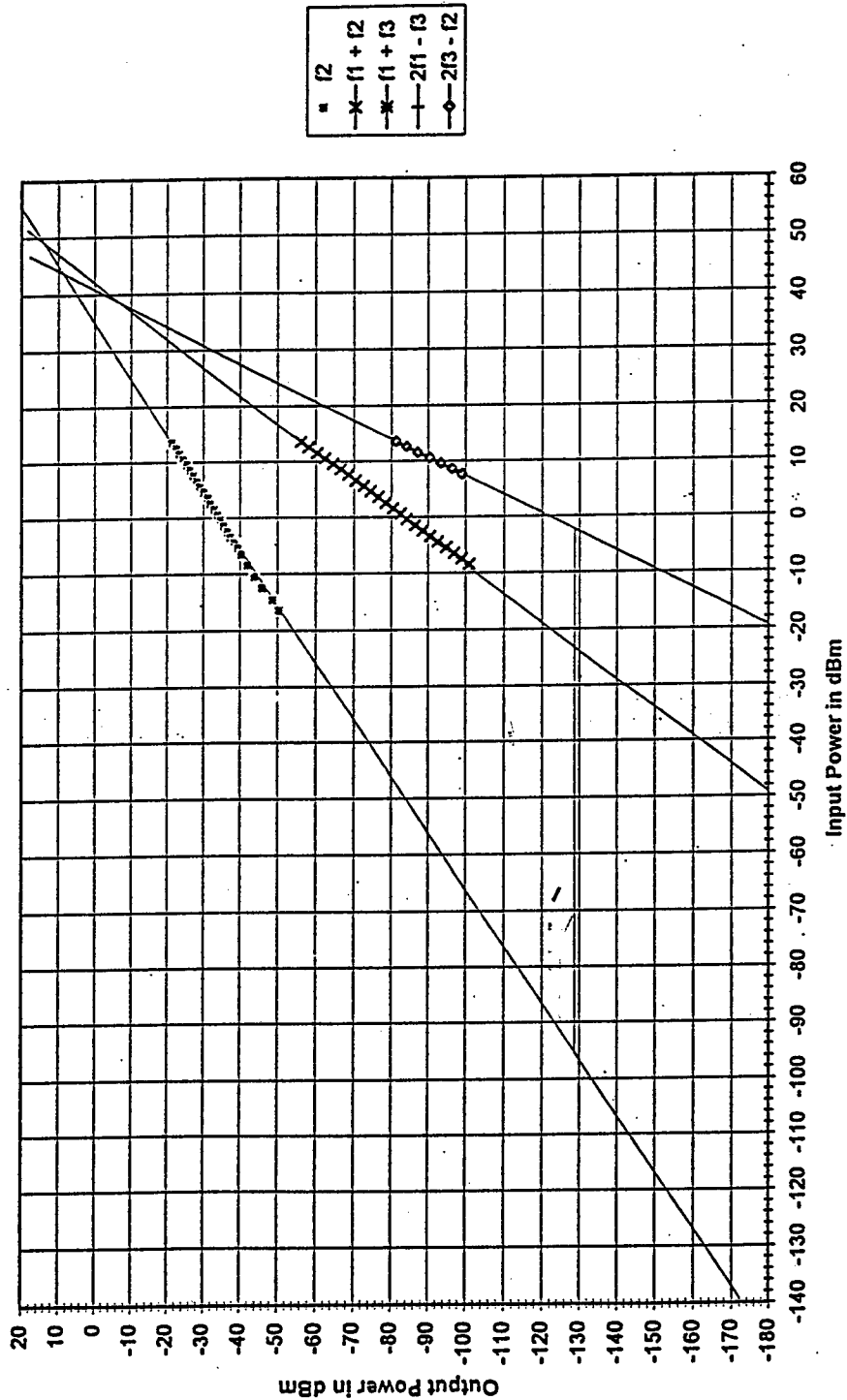


Figure B-2-1-5. Dynamic Range (DR) Estimation from the Measured IM Data of an Analog Link.

Analog Link Performance Measures

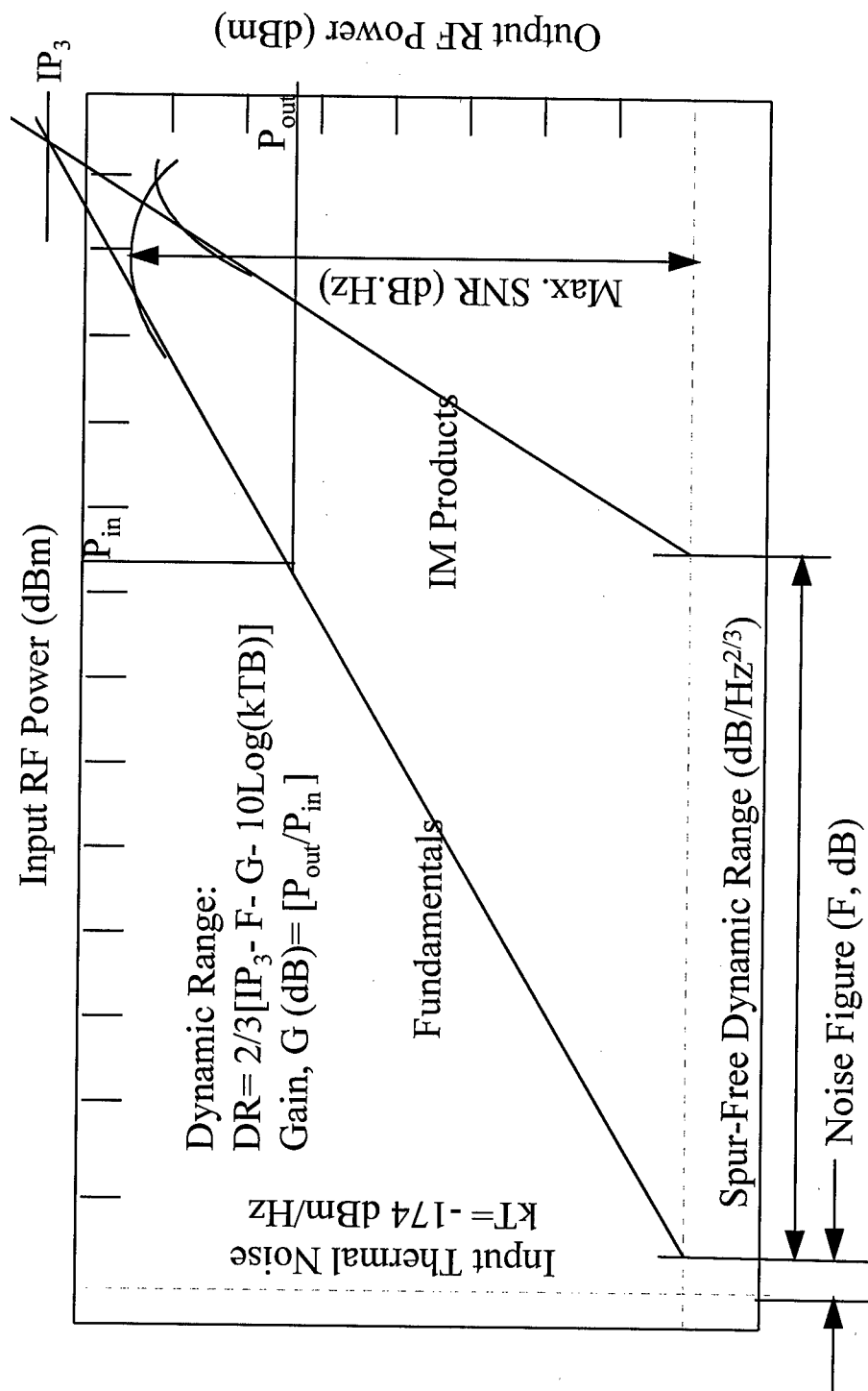


Figure B-2-1-6a. Performance Analysis of Externally Modulated Optically Preamplified Direct Detection Analog Link: Optical Hardware Configuration.

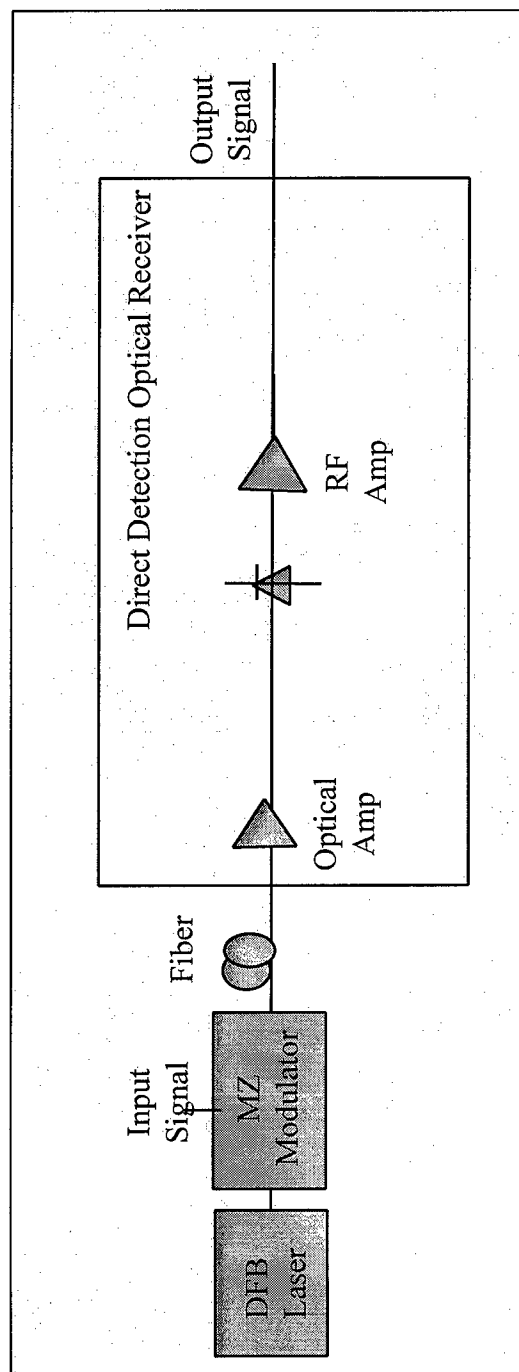


Figure B-2-1-6b. Performance Analysis of Externally Modulated Optically Pre-amplified Direct Detection Analog Link: Effect of Link Gain/Loss on Noise Figure; RIN @ -160 dB/Hz.

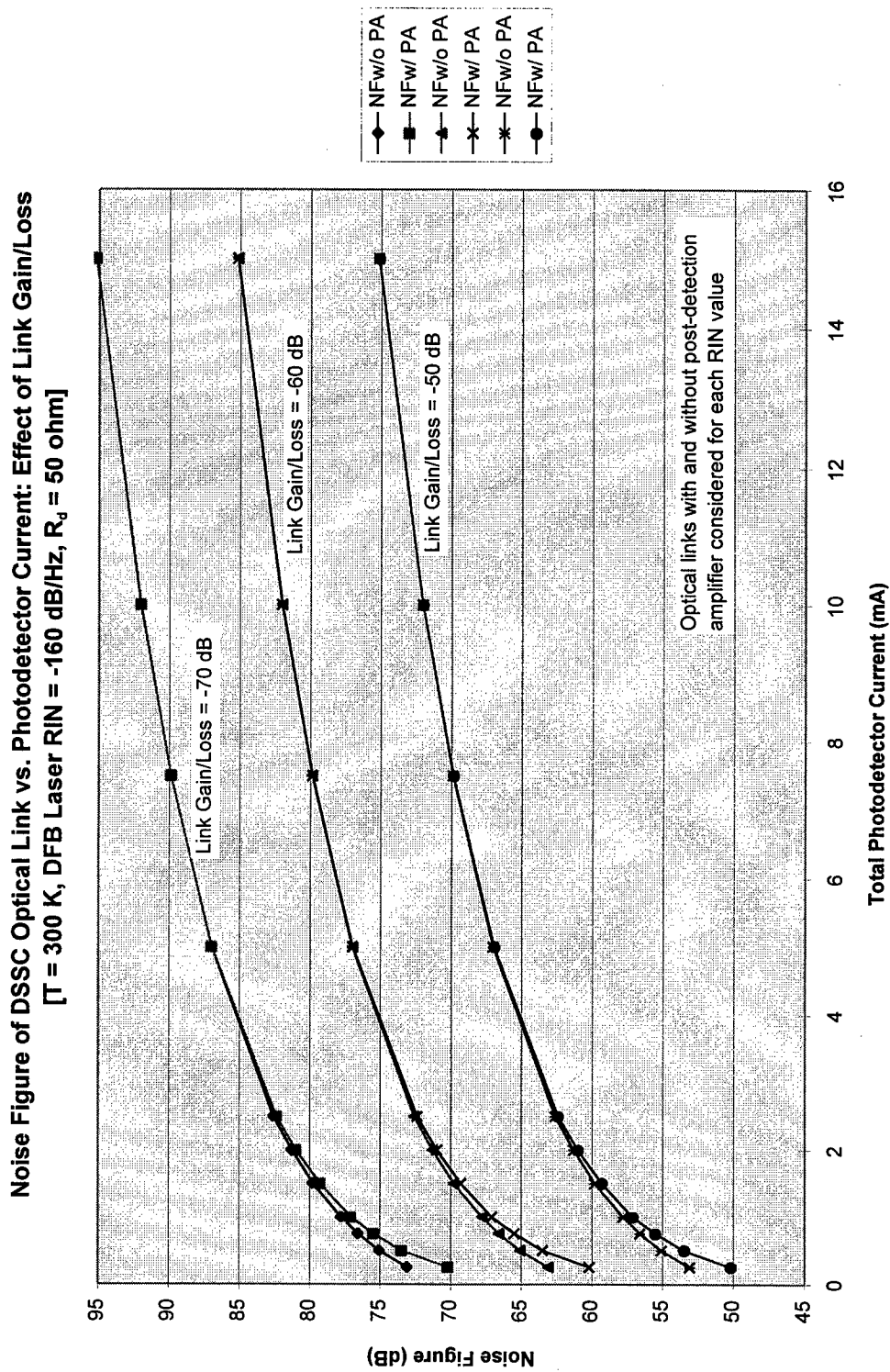


Figure B-2-1-6c. Performance Analysis of Externally Modulated Optically Preamplified Direct Detection Analog Link: Effect of Laser RIN on Noise Figure; Link Gain/Loss @ -60 dB.

Noise Figure of DSSC Optical Link vs. Photodetector Current: Effect of Laser RIN
 $[T = 300 \text{ K, Link Gain/Loss} = -60 \text{ dB, } R_d = 50 \text{ ohm}]$

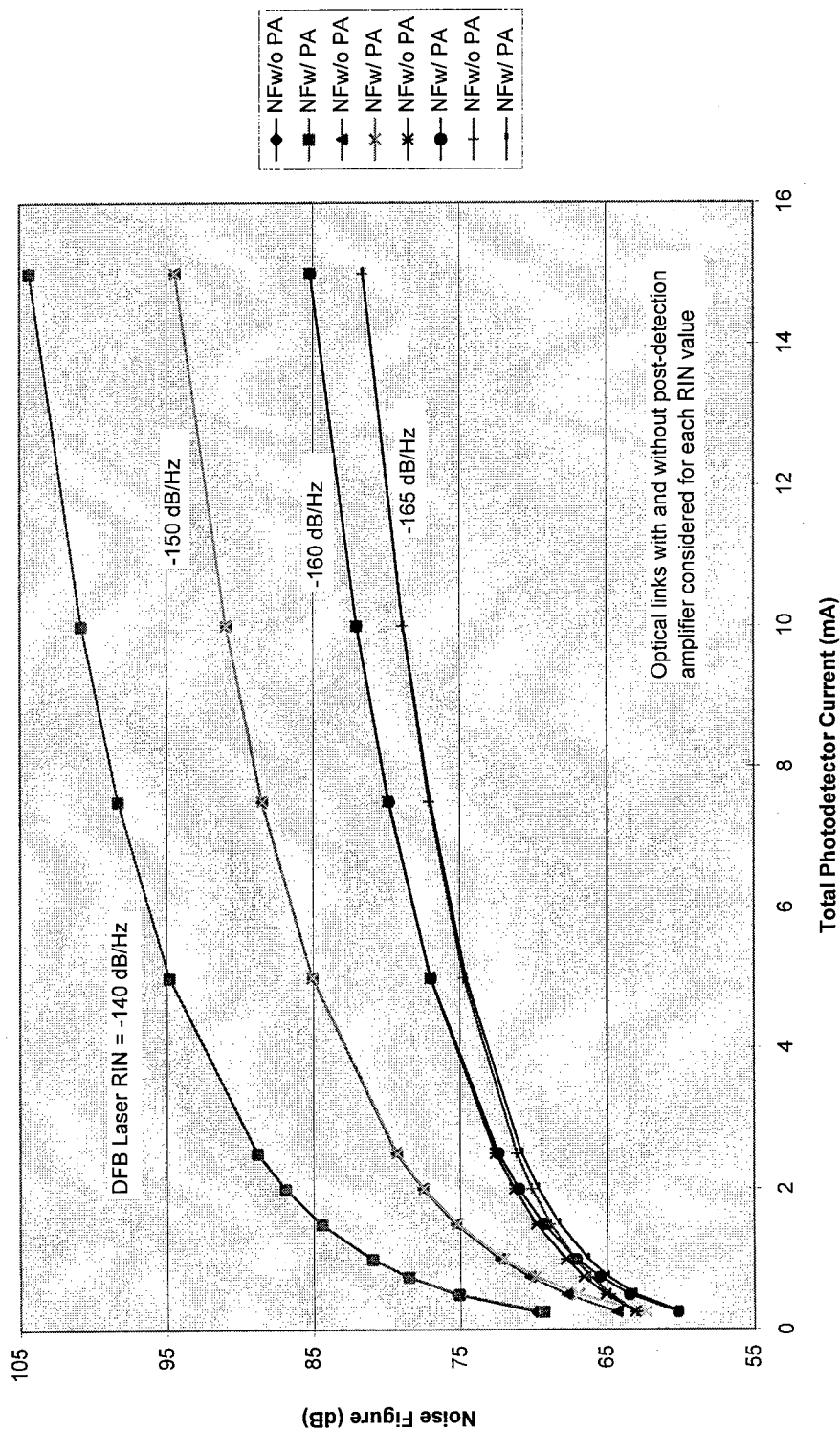


Figure B-2-1-7a. DSSC/EDFA Link: EDFA Output Measured by Optical Spectrum Analyzer; Input Optical Power Level : Low; 20-dB In-line Optical Pad to OSA

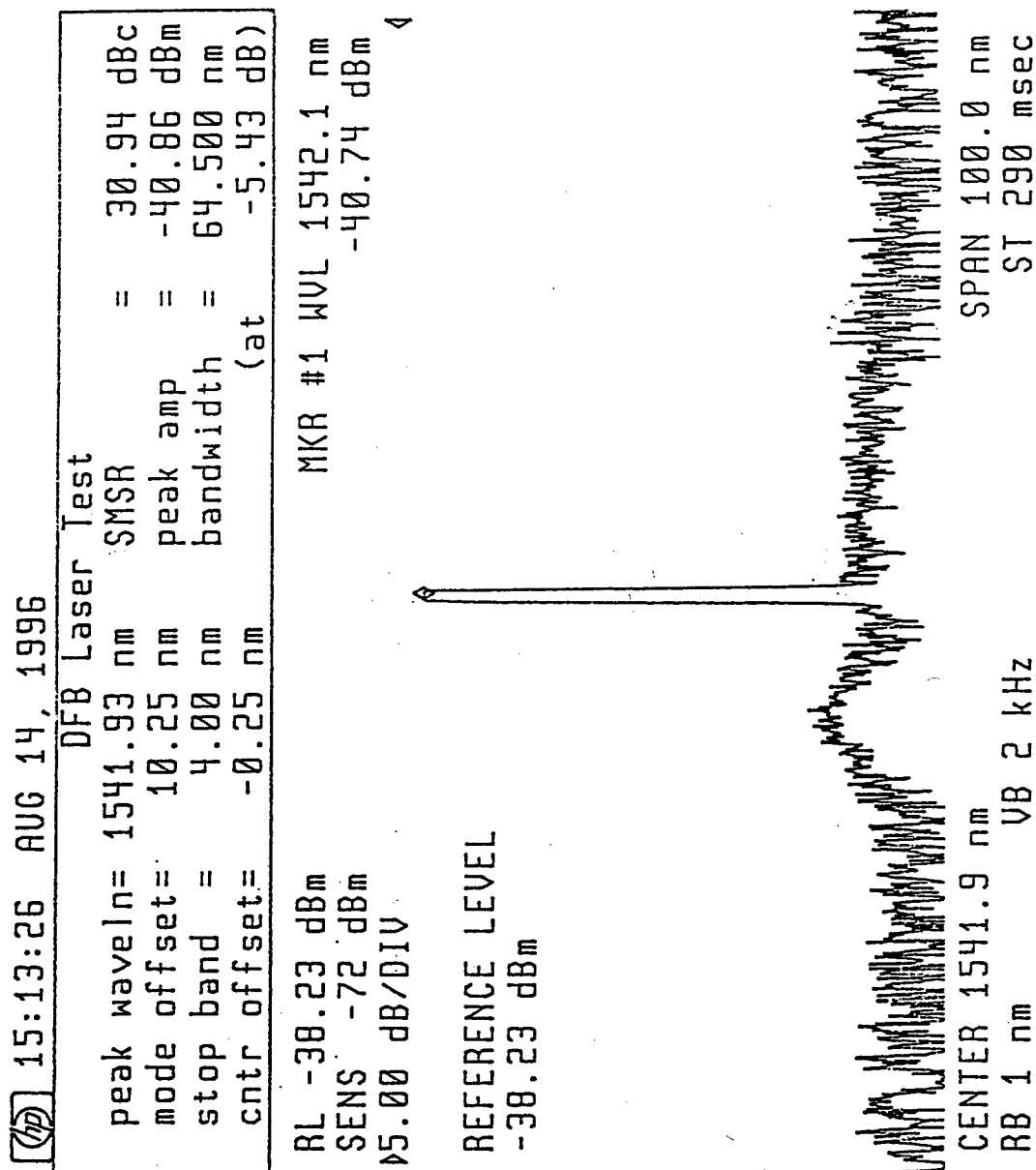


Figure B-2-1-7b. DSSC/EDFA Link: EDFA Output Measured by OSA; Input Optical Power Level : Medium; 10-dB Optical Pad Plus Variable Attenuator to OSA

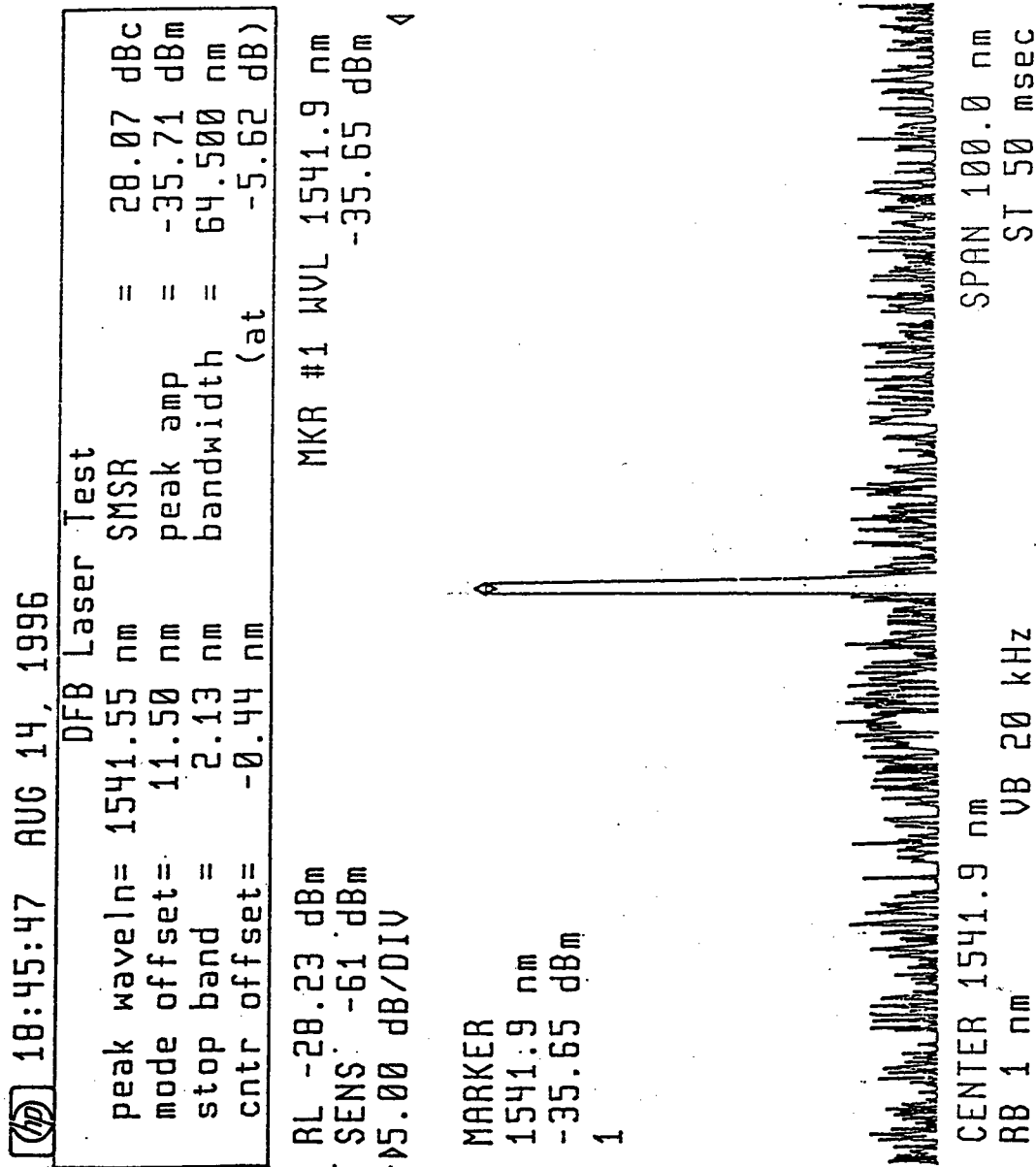


Figure B-2-1-7c. DSSC/EDFA Link : EDFA Output Measured by Optical Spectrum Analyzer; Input Optical Power Level : High; 15-dB In-line Optical Pad to OSA

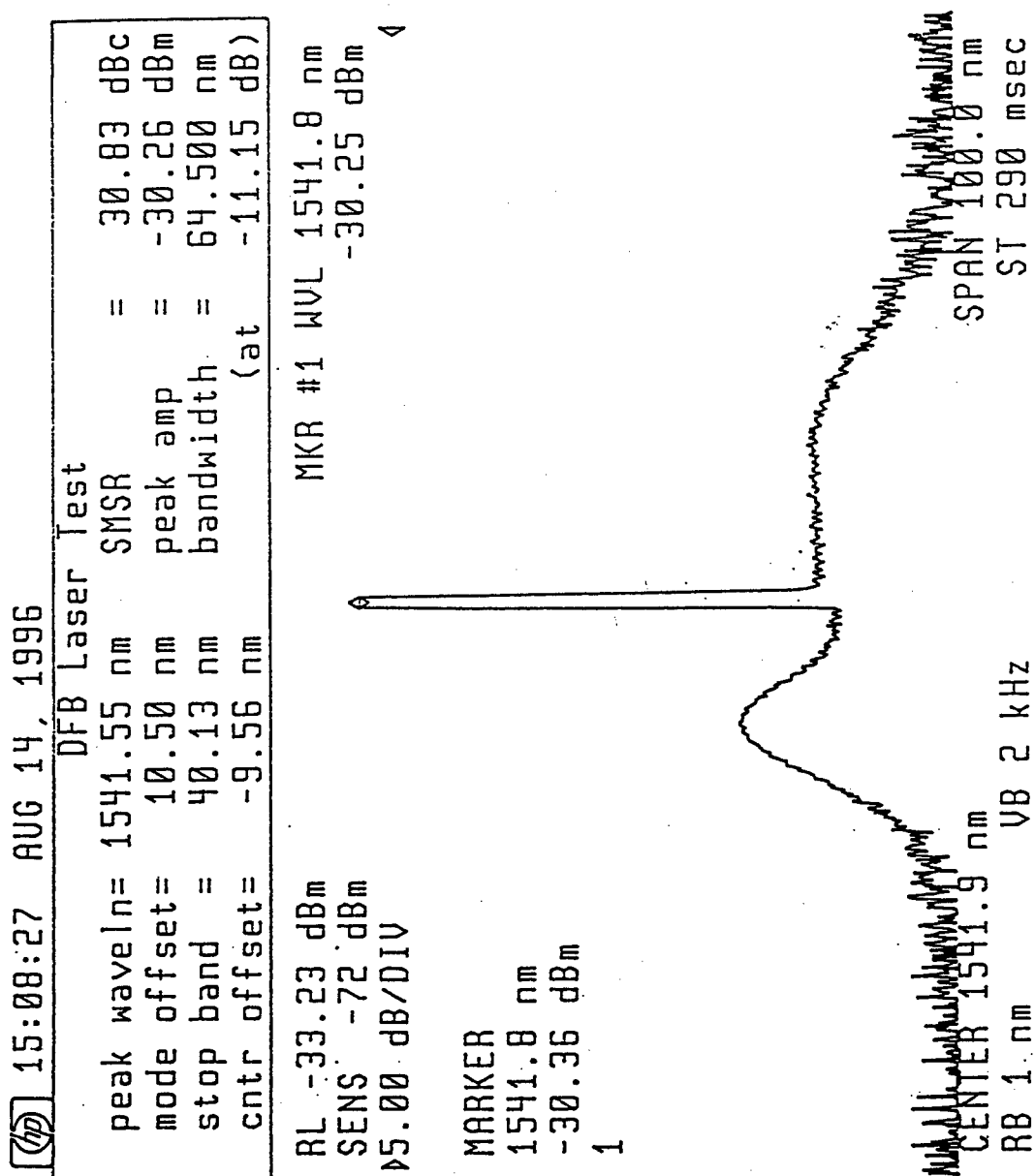


Table B-2-1-1. DSSC Performance Tests Using Optical Spectrum Analyzer (OSA)

Run #	Experiment Condition	Spectral Features
# 1	◆ 1550-nm DFB Laser Off	◆ Very Broad Spectra in a 80-nm band (basically gain spectrum w/double hump excited in the EDFA by the 980-nm pump laser)
	◆ Variable Optical Attenuator set at Maximum	◆ Broad peak @ 1531 nm, -61.5 dBm
		◆ Noise Floor @ -81 dBm
	◆ 1550 nm DFB Laser On with DSSC Mod. in the link	◆ 1541.6 nm line peaks ~ -56.96 dBm
# 2	◆ Variable Optical Attenuator set at Maximum	◆ SMSR ~ 6.04 dBc
		◆ Noise Floor @ -80 dBm
	◆ 1550 nm DFB Laser On with DSSC Mod. in the link	◆ 1541.9 nm line grows, peak ~ -47.8 dBm
	◆ Variable Optical Attenuator set at Minimum	◆ SMSR ~ 31.56 dBc
# 3		◆ Noise Floor @ -80 dBm
	◆ 1550 nm DFB Laser On with DSSC Mod. in the link	◆ 1541.9 nm line grows, peak @ ~ 66.85 dBm
	◆ Variable Optical Attenuator set at Minimum	◆ SMSR ~ 13.68 dBc
		◆ Noise Floor @ -80 dBm
# 4	◆ 1550 nm DFB Laser On with DSSC Mod. in the link	
	for 2-tone Test: Carriers at 4.00 and 4.01 GHz, total RF input drive to DSSC @ 5.31 dBm	
	◆ Variable Optical Attenuator set at Minimum	

Note: For Runs 1 through 3, the OSA was fed directly from the EDFA. A fixed optical pad (~ 10-dB rating @ 1300 nm) was used to limit the optical input to the OSA. DSSC bias stabilization achieved through internal tones and feedback loop.

Table B-2-1-2. IM Performance of the DSSC Modulator Link.

[Note: SFDRs are adjusted for the post-detection amplification used ; ~26 dB @ 1-2 GHz and ~22 dB @ 3-4 GHz; Figure B-2-1-6a]

Data File	Description	Opt. Power on PD (mW)	Id (A)	Link Gain/Loss (dB)	RF Drive (dBm)	f1 (dBm)	f3 (dBm)	IMD (dBc)	OIP3 (dBm)	Noutput (dBm/Hz)	SFDR (dB/Hz ^{2/3})
DSSC_NA_1	1.1/1.2 GHz, 100-MHz sp.	0.396	3.56E-04	-39.03	0.53	-38.50	-104.00	65.50	-6	-172.30	93.70
DSSC_NA_2	4/3.9 GHz, 100-MHz sp.	0.101	9.09E-05	-58.30	17.13	-41.17	-94.00	52.83	-15	-173.44	91.13
DSSC_NA_3	4/3.99 GHz, 10-MHz sp.	0.075	6.75E-05	-60.29	20.62	-39.67	-84.00	44.33	-18	-173.54	89.36
DSSC_NA-3 R	4/3.99 GHz, 10-MHz sp.	0.454	4.09E-04	-43.30	14.80	-28.50	-104.00	75.50	9	-172.08	106.22
DSSC_NA_4	4/3.96 GHz, 40-MHz sp.	0.513	4.62E-04	-45.42	16.92	-28.50	-104.00	75.50	9	-171.86	106.07
DSSC_NA-4 R	4/3.96 GHz, 40-MHz sp.	0.513	4.62E-04	-45.42	16.92	-28.50	-104.00	75.50	9	-171.86	106.07
DSSC_NA_5	1.1/1.2 GHz, 100-MHz sp.	0.685	6.17E-04	-39.01	0.51	-38.50	-104.00	65.50	-6	-171.22	92.98
DSSC_NA_5R	1.1/1.2 GHz, 100-MHz sp.	0.513	4.62E-04	-46.31	15.48	-30.83	-104.50	73.67	6	-171.86	101.24
DSSC_NA_6/6B	4/4.01 GHz, 10-MHz sp.	0.768	6.91E-04	-43.30	14.80	-28.50	-103.50	75.00	9	-170.92	105.28
DSSC_NA_6A	4/4.01 GHz, 10-MHz sp.	0.435	3.92E-04	-44.04	14.24	-29.80	-104.00	74.20	7	-172.15	104.97
DSSC_NA_7	4/4.1 GHz, 100-MHz sp.	0.734	6.61E-04	-45.42	16.92	-28.50	-104.00	75.50	9	-171.04	105.53
DSSC_NA_8A	4/4.04 GHz, 40-MHz sp.	0.6	5.40E-04	-46.02	18.52	-27.50	-104.50	77.00	11	-171.53	107.02
DSSC_NA_9	3883/3898 MHz, 15-MHz sp., w/EDFA adjusted to same opt. power level as w/o EDFA	0.3	2.70E-04	-26.21	-7.69	-33.90	-98.00	64.10	-2	-172.67	99.22
DSSC_NM_1	3883/3898 MHz, 15-MHz sp., w/EDFA adjusted to same opt. power level as w/o EDFA	0.396	3.56E-04	-46.25	6.35	-39.90	-98.00	58.10	-11	-172.30	92.97
DSSC_NM_2	3883/3898 MHz, 15-MHz sp., w/EDFA, opt. power level adjusted	2.05	1.85E-03	-38.41	11.21	-27.20	-98.00	70.80	8	-166.98	102.12
DSSC_NM_3	3883/3898 MHz, 15-MHz sp., w/EDFA, opt. power level adjusted	1	9.00E-04	-37.54	15.34	-22.20	-94.00	71.80	14	-170.10	107.87
DSSC_OA_1	4/4.01 GHz, 10-MHz sp., w/o EDFA	0.396	3.56E-04	-43.30	14.80	-28.50	-103.50	75.00	9	-172.30	106.20
DSSC_OA_10	3883/3898 MHz, 15-MHz sp., high opt. power	2	1.80E-03	-26.21	7.31	-18.90	-96.10	77.20	20	-167.11	109.88
DSSC_OA_2	4/4.01 GHz, 10-MHz sp.	0.4	3.60E-04	-47.30	18.10	-29.20	-99.50	70.30	6	-172.29	104.16

B-2.2 Noise Performance of DSSC Modulator

Amplitude and phase noise characteristics of the DSSC modulator link were measured using the test equipment shown in Figures B-2-0-2 through B-2-0-4. Because of interests in MW/MMW optical transmission and distribution of signals, these measurements were conducted at high frequencies (2-4 GHz). The 4-GHz limitation was imposed by the built-in RF combiner used in the DSSC unit. The amplitude noise figure test configuration (Figure B-2-0-2) uses a conventional set up consisting of a noise generator (HP 3468), a noise figure meter (HP 8970A), a low-noise mixer and LO synthesizer, the DUT and other accessories (high gain low-noise preamplifiers). The mixer stage was needed to down-convert the high GHz signals to 1.5 GHz capability of the noise meter. Also, a high gain, low-noise preamplification of the RF input signal to the modulator was necessary to keep the measured NF data within the range (~ 15 dB) of the test set up. These tests were conducted using both Ortel (high power, 10-12 mW, provided by the Rome Lab.) and the built-in Lasertron (lower power, ~ 2 mW) photodetectors. Four test configurations were employed:

- Config. 1: DSSC modulator and Lasertron PD
- Config. 2: DSSC modulator and Ortel PD
- Config. 3: DSSC Modulator plus EDFA and Lasertron PD
- Config. 4: DSSC modulator plus EDFA and Ortel PD

These tests allowed making a comparison of the photodetectors and also characterizing the DSSC noise performance under both amplified and unamplified conditions. These results are included in this subsection. The DSSC link gain and NF data measured using Lasertron and Ortel PDs at various input optical power levels are shown in Figures B-2-2-1 through B-2-2-4. Note that for the link gain and NF test configuration used (see Figure B-2-0-2), the DUT includes a substantial preamplification (~ 71 dB total from two LNAs in cascade, the first LNA with 39.5 dB gain and 3.6 dB NF followed by a second LNA with 31.5 dB gain and 9 dB NF) of the Noise Generator signal driving the EO modulator. In these measurements, however, there was no post-detection amplification required. To estimate the true gain/loss in the DSSC modulator, the measured gain data (as shown in Figures B-2-2-1 and B-2-2-2) must therefore be corrected by the LNA gain. As expected, the noise figure is reduced and the link gain enhanced with increased optical power to the modulator. By using Frii's formula for the cascaded gain stages, the true noise figure of the DSSC modulator chip was determined from the test data taken over a range of 3-4 GHz. Typical NF values ranged between 60-70 dB. Effect of higher optical power on the NF and a comparison of the two detectors are shown in these figures. We found the Ortel detector less sensitive

Table B-2-1-2. IM Performance of the DSSC Modulator Link (Continued).

[Note: SFDRs are adjusted for the post-detection amplification used ; ~26 dB @ 1-2 GHz and ~22 dB @ 3-4 GHz; Figure B-2-1-6a]

DSSC_OA_3	4/4.01 GHz, 10-MHz sp.	0.355	3.20E-04	-48.84	17.34	-31.50	-98.50	67.00	2	-172.46	101.64
DSSC_OA_4	4/4.01 GHz, 10-MHz sp.	1.02	9.18E-04	-38.97	17.37	-21.60	-89.00	67.40	12	-170.04	106.76
DSSC_OA_5	4/4.01 GHz, 10-MHz sp.	1.41	1.27E-03	-37.68	17.38	-20.30	-97.00	76.70	18	-168.78	109.89
DSSC_OA_6	3883/3898 MHz, 15-MHz sp., w/EDFA, opt. power level adjusted	0.85	7.65E-04	-37.29	3.39	-33.90	-98.00	64.10	-2	-170.62	97.85
DSSC_OA_7	3883/3898 MHz, 15-MHz sp., opt. power varied	0.513	4.62E-04	-37.55	12.45	-25.10	-93.50	68.40	9	-171.86	105.97
DSSC_OA_8	3883/3898 MHz, 15-MHz sp., medium opt. power	1.04	9.36E-04	-31.61	7.41	-24.20	-97.00	72.80	12	-169.97	106.78
DSSC_OA_9	3883/3898 MHz, 15-MHz sp., high opt. power	1.5	1.35E-03	-28.73	7.43	-21.30	-97.00	75.70	17	-168.51	108.71
DSSC_IT_1	3-tone test, ~2.7 GHz	0.474	4.27E-04	-43.50	10.00	-33.50	-106.00	72.50	3	-172.01	101.84
DSSC_IT_2	3-tone test, ~2.7 GHz	1.95	1.76E-03	-31.50	7.50	-24.00	-100.00	76.00	14	-167.24	106.16
DSSC_IT_3	3-tone test, ~2.7 GHz	0.95	8.55E-04	-40.00	10.00	-30.00	-104.50	74.50	7	-170.27	103.68

(by ~ 17 dB initially) than the Lasertron detector (see Table B-2-2-1). Also, we noted severe performance degradation (by another 9 dB) during our use at AEL. A report on the subject matter is provided in Table B-2-2-2.

The phase noise data were taken in two different test configurations:

- A sophisticated phase noise test set up with capabilities of establishing a low-noise reference phase and using methods to cancel out most unwanted phase changes commonly encountered in the simpler techniques. The test set up is automated.
- On the other hand, an RF spectrum analyzer with phase-noise test accessories (available in HP 8563E) can provide a quick and reasonable estimate of the phase-noise.

The results presented in Figures B-2-2-5 through B-2-2-9 were taken using both configurations. The measurements were repeated several times for the DSSC link both with and without the EDFA. Also, the sensitivity of the test setup only was determined from a test conducted without the DSSC link. It was observed that the internal pilot tones (@ 872 and 882.7 MHz) of the DSSC bias control circuit produced phase jitters. Therefore, a set of measurements were taken with the pilot tones turned off. Note that the DSSC modulator chip operated under this condition could easily drift from its third-order IM null. The measured phase noise of the 1550-nm DFB laser/DSSC link is less than -125 dBc/Hz for frequencies up to ~ 1 MHz. We have measured a 10 to 15 dB better performance in 1310-nm Nd:YAG laser/lithium niobate modulator links. It should be noted that those links were operated at much higher optical power levels, ~ 100 mW and higher. For the DFB laser used, the RJN is higher and the optical power is much too weak compared with the Nd:YAG laser.

Figure B-2-2-1. DSSC Link Gain and Noise Figure Measured Using Lasertron PD at Various Input Optical Power Levels.

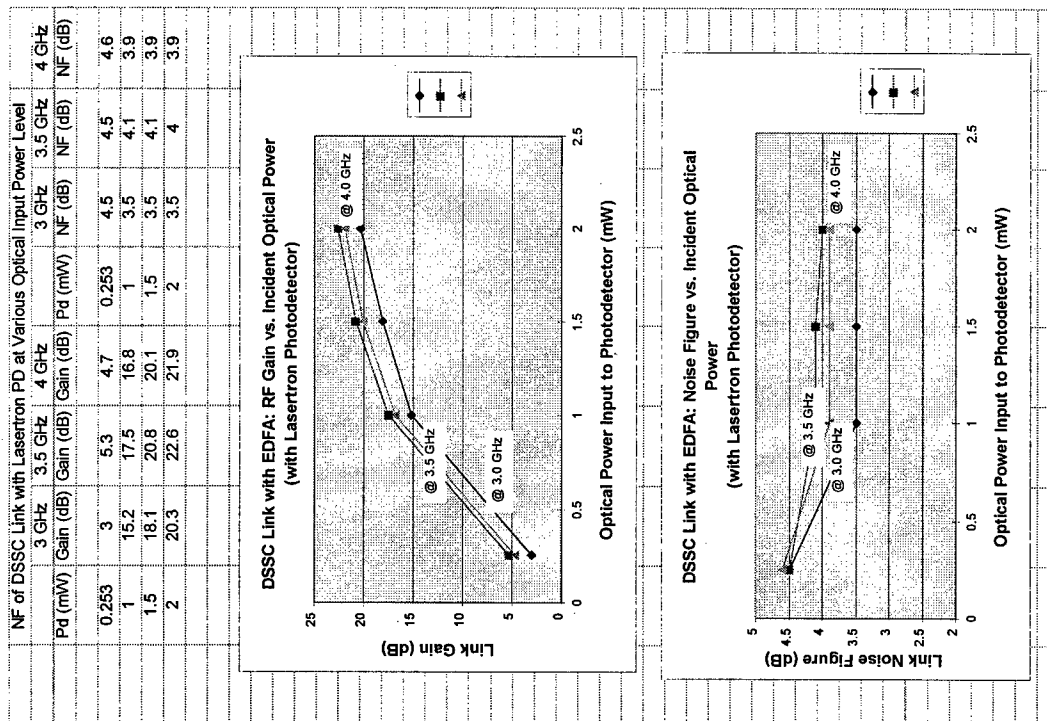


Figure B-2-2-2. DSSC Link Gain and Noise Figure Data Measured Using Ortel PDs at Various Input Optical Power Levels.

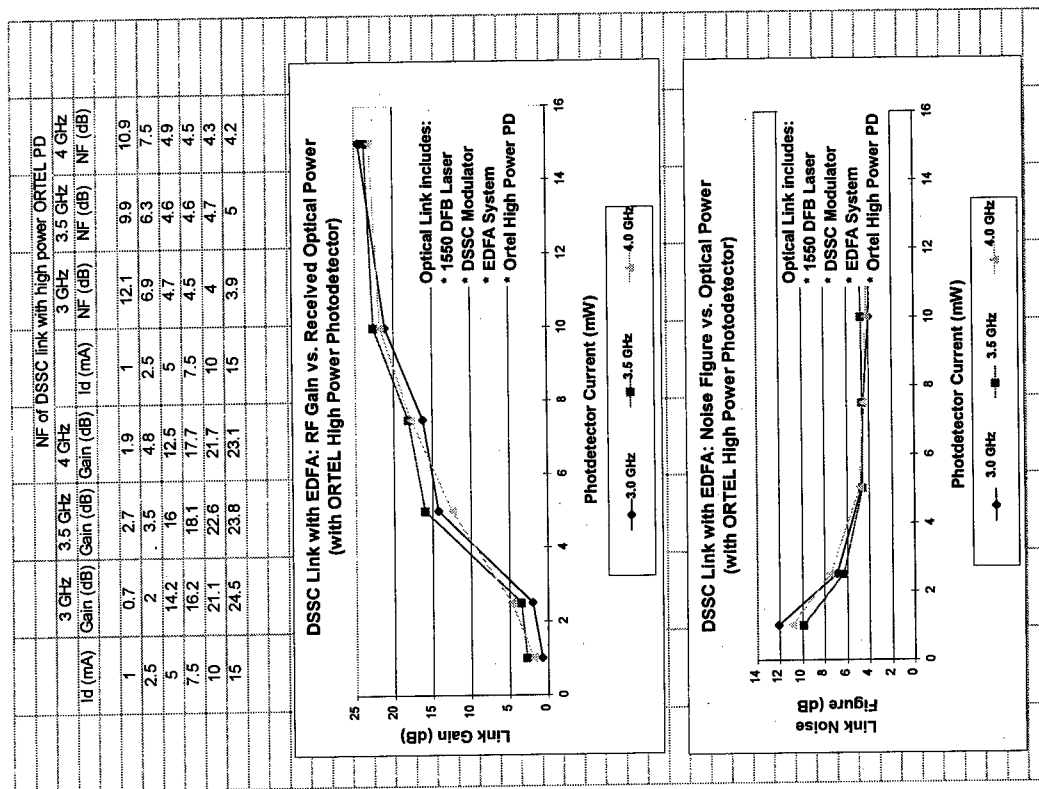


Figure B-2-2-3. DSSC Link Performance at C-band: Noise Figure vs. RF Carrier Frequency (w/Lasertron PD).

DSSC Modulator Link Performance

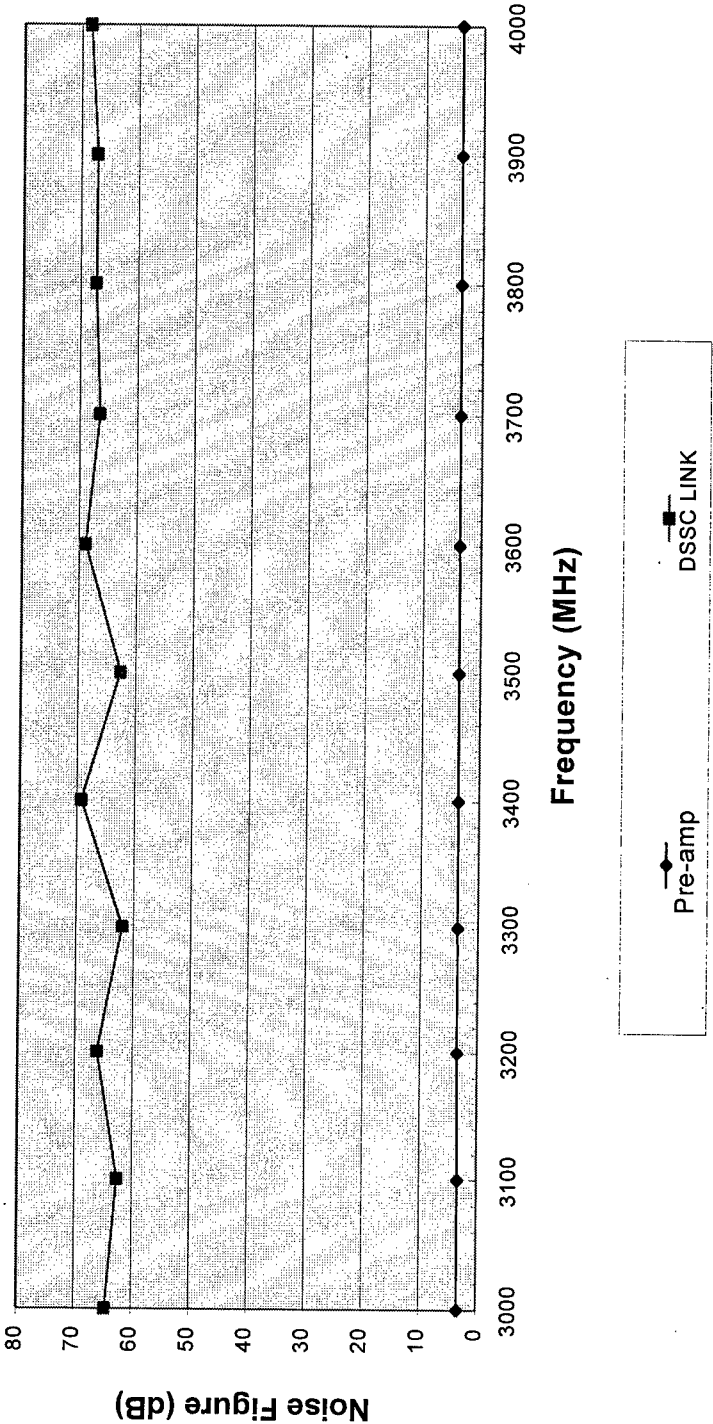


Figure B-2-2-4. DSSC Link Performance at C-band: Noise Figure vs. RF Carrier Frequency (w/Ortel PD).

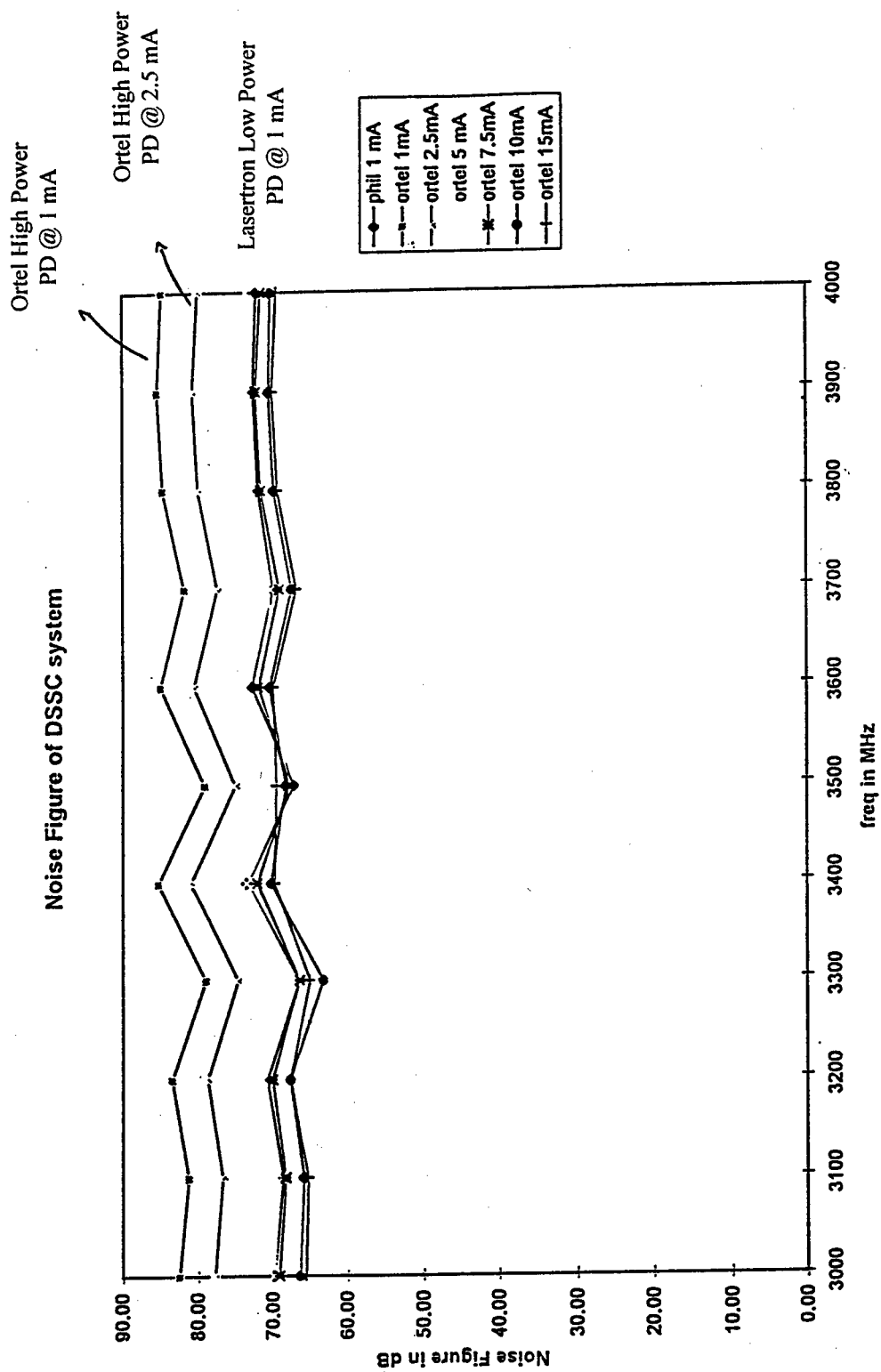


Figure B-2-2-5. DSSC Link Phase Noise Test data: Link with EDFA, Input Optical Power @ 0.95 mW.

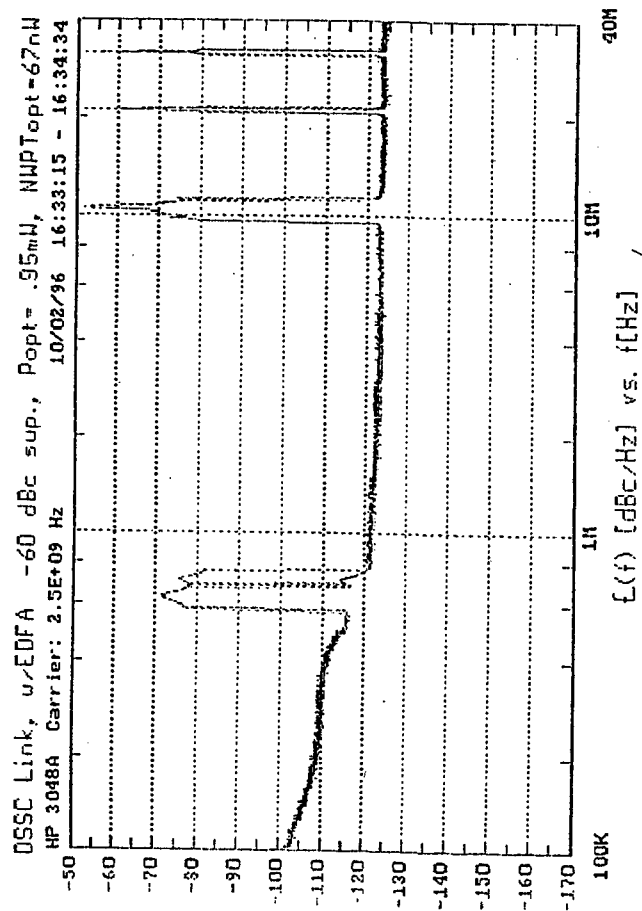
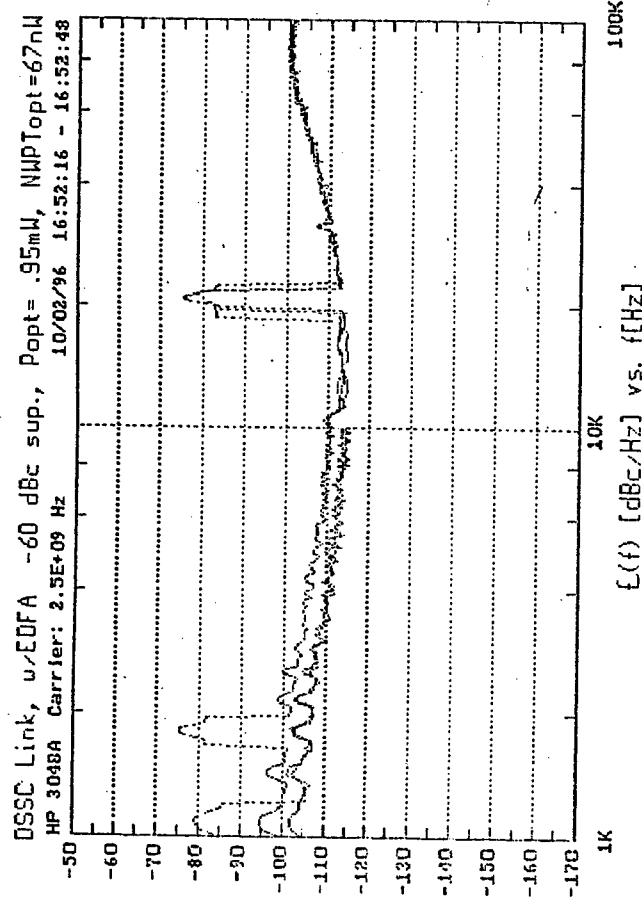


Figure B-2-2-6. DSSC Link Phase Noise Test Data: Link with EDFA, Input Optical Power @ 1.9 mW.

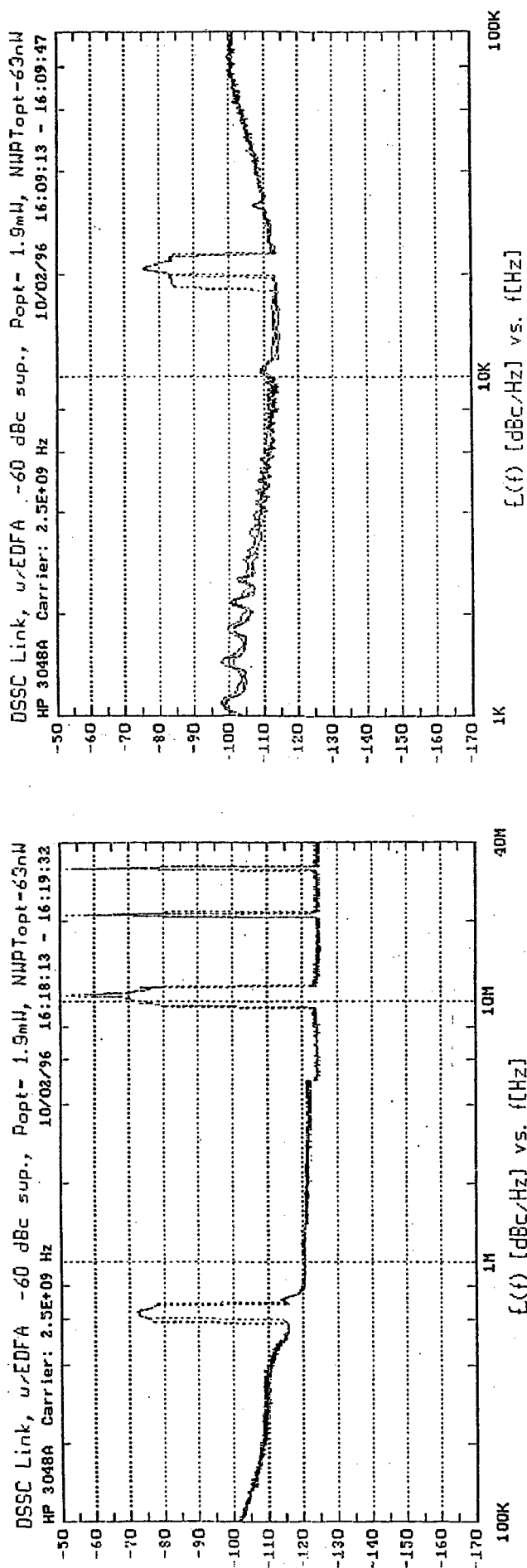


Figure B-2-2-7. Phase Noise Test data: w/o DSSC Link.

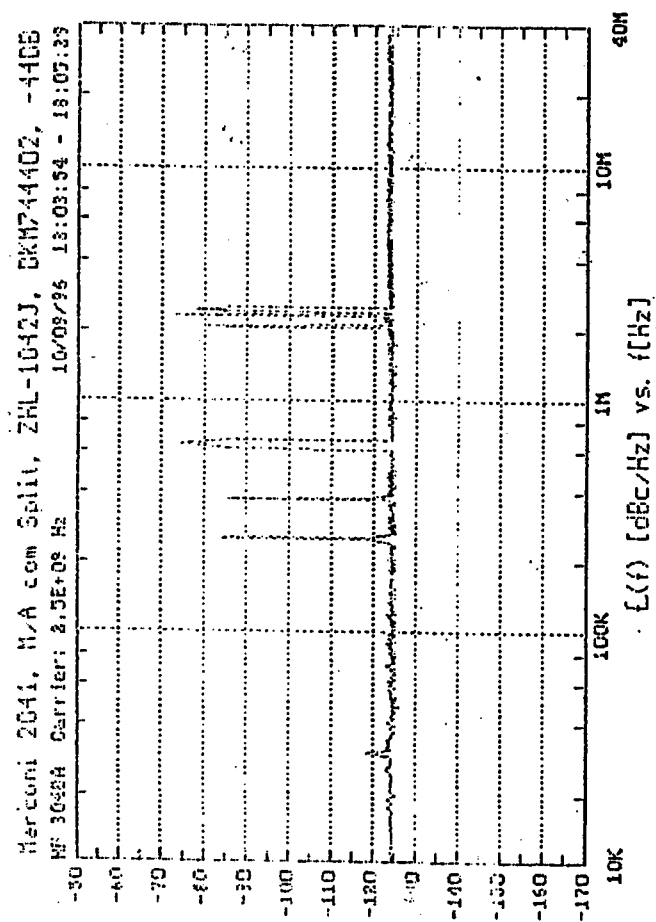
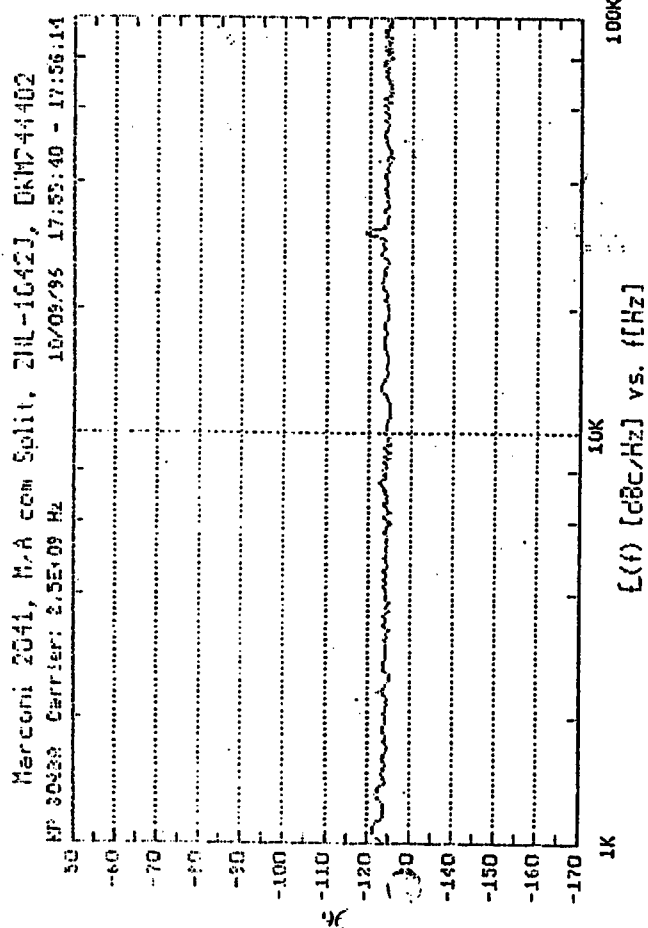


Figure B-2-2-8. DSSC Link Phase Noise Data: Link with EDFA, but w/o Pilot Tones, Input Optical Power @ 3 mW.

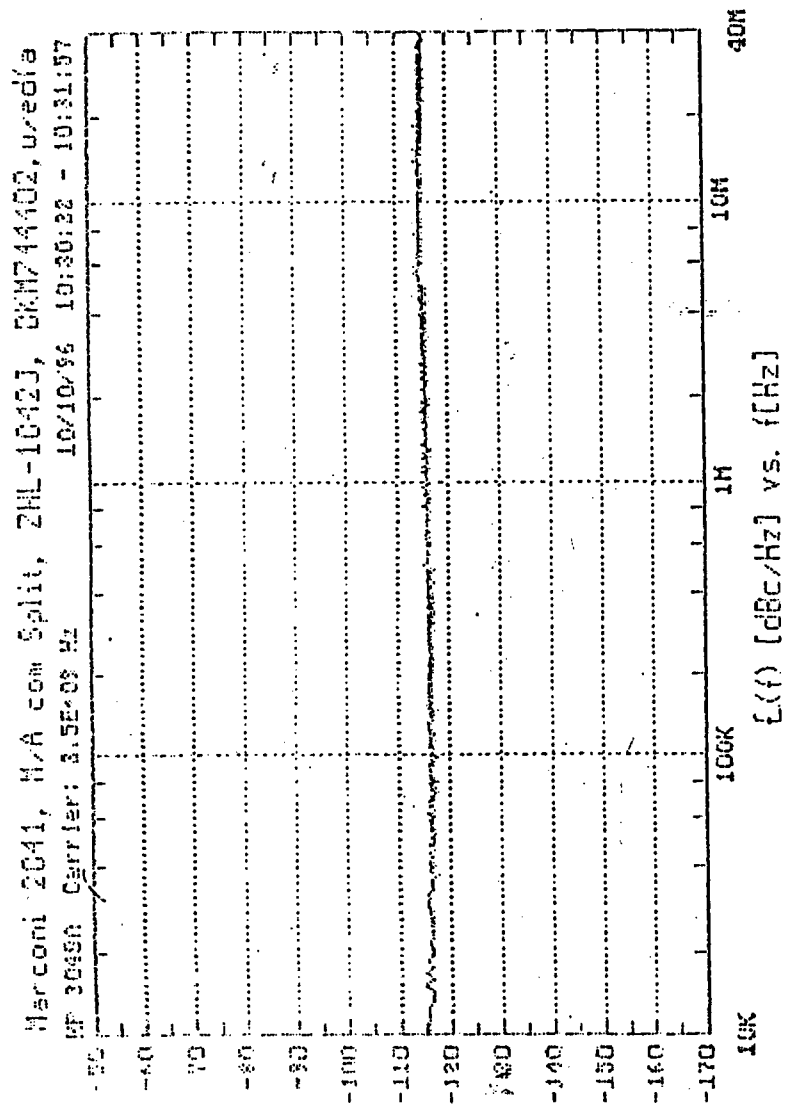


Figure B-2-2-9. DSSC Link Phase Noise Data: Link w/EDFA, Measured using Network Analyzer (HP8563E), 2.5 GHz RF Carrier.

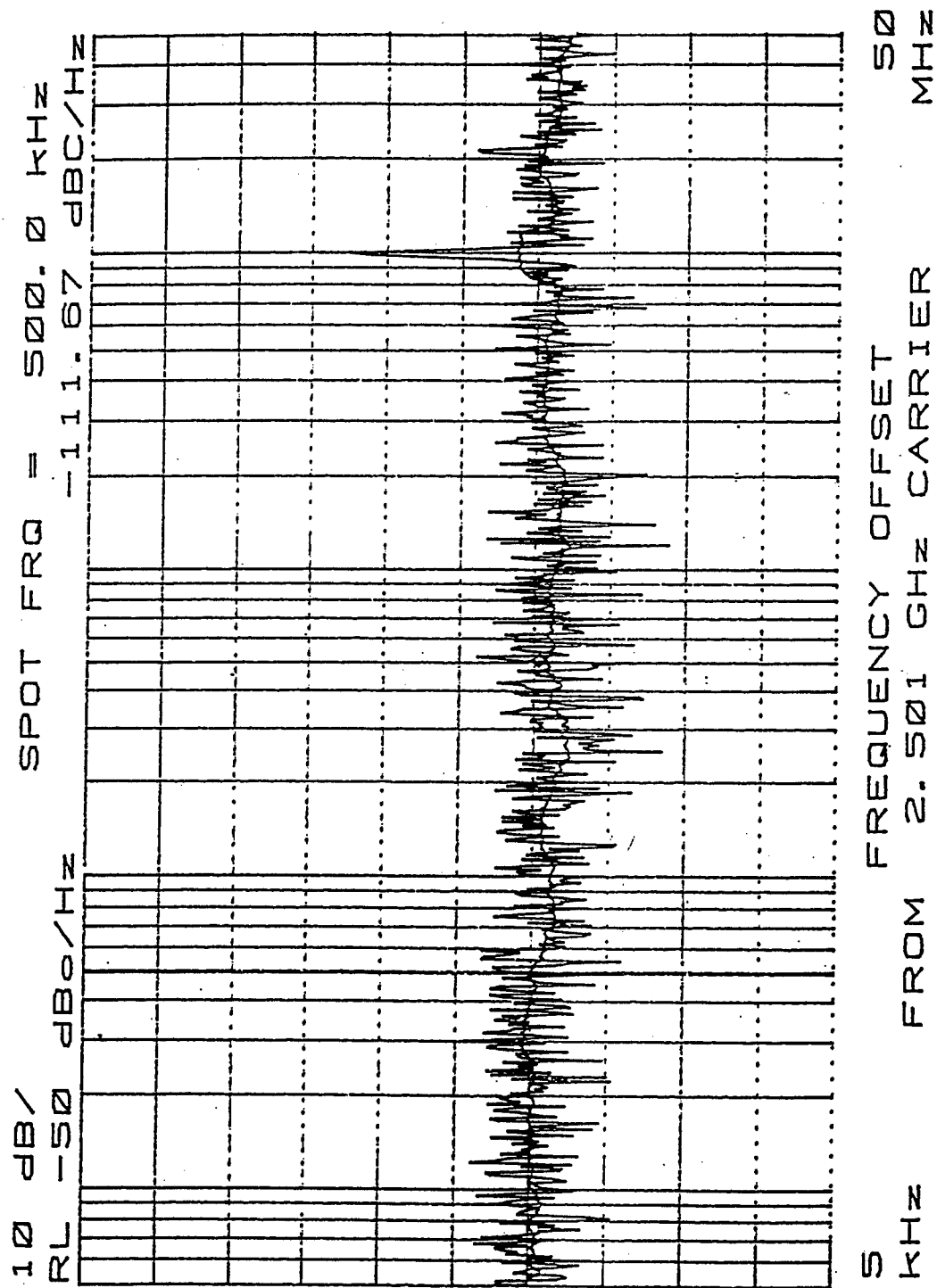


Table B-2-2-1. Comparison of Lasertron and Ortel PDs. Data compiled from the results reported in Figures B-2-2-1 and B-2-2-2, per link gain/NF test configuration shown in Figure B-2-0-2]

Comparison of Lasertron and ORTEL PDs									
Pd (mW)	Gain & Noise Figure (dB)								
	@ 3.0 GHz			@ 3.5 GHz			@ 4.0 GHz		
	ORTEL	Lasertron		ORTEL	Lasertron		ORTEL	Lasertron	
0.25									
0.5									
1	0.7/12.1	15.2/3.5		2.7/9.9	17.5/4.1		1.9/10.9	16.8/3.9	
1.5	1.1/10.4	18.1/3.5		3/8.7	20.1/4.1		2.85/9.8	20.1/3.9	
2	1.6/8.7	20.3/3.5		3.3/7.5	22.6/4		3.85/8.7	21.9/3.9	
2.5	2/6.9	-		3.5/6.3	-		4.8/7.5	-	
3		-			-			-	
3.5		-			-			-	

Table B-2-2-2. Degradation of Ortel High-power PD.

The following experiment was conducted to test and compare the performance of Lasertron and ORTEL high power PD used in the DSSC optical link set up. The link included the following 2-tone test arrangement comprising--

- A. Signal Source/Driver for the DSSC Modulator
 - _ two synthesizers operated in the C-band;
 - _ two Mini-circuit preamplifiers to amplify the output of the synthesizers,
 - _ 90-degree hybrid to combine these carrier signals,
 - _ variable attenuator (110-dB range)
- B. DSSC Modulator/Transmitter with its bias adjusted for third-order IMD minimum
 - _ DFB laser @ 1550-nm
 - _ DSSC Modulator on lithium niobate with bias circuitry and internal 872 and 882.7 MHz tone generators
- C. Optical Receiver with two options:
 - _ Lasertron PD rated for 2-mW max. optical input power, -15-V bias
 - _ ORTEL high power PD, 15-mW max. optical input power, +10-V bias
- D. Post-detection Amplifier (Mini-circuit)
- E. Spectrum Analyzer

Table B-2-2-2. Degradation of Ortel High-power PD (continued).

- F. The tests were conducted with the following test parameters but without EDFA:
 - Carrier #1 @ 3883 MHz, +6.23 dBm RF power at the -13 dB output port of a coupler
 - Carrier #2 @ 3898 MHz, +6.70 dBm RF power at the -13-dB output port of the coupler
 - The signals combined to a max. input power of +9.45 dBm [measured at the power meter] for 22.45 dBm total driving the DSSC modulator.
 - The bias settings for the third-order minimum condition:
 - $V_{b1} = -8.1818$ V, $V_{b2} = -1.04$ V, $V_{p2} = -0.31$ V and
 - Optical Power Measured at the Newport Power Meter: 49-nW
 - Optical Power incident on the PD: 0.25 mW
- G. The test data is summarized below.

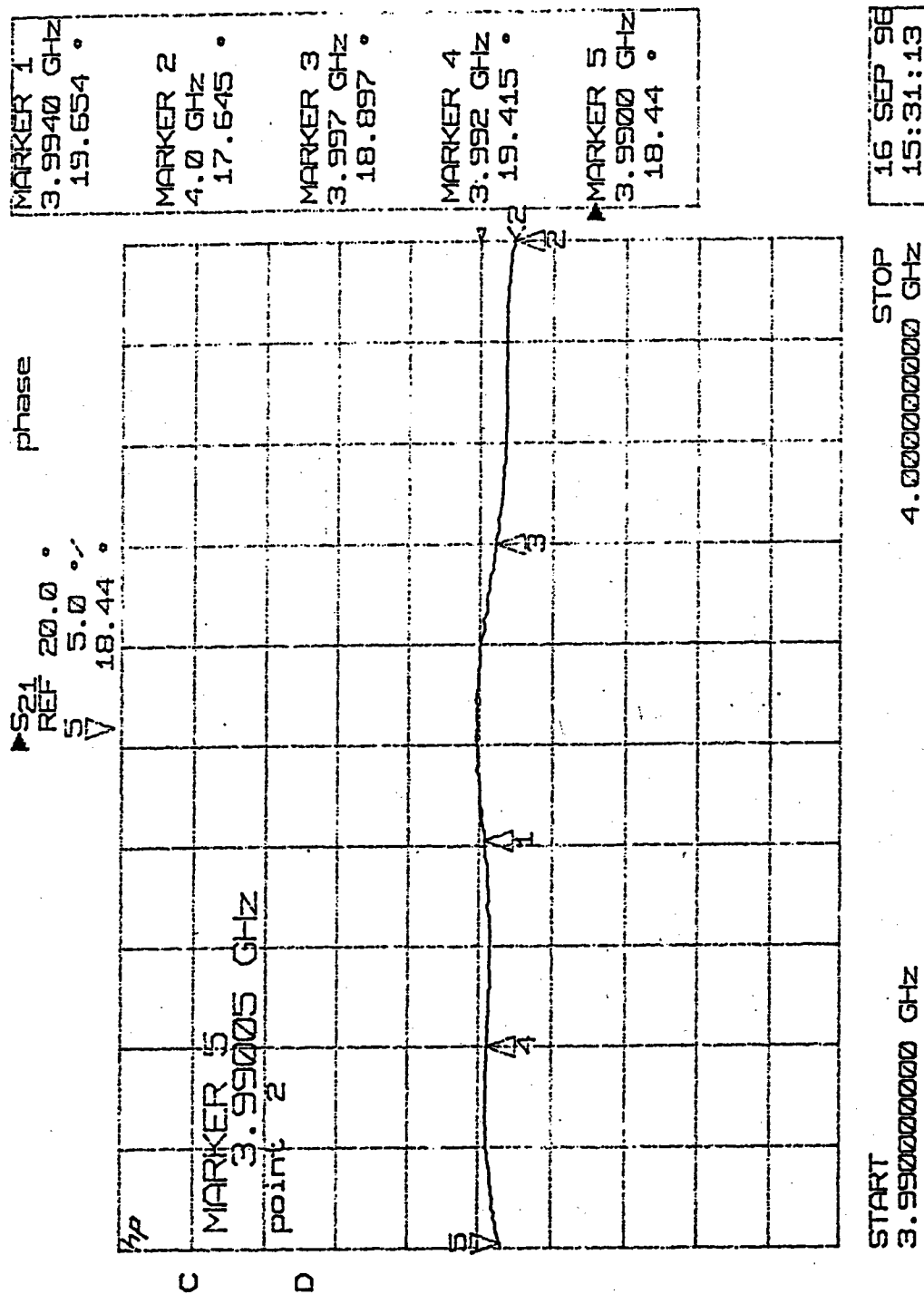
Case 1.		ORTEL PD									
Freq. (MHz).	3883	3898	3868	3913	15	872	882.7	861.3	893.4	1754.7	
Ampl. (dBm)	-46.8	-50.5	-90.2	-91	-68	-47.1	-48.8	-87.2	-87.4	-62.9	

Case 2.		Lasertron PD									
Freq. (MHz).	3883	3898	3868	3913	15	872	882.7	861.3	893.4	1754.7	
Ampl. (dBm)	-21.3	-24.3	-76.8	-82.4	-37	-21.8	-22.7	-76.4	-76	-38.2	
- H. Conclusion: ORTEL PD sensitivity is worse by ~26 dB

B-2.3 Phase Stability

The phase stability testing was conducted in a closed loop using a network analyzer (HP 8510). The schematic shown also includes other accessories for the DSSC operation (see Figure B-2-0-5. For short links, the phase instability arises due to the bias/thermal drifts and chirping of the lithium niobate modulator. The tests continued in ambient temperature (laboratory environment) for long hours (six). The measured phase drift was very nominal; less than 2-degree for this period (see Figure B-2-3-1). At 1550-nm, a 1-meter long Corning SMF-28 fiber will experience an optical phase shift of 2,500 degree/°C change in temperature.. For microwave-fiber optic transmission, the corresponding RF phase shift is, however, very small (0.35 degree @ 18 GHz and 0.02 degree @ 1 GHz). For long MMW/fiber links, the optical phase drift attributable to the (dn/dT) and modal characteristics of single-mode fibers could be substantial. However, the phase stability can be improved by adequate thermal stabilization and/or corrective phase-cancellation measures

Figure B-2-3-1. Phase Stability Test Data of the DSSC Modulator Link.



Appendix- C. DSSC Performance Simulation

C-1. Optimum Performance of DSSC Modulator Chip

In an attempt to find an answer to optimum operating conditions for the DSSC modulator chip developed under this program and its usefulness in enhancing the link performance, computer simulations of the link characteristics were run. Both two and three-carrier transmission characteristics and relative performance of the fundamental and third-order IMDs of the DSSC chip were compared vis-a-vis a standard MZ modulator device biased for second-order null. It was observed from this analysis that a suitably biased DSSC chip, i.e., a modified DSSC biased @ 1.48V_r on the signal port and 0.6V_r on the parallel port, can improve the link performance considerably (the fundamental-to-DC signal power ratio is increased by 8 dB and the third harmonic is suppressed with a dynamic range of 128-dB/Hz^{2/3}).

Because of the overall cost and complexity of the DSSC chip and the difficulty in maintaining a long-term stable operation at the third-harmonic null, several alternate modulator chips were also considered in the analysis. These configurations included simple EO modulator chips such as standard MZMs with differential detection capability (for example, an "X-type" modulator chip with dual balanced outputs) operated both with and without optical carrier injection. Unlike the DSSC or the modified DSSC chips, both standard MZM and MZM w/carrier injection have a much wider bandwidth. Furthermore, in comparison with the modified DSSC, standard MZMs with carrier injection require a simple bias and have the signal (fundamental) enhanced by ~1-dB while nulling the second harmonic and suppressing the third harmonic for a comparable dynamic range (129-dB/Hz^{2/3} vs. 128-dB/Hz^{2/3} in modified DSSC). Currently additional tests are planned/conducted to validate this observation. The details of the simulation/analytical results are provided in **Section E, Appendix III: DSSC Modulator Performance Enhancement Simulations.**

Appendix- D. Summary and Recommendation

An exhaustive series of measurements have been performed on the DSSC modulator link which included multicarrier transmission test for linearity and intermodulation distortion, amplitude and phase noise, and phase stability. Maintaining the DSSC chip at the third-order null seemed a very difficult task. From these measurements, we determined a link noise figure of 65 to 70 dB, an SFDR of 110 dBm.Hz^{2/3}, and a phase noise of < -125 dBc at 1 MHz offset from the 2.5-GHz carrier. Also, an analysis has been made on the optimum performance of the DSSC modulator chip which led to the conclusion that biasing at $0.6V_{\pi}$ could enhance its performance by 10 to 15 dB over the current biasing scheme. We have made preliminary verification of this operating point. A detailed investigation might produce other interesting potentials for the DSSC modulator chip.

The major conclusions and suggestion for future work are summarized below:

- ◆ Various systems functionality of DSSC modulator chip used in a C-band microwave optical link are characterized:
 - I/O linearity, IMD, SFDR, Noise Figure, Phase Noise, and Phase Drift
 - Both amplified (w/EDFA) and unamplified link architectures used with low and high power photodetectors
 - DSSC control of the third-order IMD minimum is unstable
 - High noise figure of the externally modulated optical link (60-70 dB)
 - Phase noise @-125 dBc/Hz for frequencies to 1 MHz, thereafter increasing to ~ -110 dBc/Hz; DFB link is 10-15 dB worse than the Nd:YAG link
 - Reasonable phase drift (>2 degree) in 6-hours continuous operation
 - Ortel detector less sensitive and also more noisy than the lower power Lasertron detector
 - SFDR ranges between 90-110 dB/Hz^{2/3}; increased at higher optical power
- ◆ Alternative bias condition to optimize DSSC performance investigated:
 - DSSC chip biased at @ $1.48V_{\pi}$ on the signal port and $0.6V_{\pi}$ on the parallel port improves the link performance by at least 8 dB and the third harmonic is suppressed with a dynamic range of 128-dB/Hz^{2/3}. Preliminary experiments performed to validate above observation.
- ◆ Proposed investigation of the system level performance of the modified DSSC chip biased as above. Also, explore other bias conditions conducive for new applications of the EO modulator chip developed.

Appendix-E: DSSC Modulator Performance Enhancement Simulations

Introduction

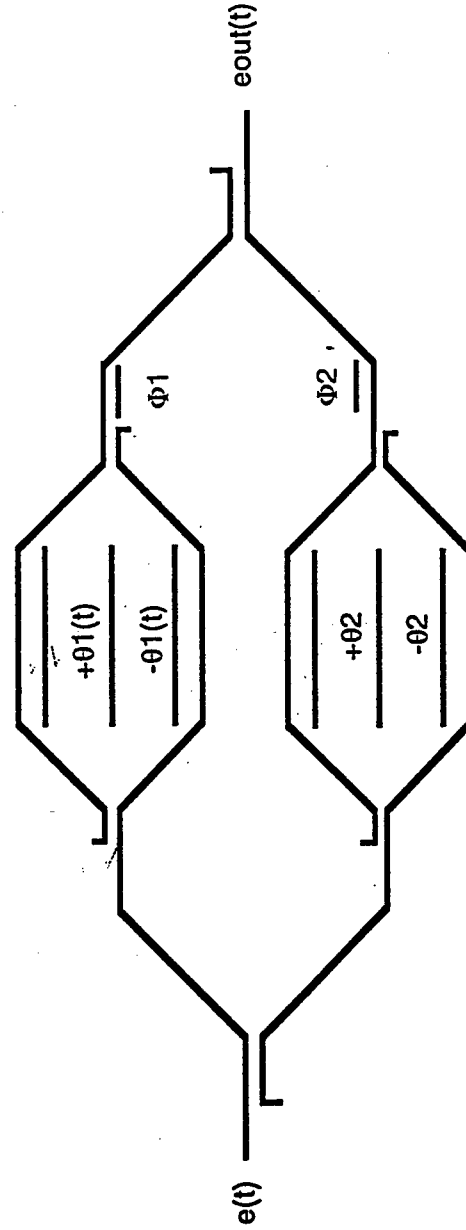
- **The Characteristics of DSSC Have Been Analyzed and Verified Experimentally**
- **Alternate Operating Points on DSSC Were Examined to Look for Optimal Performance of the Modulator Chip**
 - 1.48 π on Signal Port Bias, 0.6 π Bias on Parallel Port
- **Alternate Modulator Configurations Were Examined to Compare How DSSC's Performance Compared**
 - Standard MZM
 - Standard MZM with Differential Detection
 - » "X" Type Modulator
 - Standard MZM with Carrier Injection and Differential Detection
 - » "X" Type Modulator

Optimum Modulator Characteristics

- **Several Characteristics Are Key When Comparing Different Modulator Configurations**
 - Amount of Power in Sidebands
 - Difference in Power Between DC and Carrier
 - » Desire Signal Saturates Detector
 - » Ensure Always Enough Optical Power Present to Saturate EDFA
 - Minimizes NF of EDFA
 - Harmonic Signal Content; Especially 2nd and 3rd Order Terms
 - Simplicity of Bias Control Network
 - Ease of Manufacturing

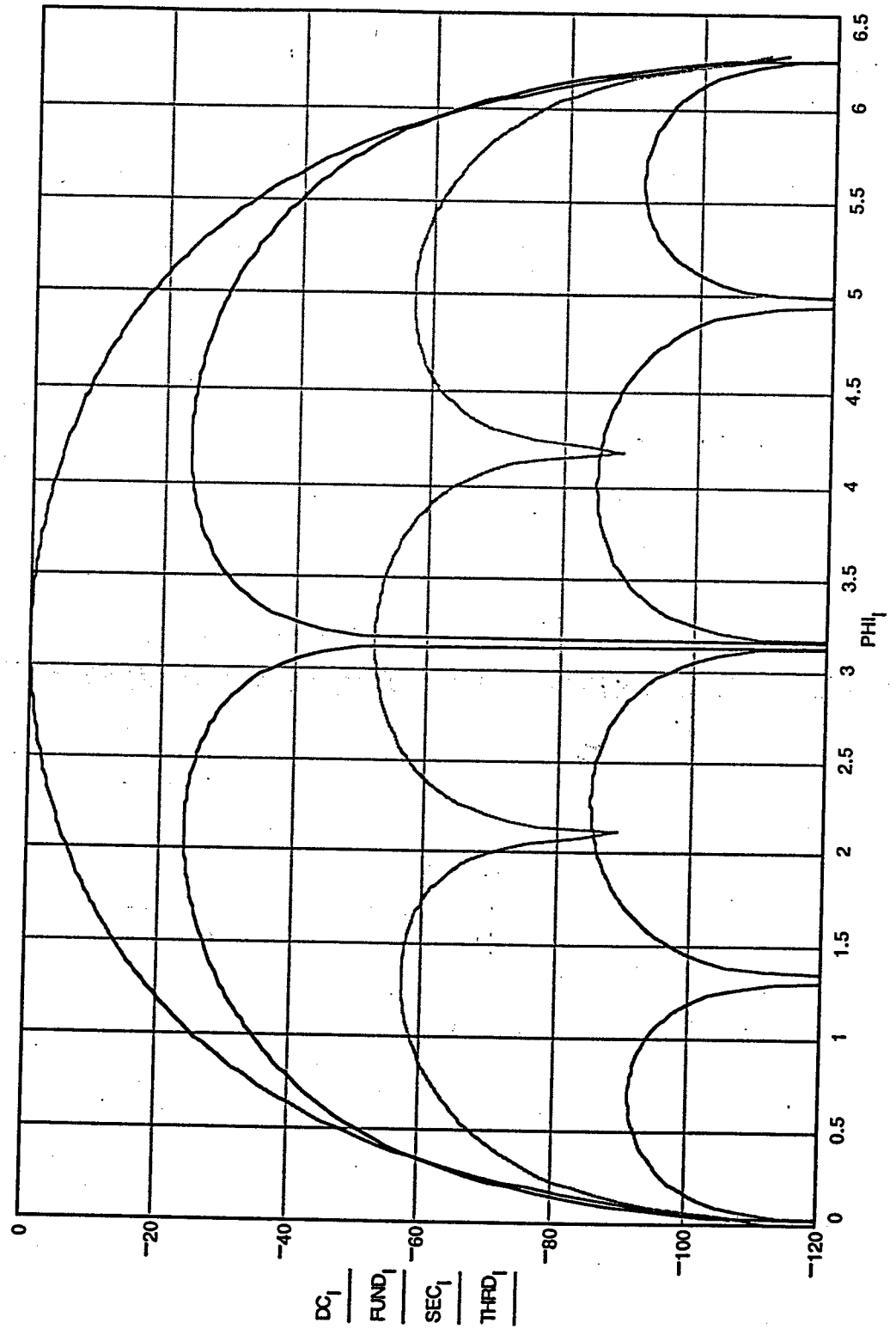
DSSC Operation

- **DSSC Was Conceived As a Way to Reduce the Carrier Power so More Signal Power Could Be Transmitted Before Detector Saturation**
- **Asymmetry of DSSC Response Created Operating Points Where 3rd Order Distortions Could Be Nulled Out**
 - Nominal Operation is With Maximum Power Out of Parallel Leg and a 180° Phase Shift Between Two MZM Paths



DSSC Harmonic Content

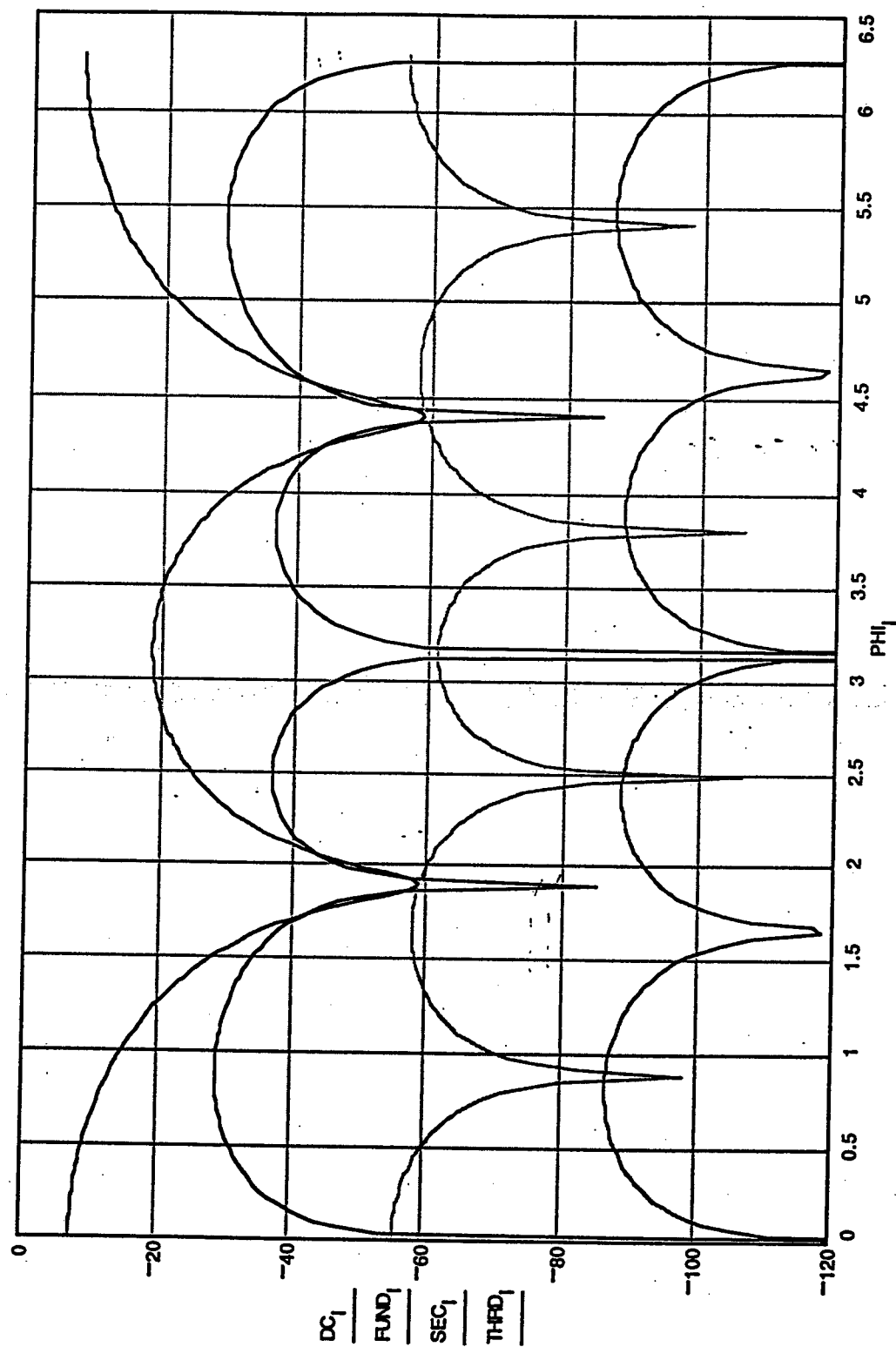
MOD = 0.1 PH2 = 0 DELPH = 3.142



Modified DSSC

- The Operating Point of DSSC Was Modified
- The “Optimal” Configuration is One Where the 3rd Order Terms Are Suppressed and the Carrier and Signal Power Levels Are Equal
 - Allows Use of EDFA to Achieve “Lossless” Link
- This Condition Occurs at a Signal Port Bias of 1.48π and a Parallel Port Bias of 0.6π
- The Penalty for Operating at This Point is:
 - Very Sensitive to Bias
 - Bias Control Becomes More Complex
 - Very Large Optical Gain Required; ≥ 50 dB

Modified DSSC Harmonic Content

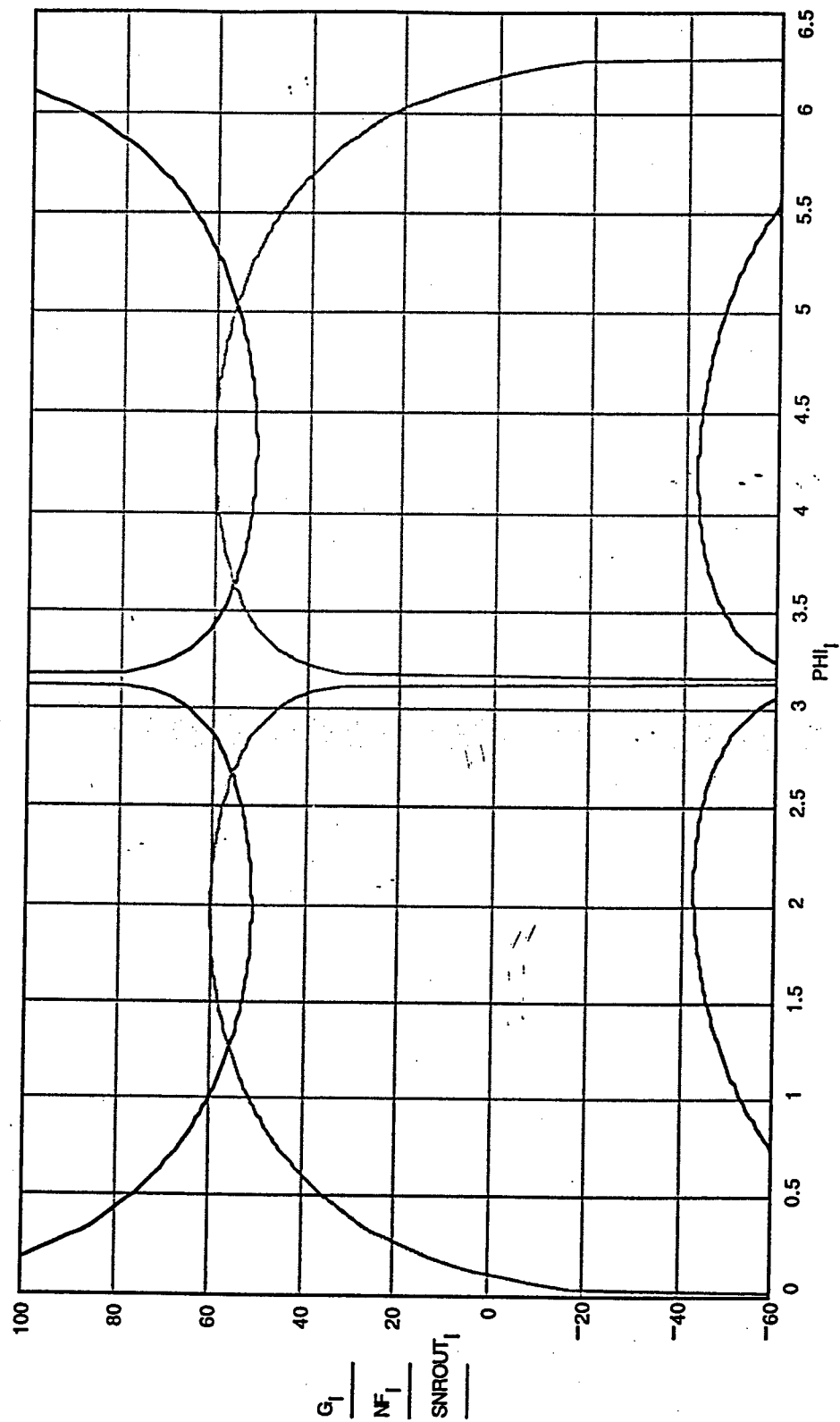


Optical Parameters for Link Evaluation

■ The Parameters Used to Characterize the Links Are Based on Current COTS Components

– Optical Power (30 mW Diode)	10 mW
– Modulator V_{pi}	8 V
– Detector Responsivity	0.9 A/W
– Modulator Impedance	50 Ω
– Load Impedance	50 Ω
– RIN (w/in 5 dB of Theoretical)	-165 dBc
– Noise Power (Thermal Limit)	-168 dBm/Hz
– Optical Loss	9 dB
– Modulation Index	0.2
– Analysis BW	10 MHz

Link Characteristics; DSSC

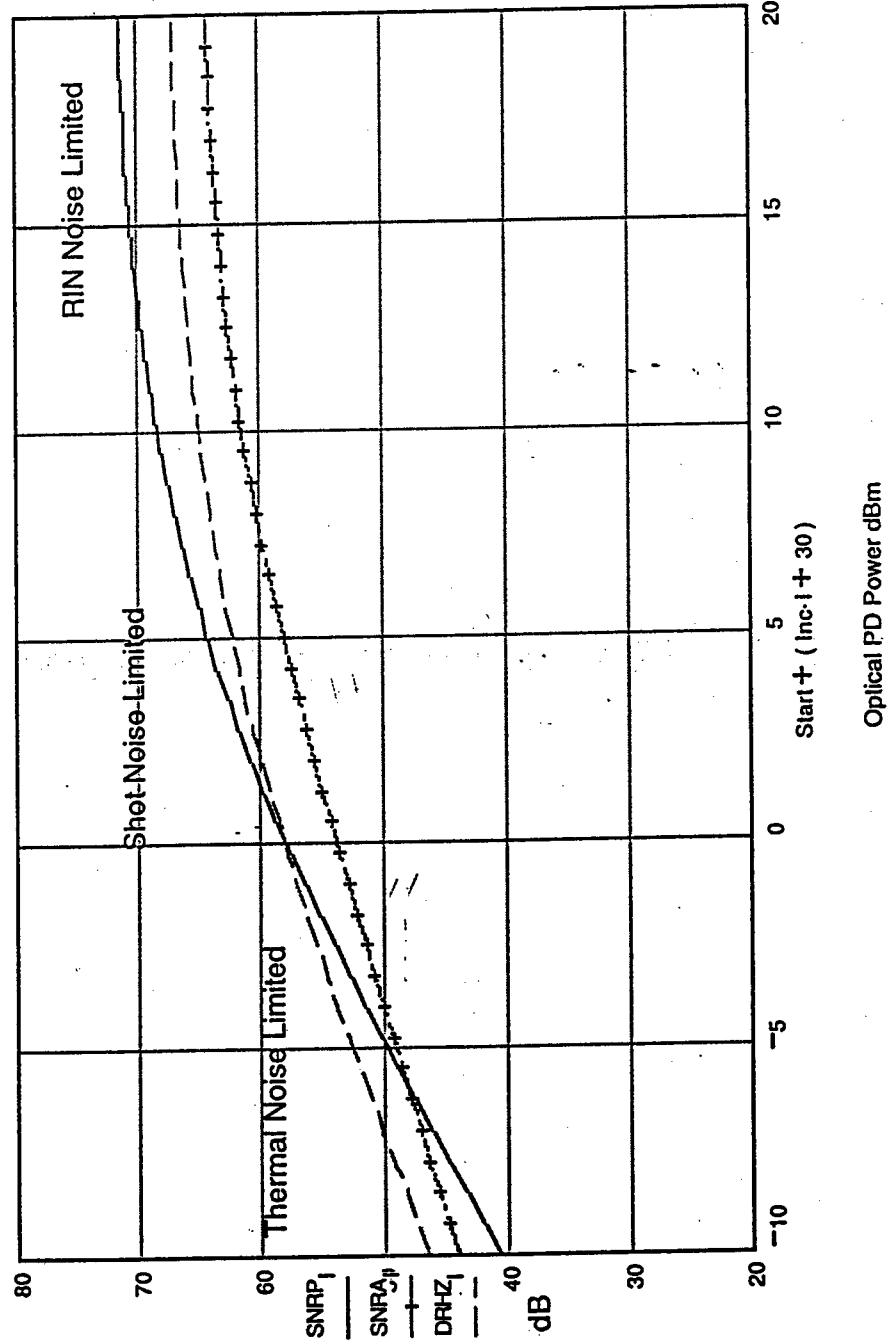


Variation in Performance With Increased Optical Power

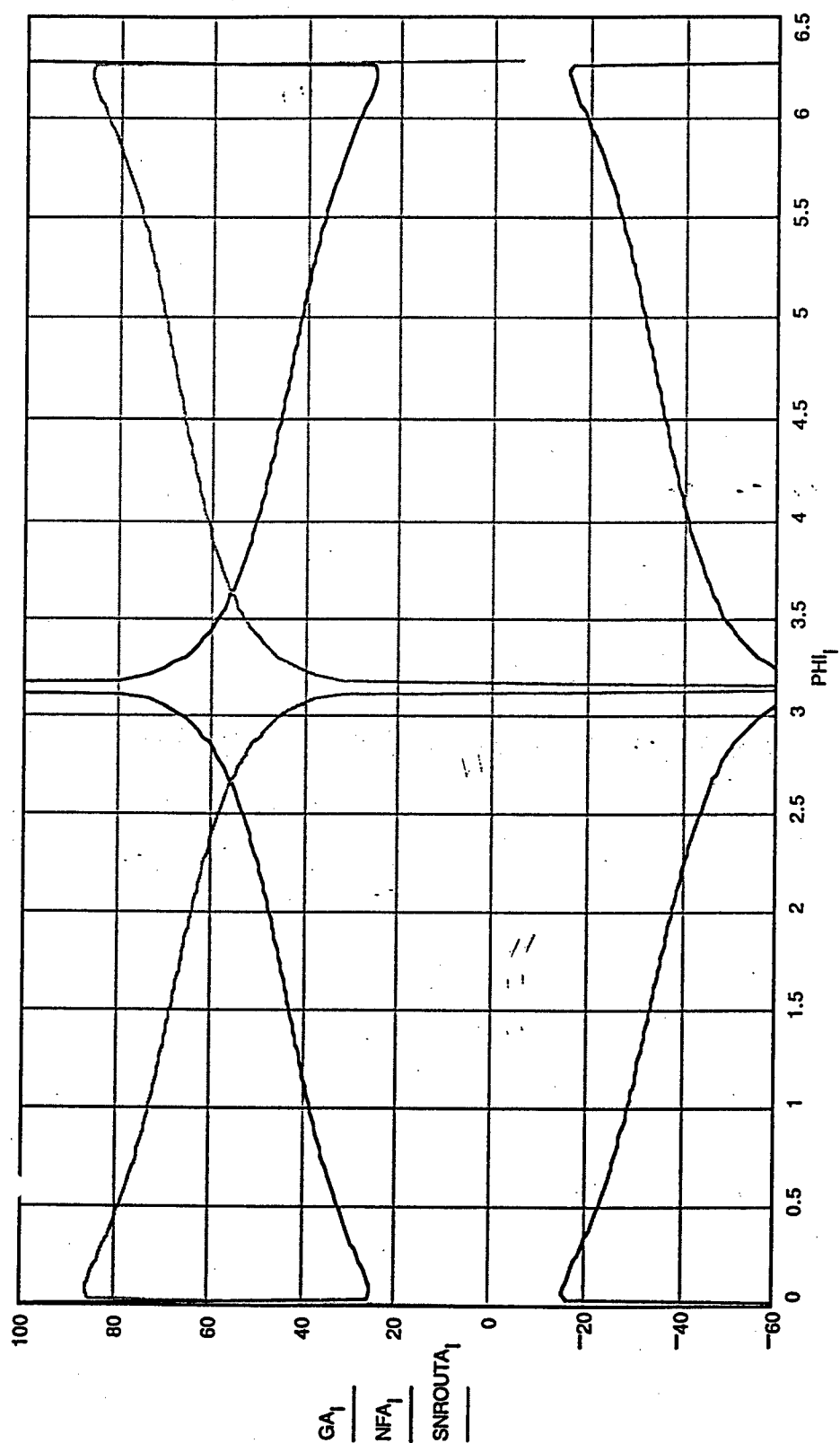
$BW = 1 \cdot 10^7$ $RL = 50$ $MD = 0.1$ $ID = 1 \cdot 10^{-8}$ $R = 0.9$ $RIN = -165$

$M = 12$ $F = 5.4$ $SEN = -62.5$

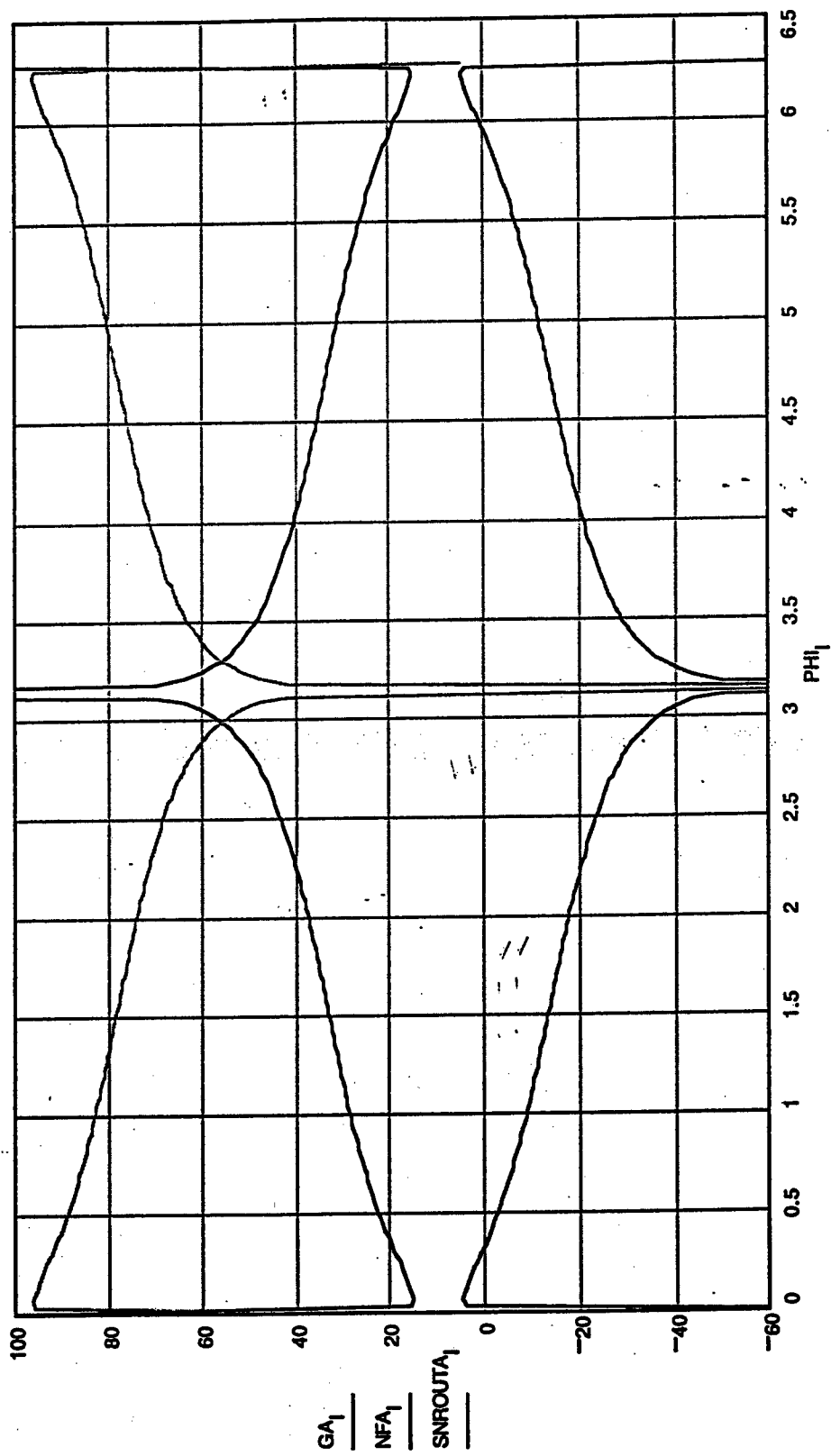
$SFDR = 59.085$



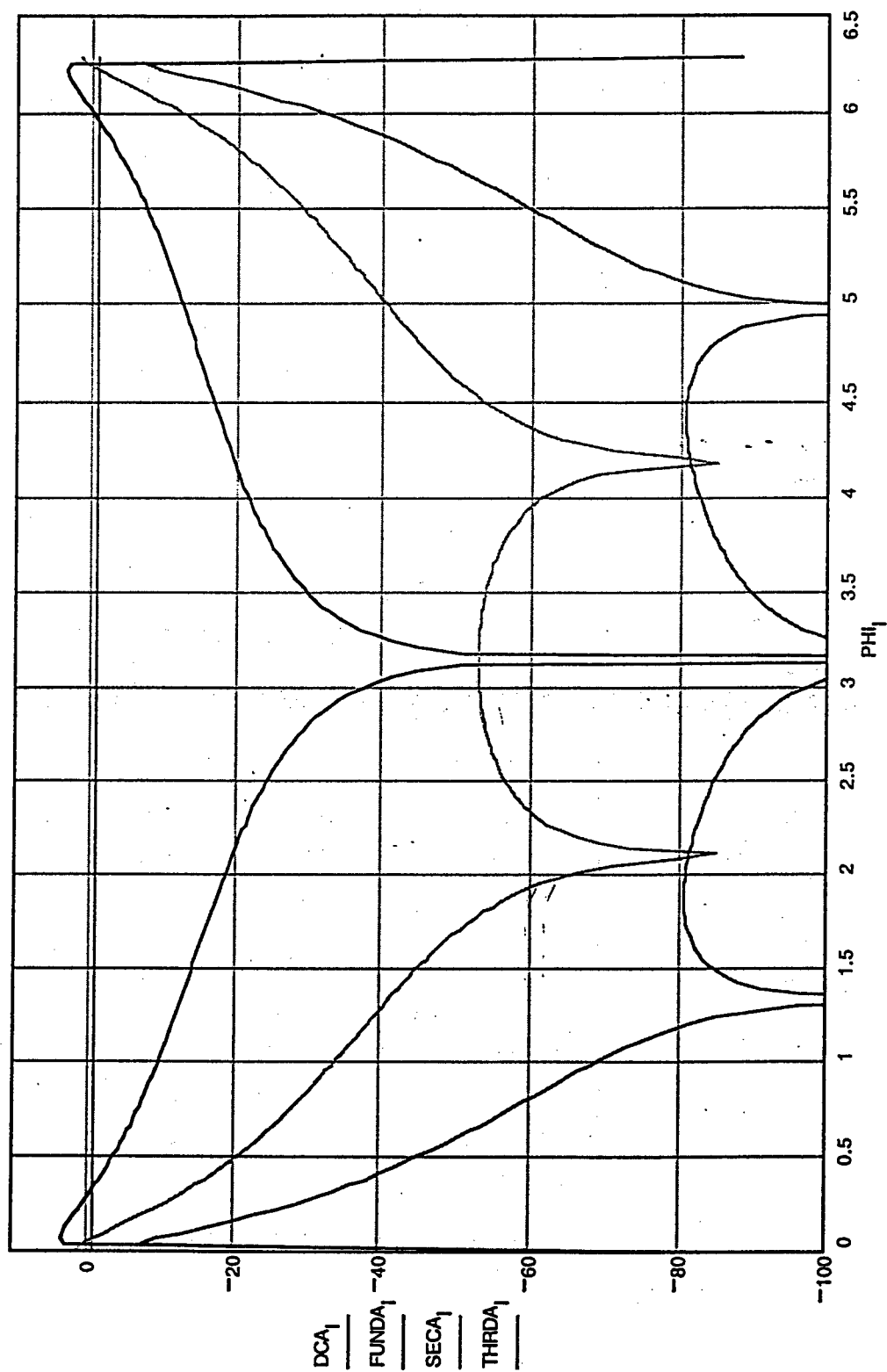
*Link Characteristic w/ EDFA
and $I_{\text{sat}} = 1 \text{ mA}$*



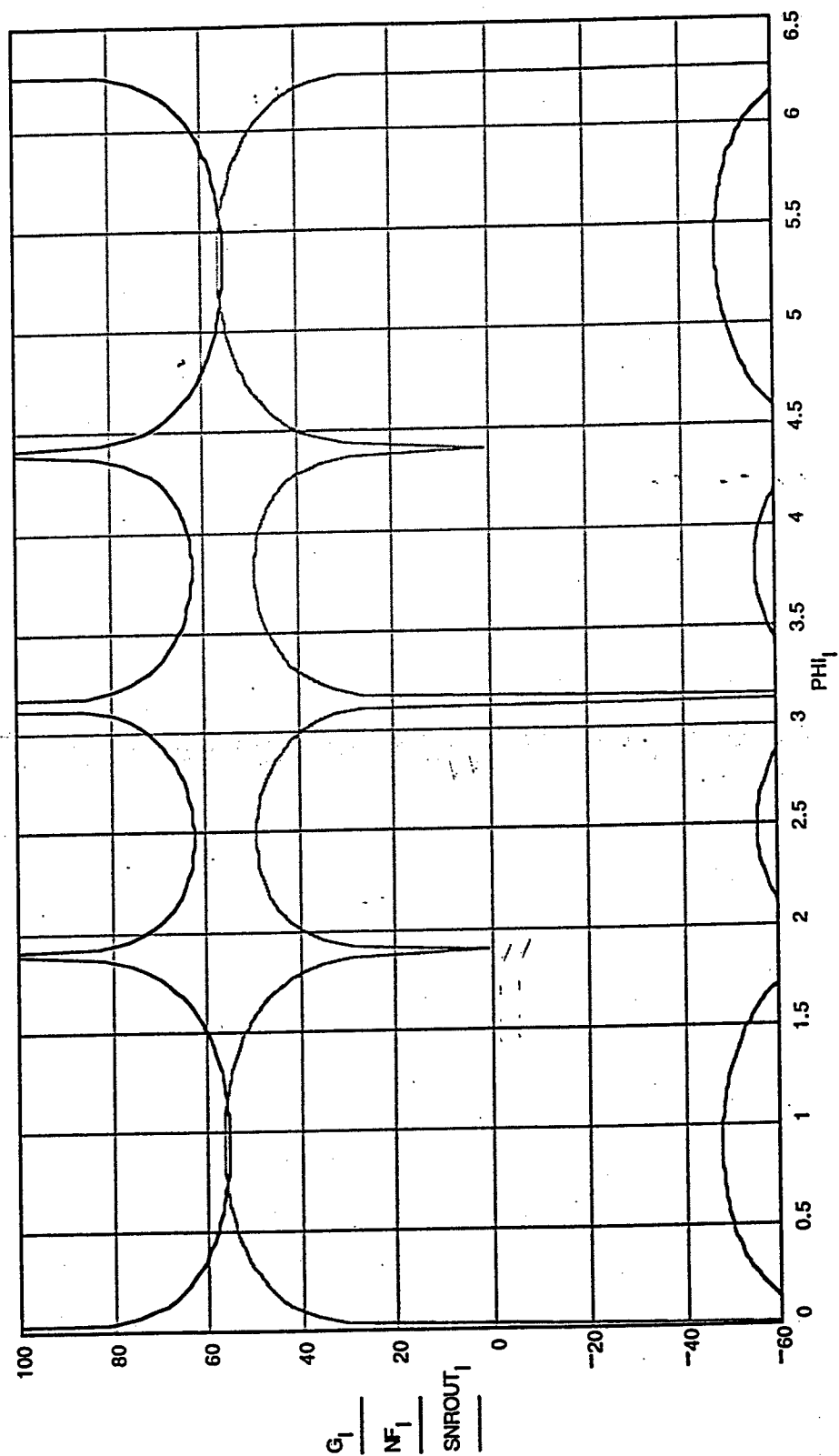
Link Characteristic w/ EDFA and $I_{sat} = 10 \text{ mA}$



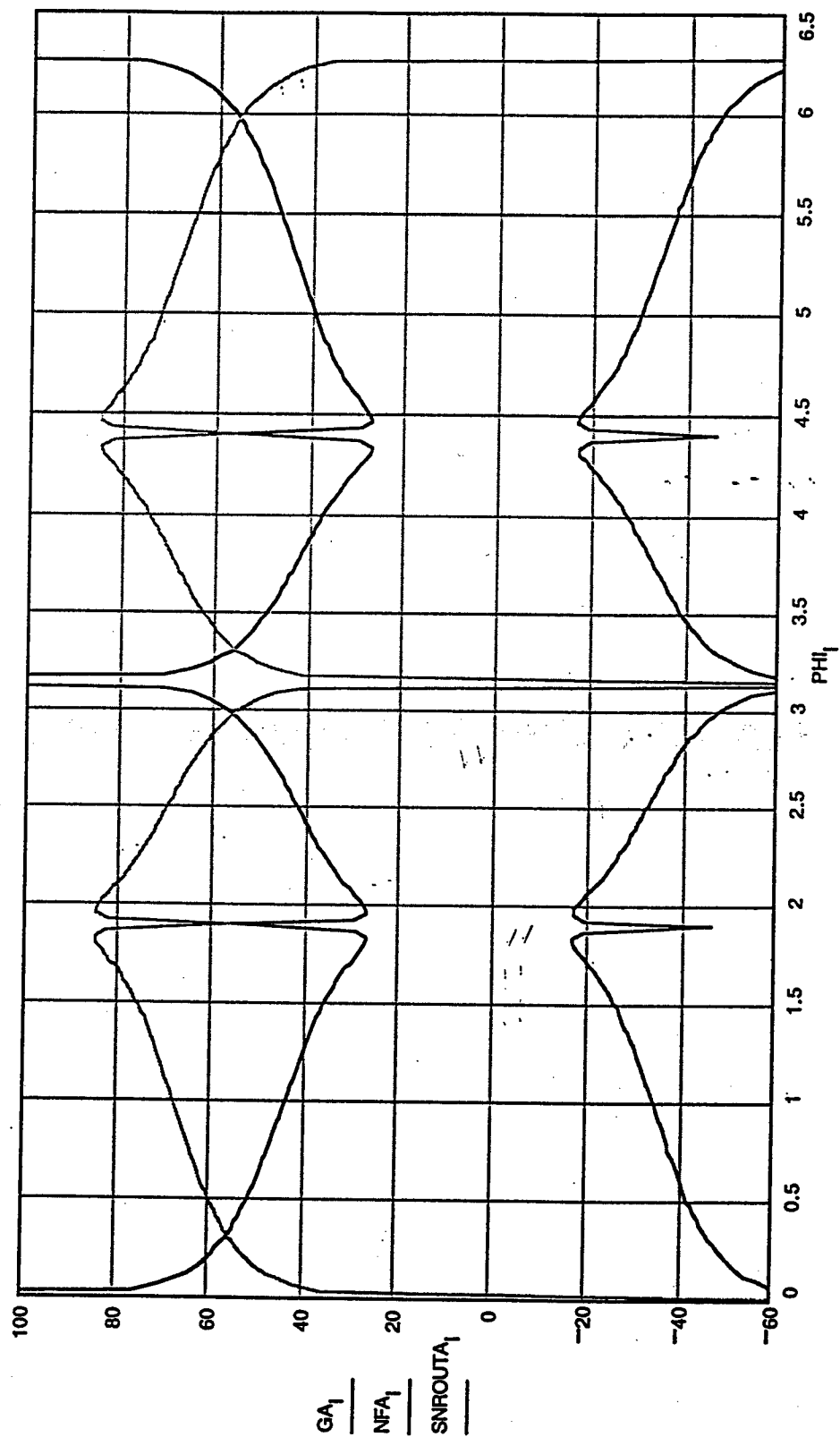
Harmonic Content w/ EDFA



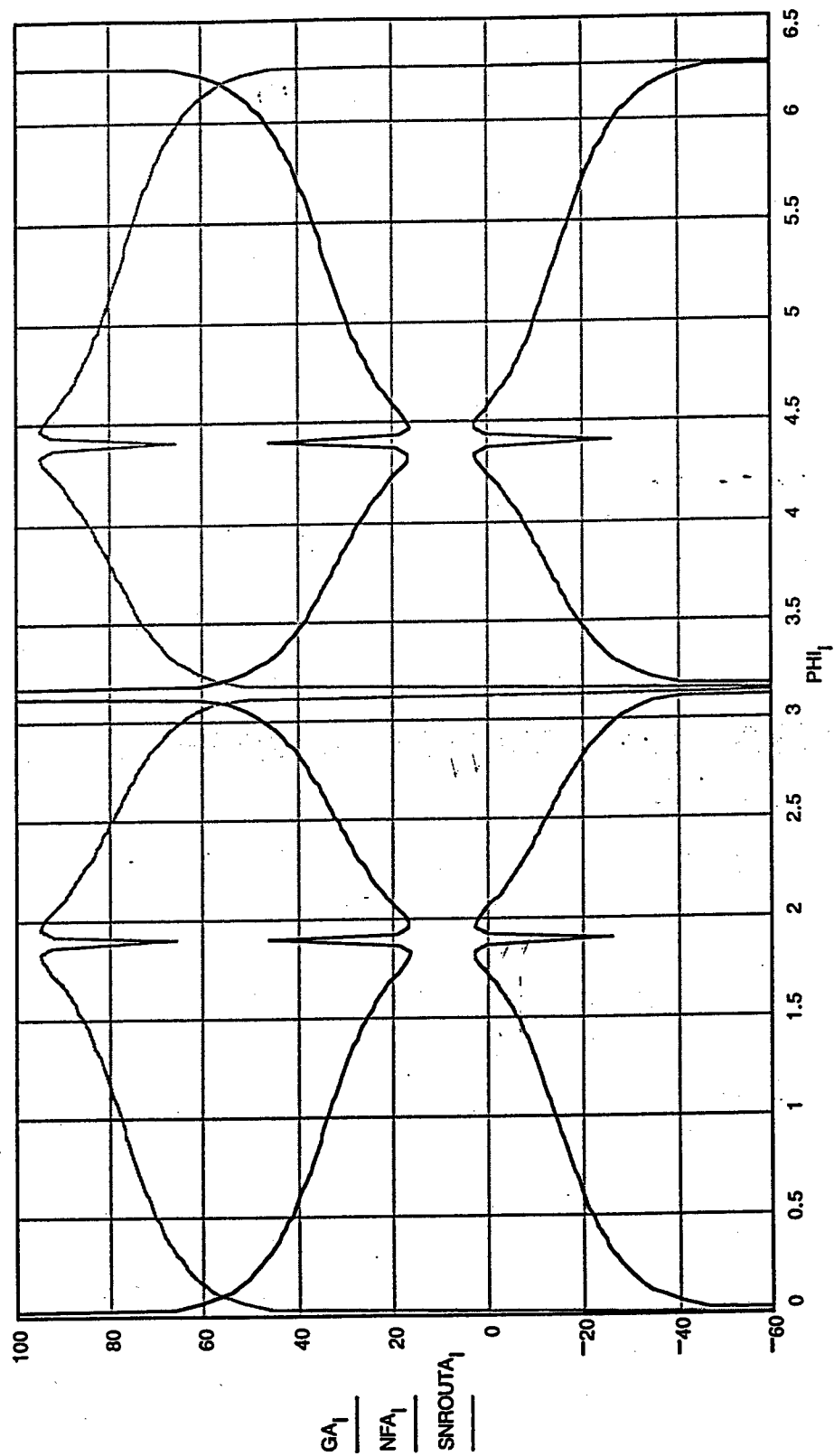
Link Characteristics; DSSCM



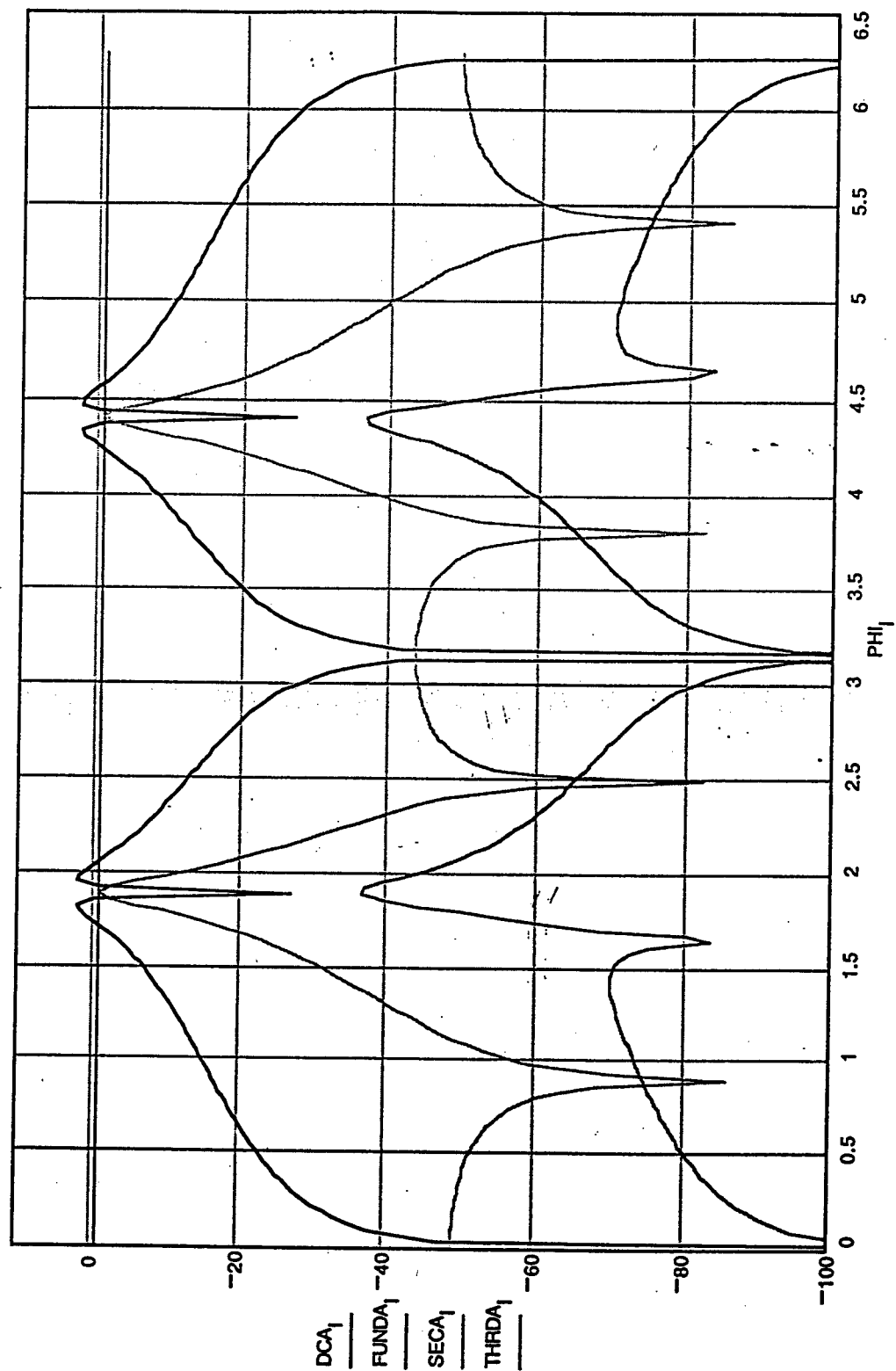
Link Characteristic w/ EDFA and $I_{\text{sat}} = 1 \text{ mA}$



*Link Characteristic w/ EDFA
and $I_{\text{sat}} = 10 \text{ mA}$*



Harmonic Content w/ EDFA

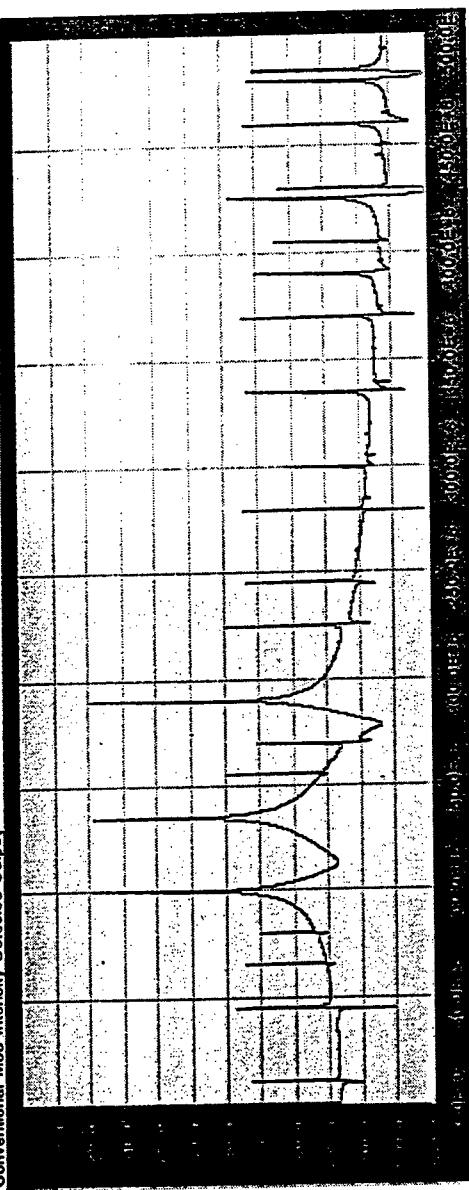


DSSC Output w/ Higher Order Spurious Signal Content; $m=.2$

Modulation Frequency 1 (MHz) Modulation Frequency 2 (MHz) Modulation Frequency 3 (MHz) Voltage Modulation Index

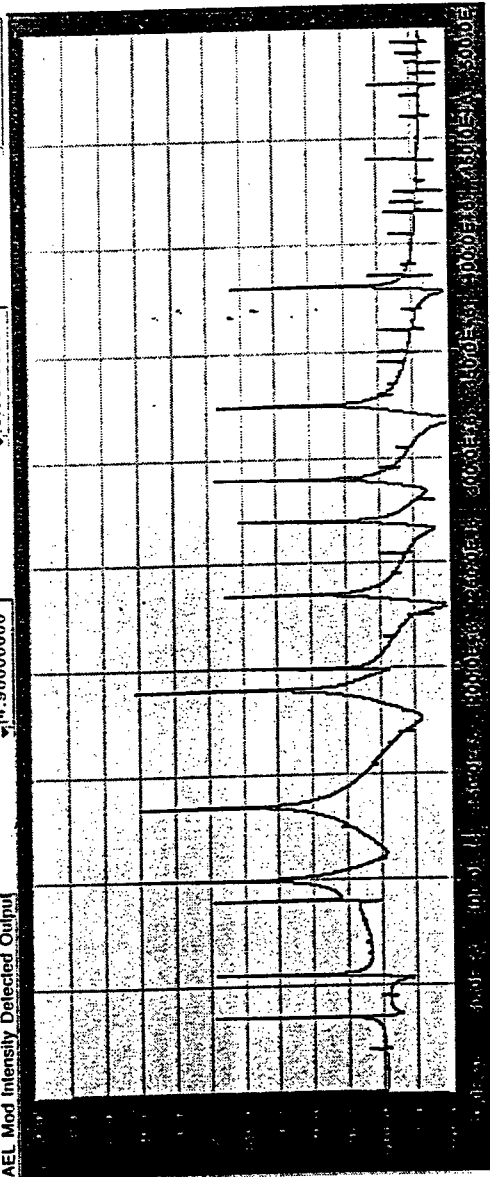
Phase Offset: Conv (radians)

Conventional Mod Intensity Detected Output



AEL Mod Intensity Detected Output

Amp Phase Offset1: AEL (radians) Amp Phase Offset2: AEL (radians) Delta Phase Offset: AEL (radians)

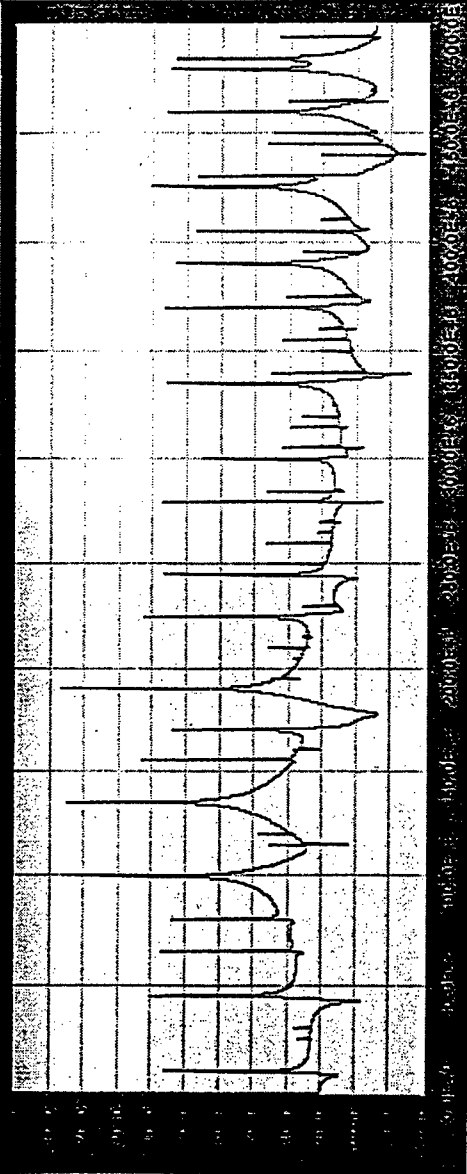


DSSC Output w/ Higher Order Spurious Signal Content; $m=5$

Modulation Frequency 1 (MHz) Modulation Frequency 2 (MHz) Modulation Frequency 3 (MHz) Voltage Modulation Index

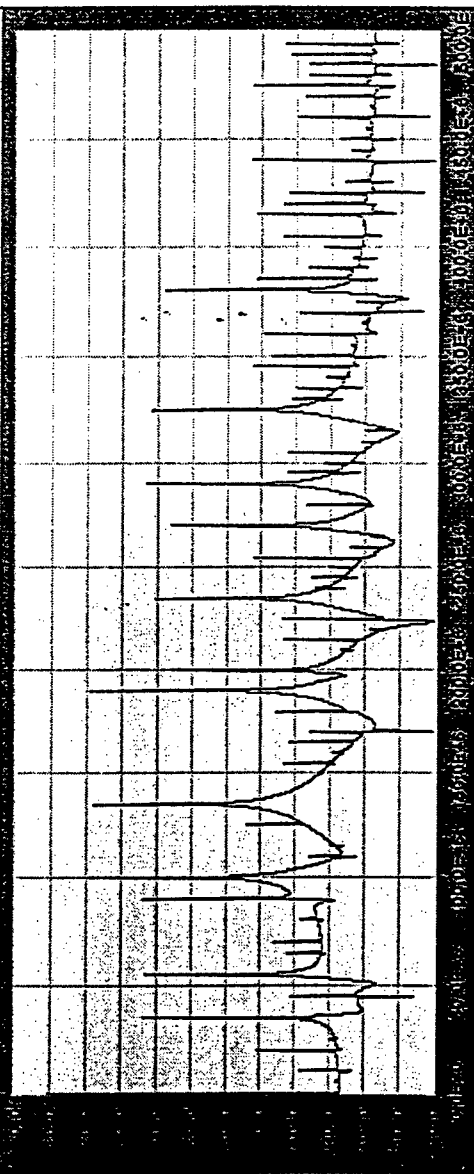
Phase Offset: Conv (radians)

Conventional Mod Intensity Detected Output



AEL Mod Intensity Detected Output

Amp Phase Offset1: AEL (radians) Amp Phase Offset2: AEL (radians) Delta Phase Offset: AEL (radians)

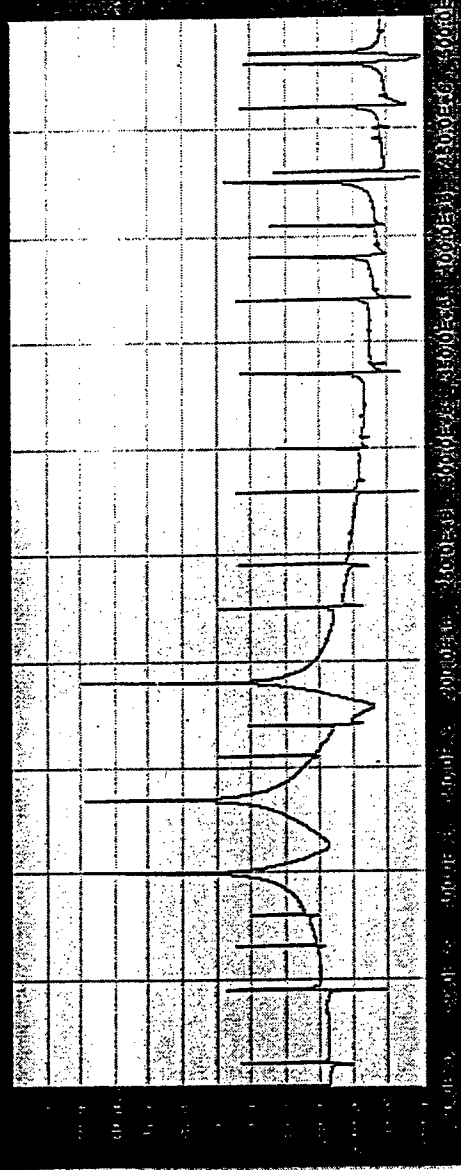


DSSCM Output w/ Higher Order Spurious Signal Content; $m=.2$

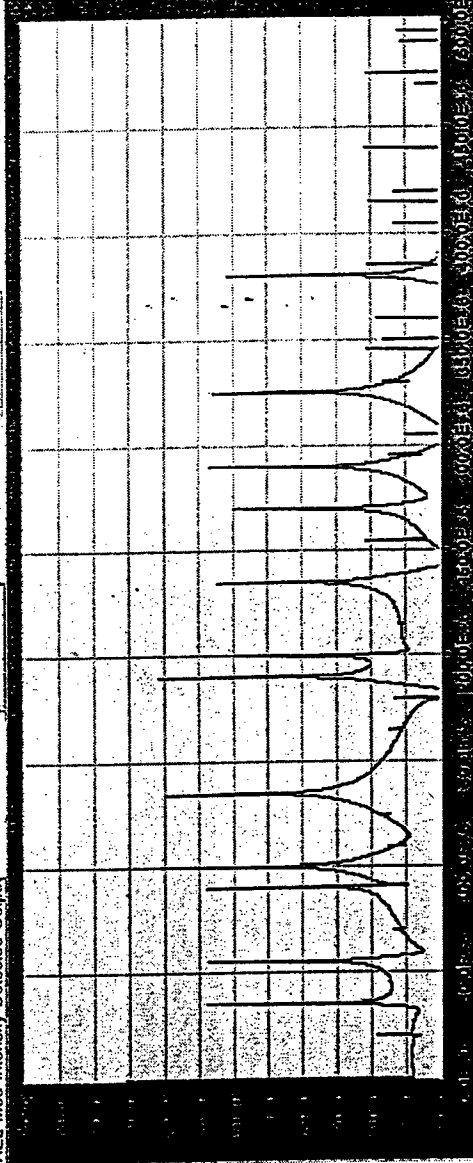
Modulation Frequency 1 (MHz) Modulation Frequency 2 (MHz) Modulation Frequency 3 (MHz) Voltage Modulation Index

Phase Offset; Conv (radians)

Conventional Mod Intensity Detected Output



AEL Mod Intensity Detected Output Amp Phase Offset1; AEL (radians) Amp Phase Offset2; AEL (radians) Delta Phase Offset; AEL (radians)

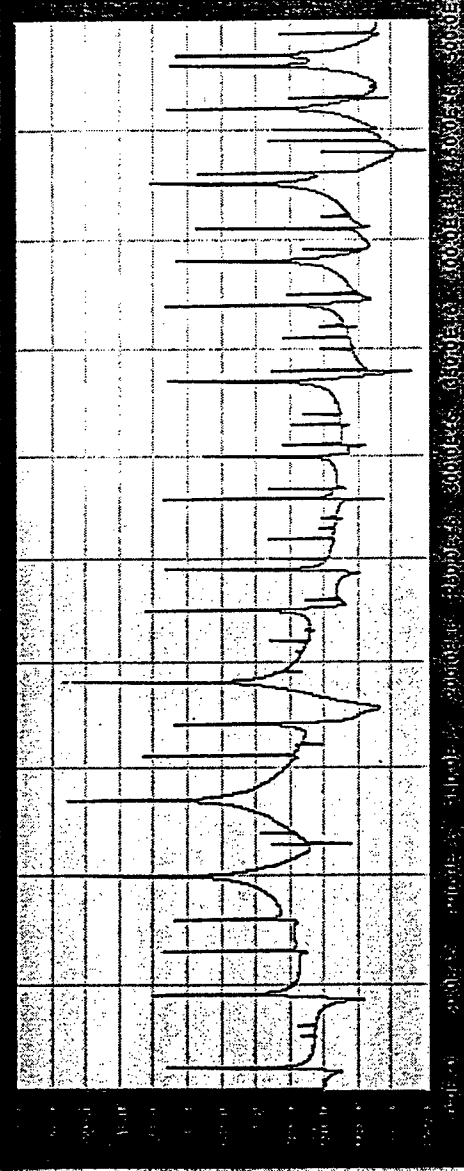


DSSCM Output w/ Higher Order Spurious Signal Content; $m=.5$

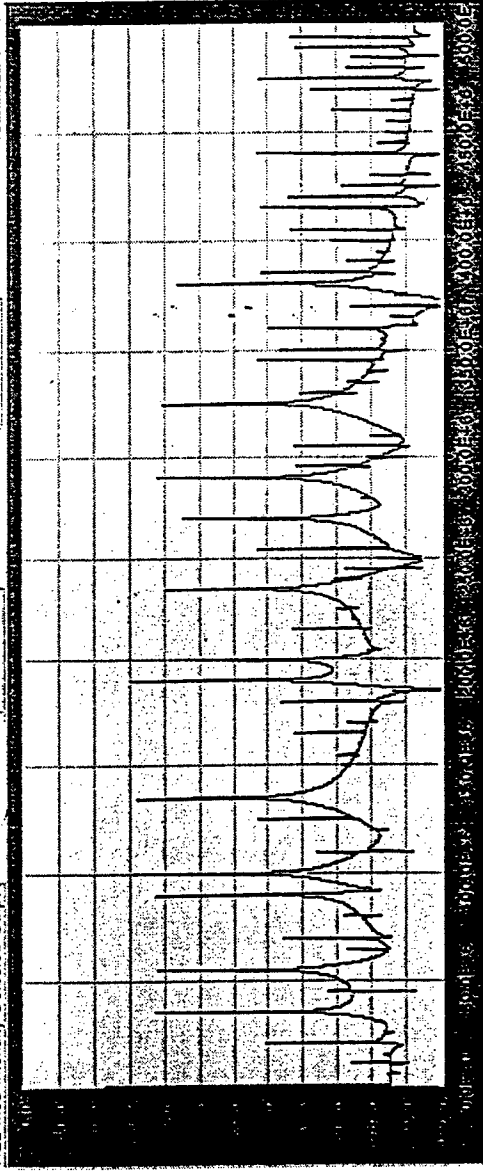
Modulation Frequency 1 (MHz) Modulation Frequency 2 (MHz) Modulation Frequency 3 (MHz) Voltage Modulation Index

Phase Offset: Conv (radians)

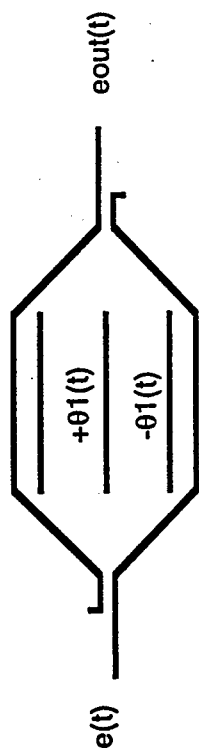
Conventional Mod Intensity Detected Output



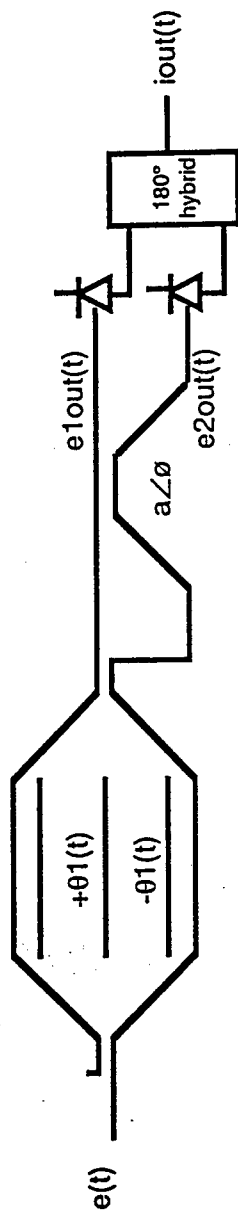
AEL Mod Intensity Detected Output Amp Phase Offset1: AEL (radians) Amp Phase Offset2: AEL (radians) Delta Phase Offset: AEL (radians)



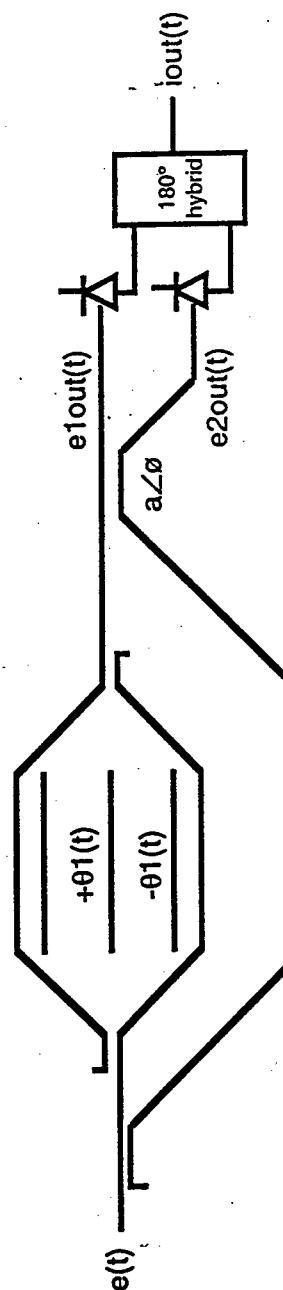
Alternate Modulator Configurations



Standard MZM

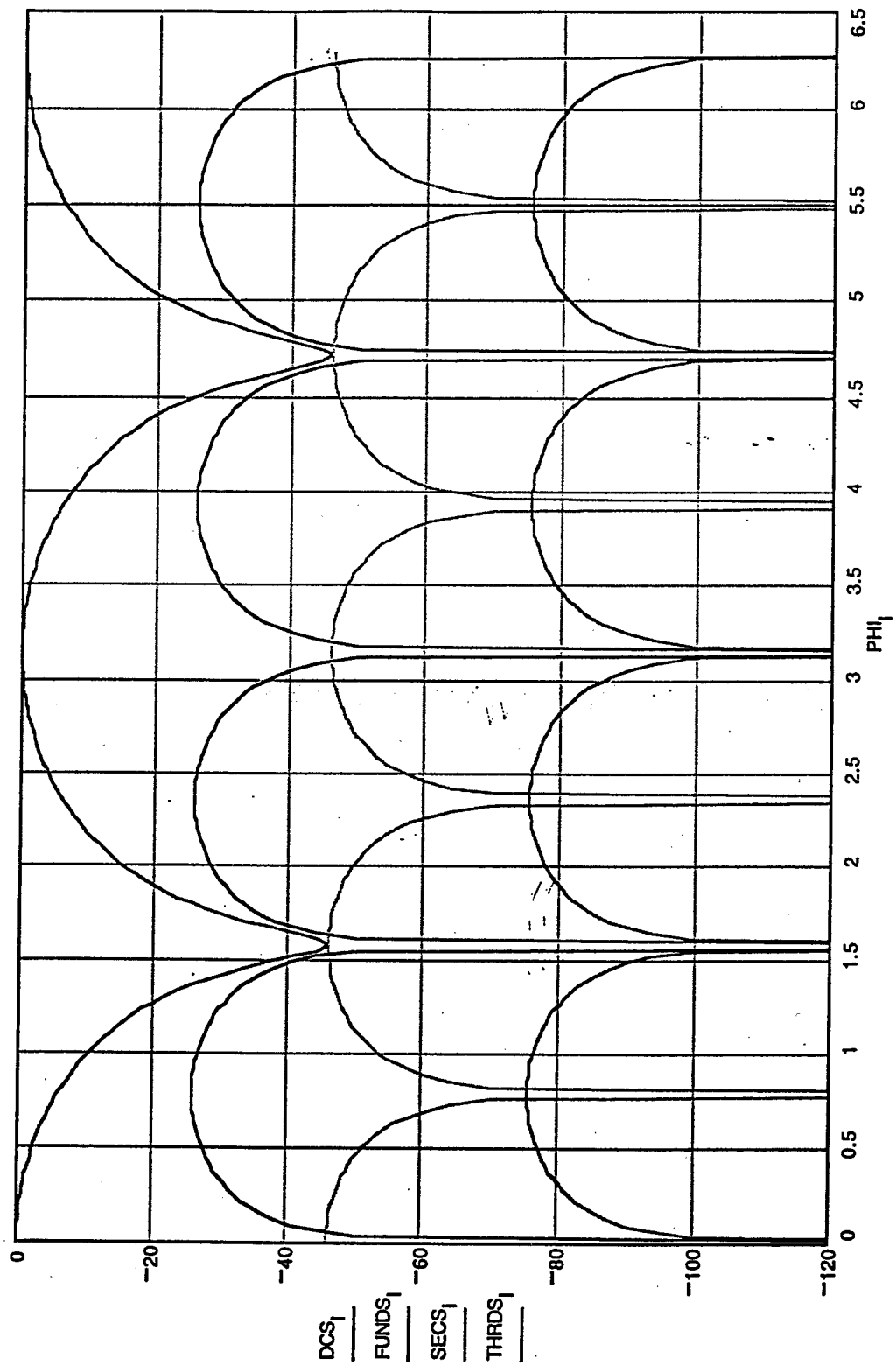


Standard MZM w/
Differential Detection

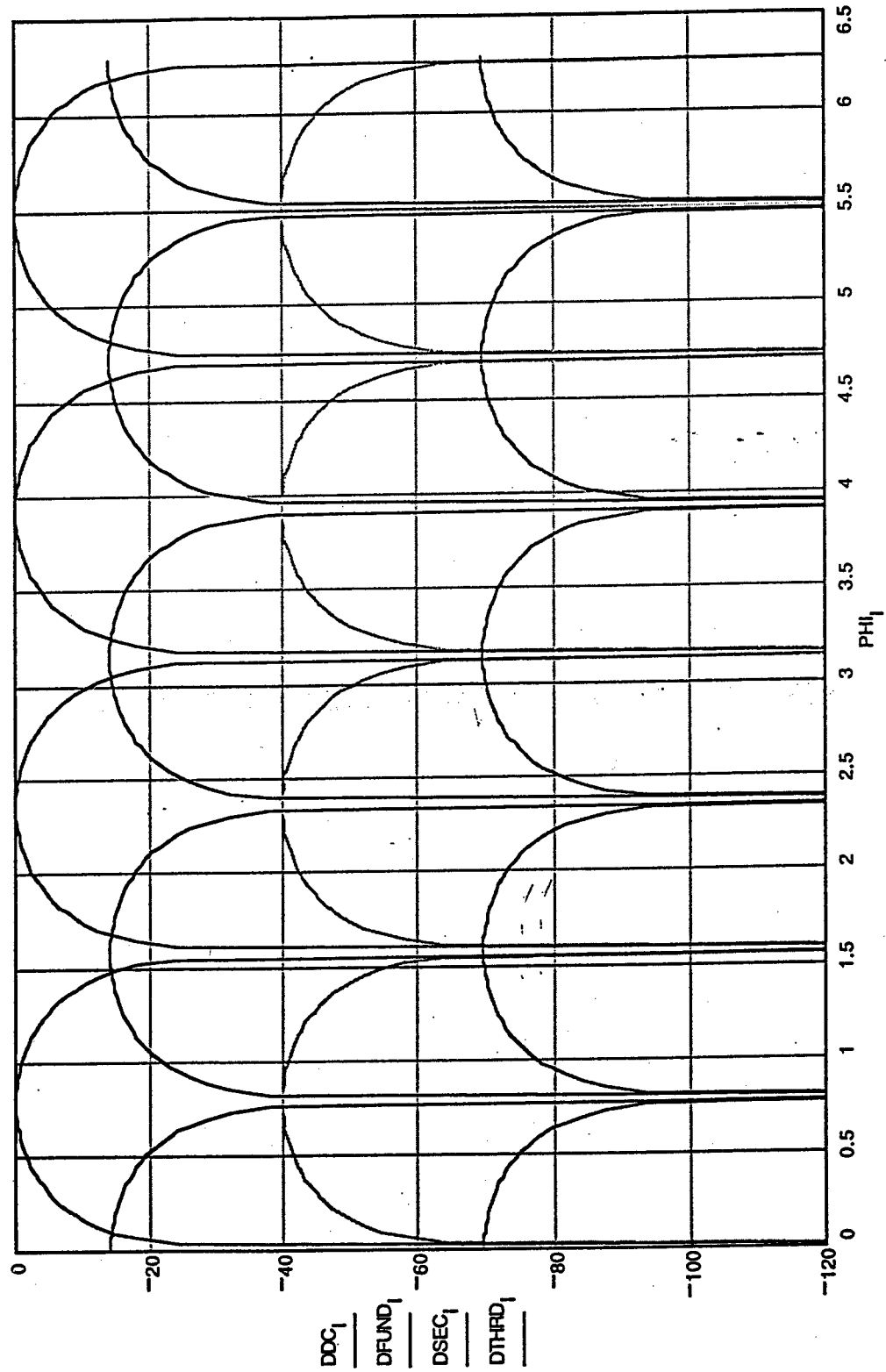


Standard MZM w/
Carrier Injection and
Differential Detection

Harmonic Content of Standard MZM

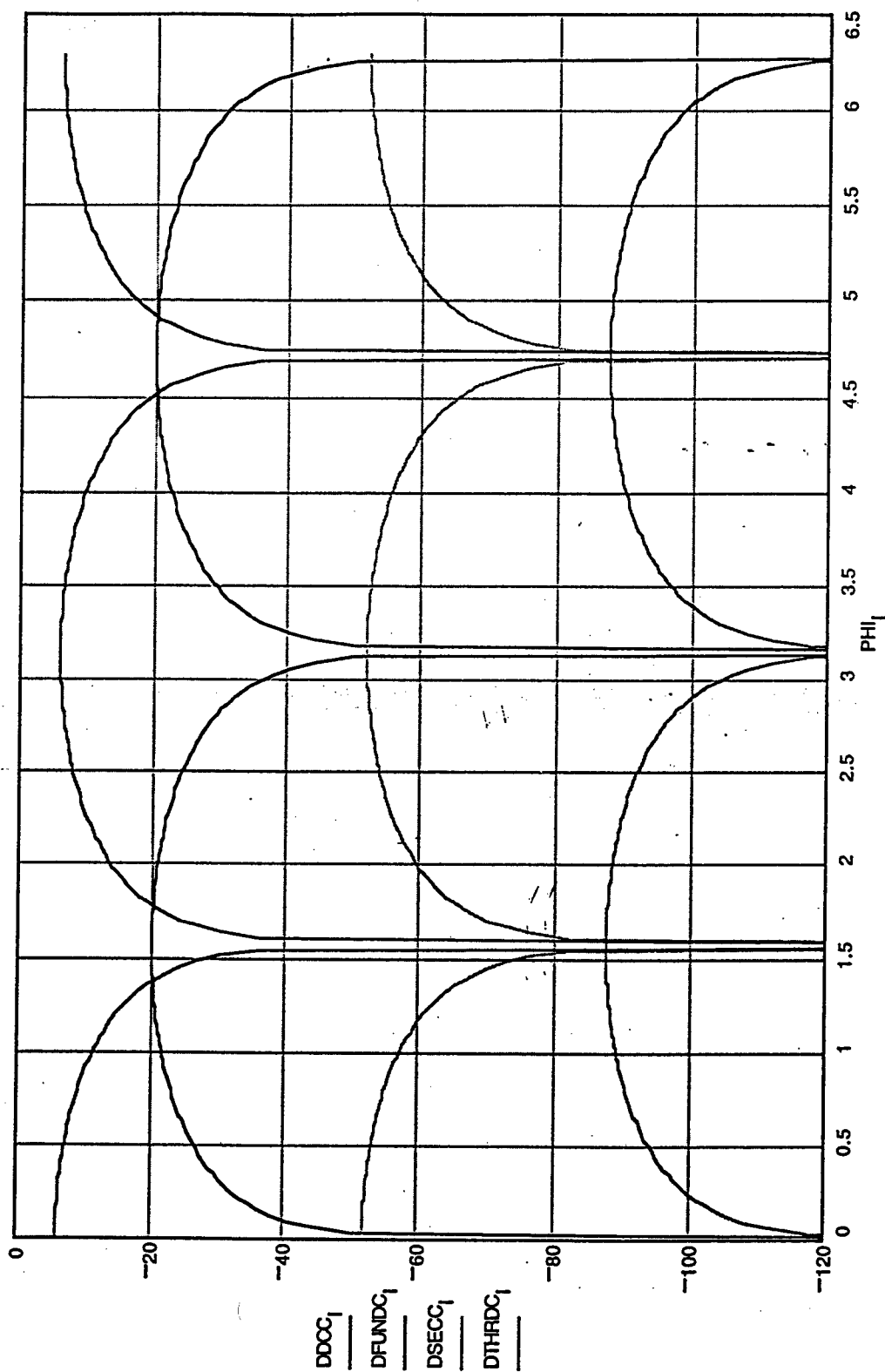


Harmonic Content of Standard MZM with Differential Detection



DC is Suppressed After Photodetector; Doesn't Improve Saturation Point

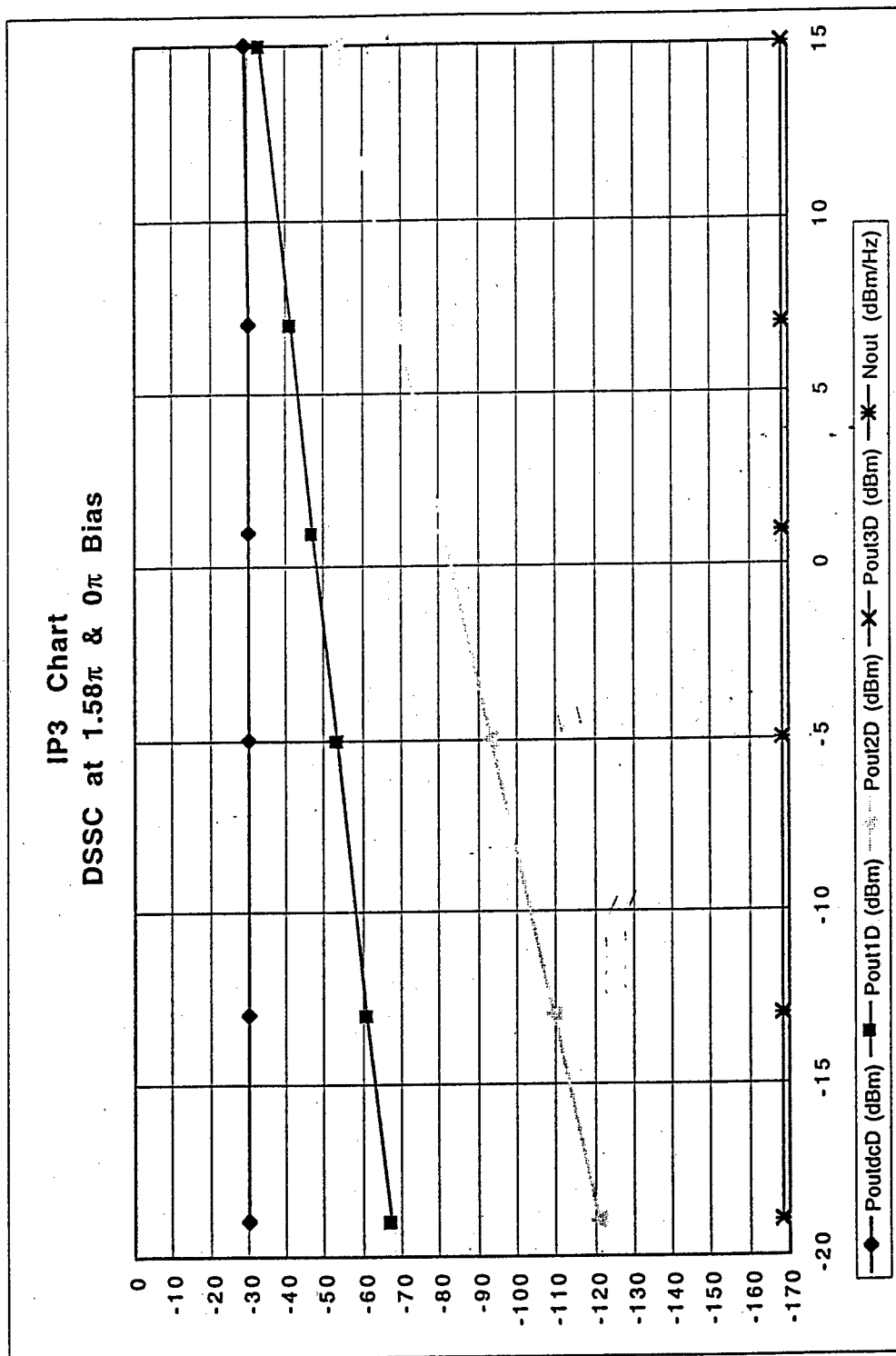
Harmonic Content of MZM w/ Carrier Injection



DC 2 dB Stronger Than Fundamental
DC and Even Harmonics Suppressed By Detection

Power Transfer Characteristics

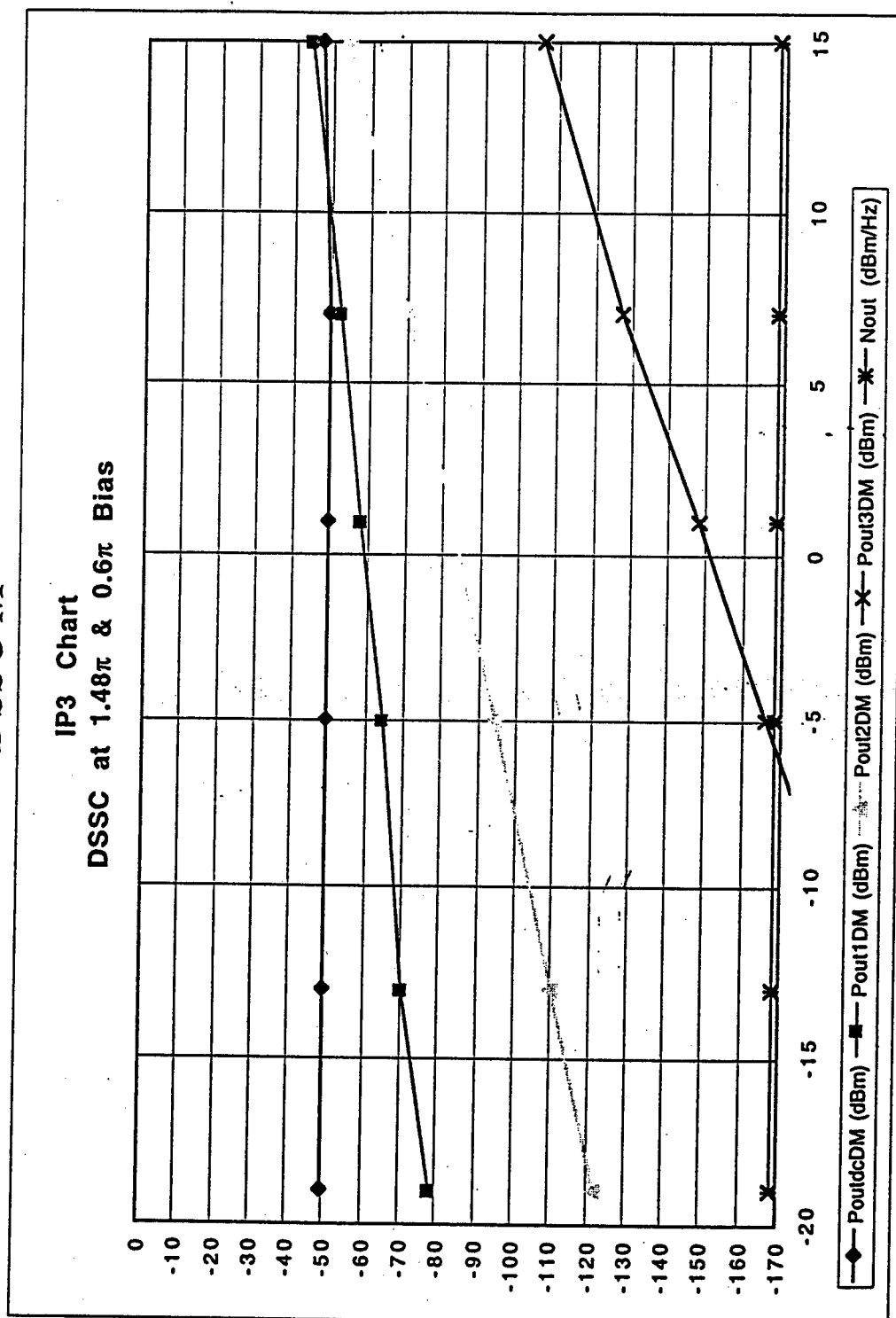
DSSC



Spurious DR Limited by 2x2 for Suboctave Applications

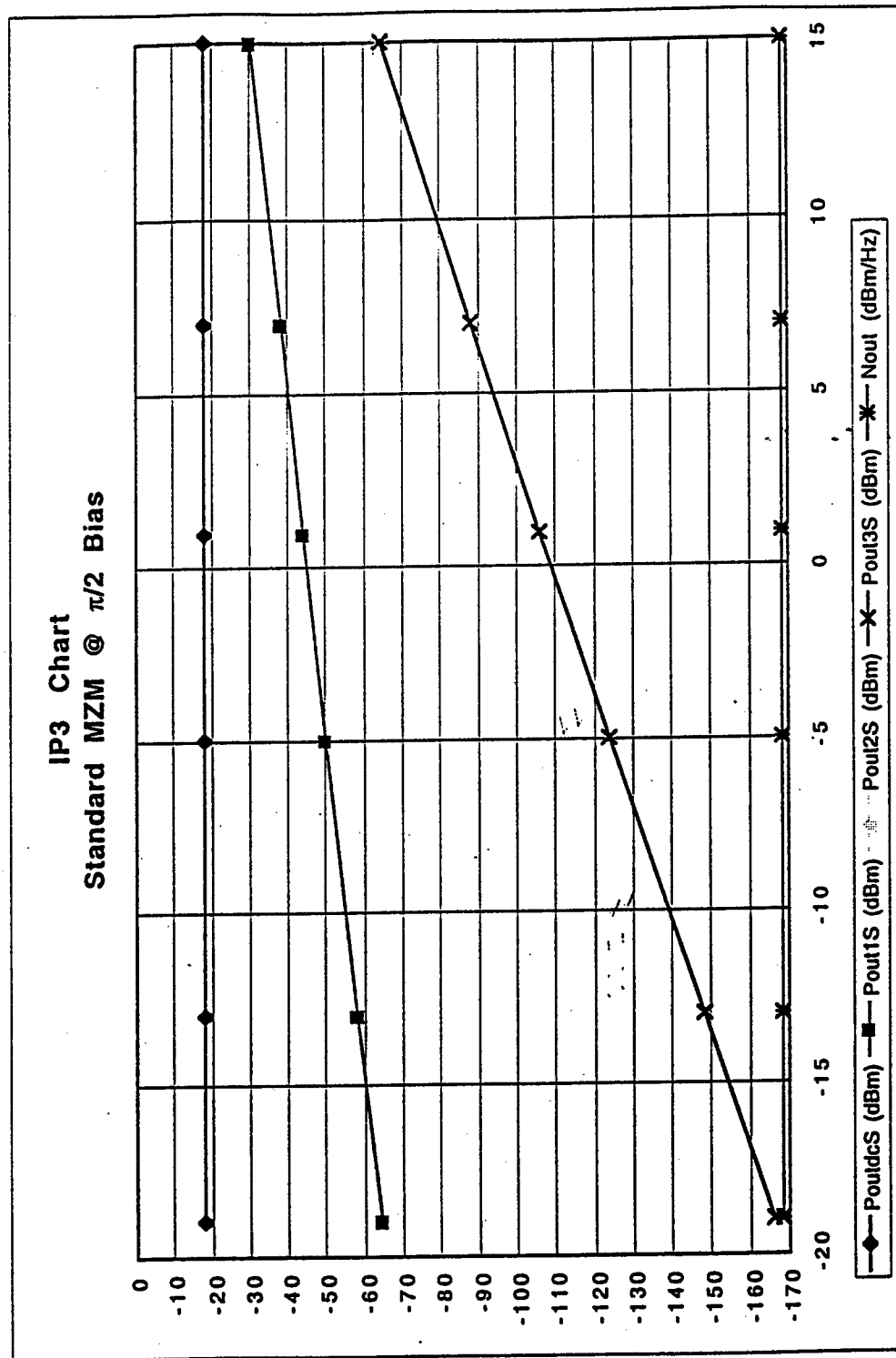
Power Transfer Characteristics

DSSC M



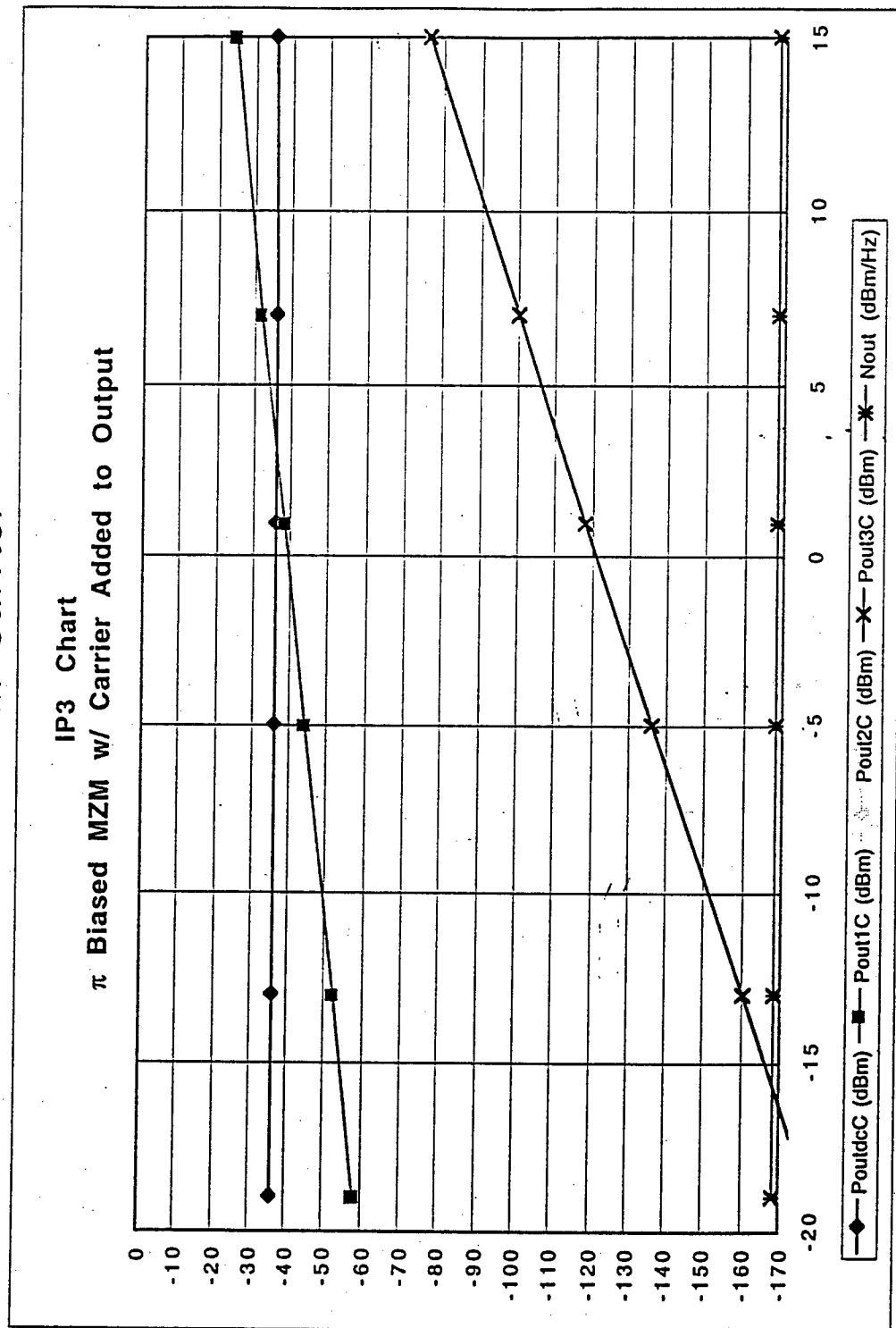
Spurious DR Limited by 2x2 for Suboctave Applications
 DR ~ 103 dB/Hz^{2/3}; Add EDFA w/ 1mA Detector ~ 128 dB/Hz^{2/3}

Power Transfer Characteristics MZM



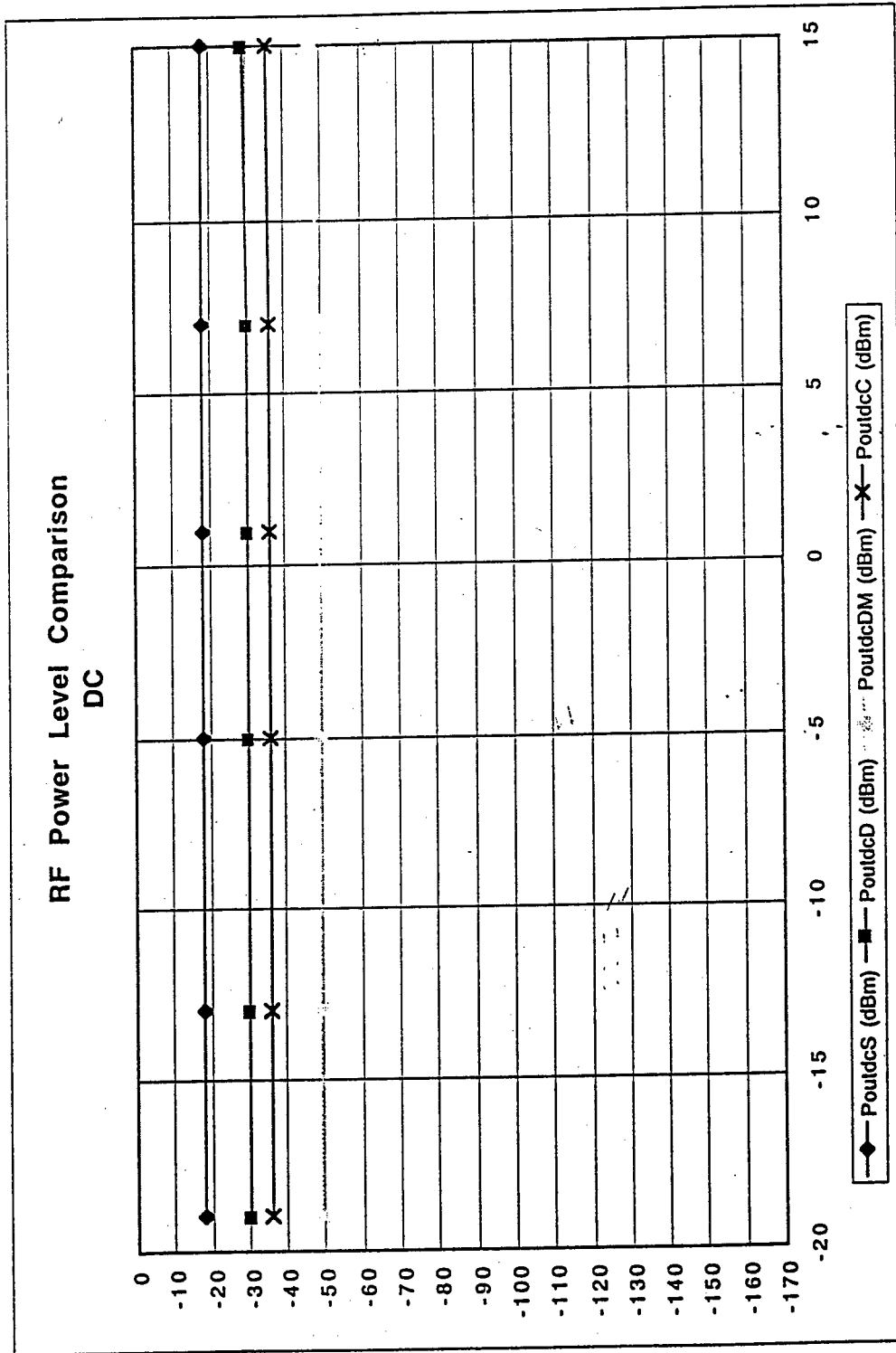
DR ~ 103 dB/Hz^{2/3}; Add EDFA w/ 1mA Detector ~ 107 dB/Hz^{2/3}
2nd Order Terms Are Suppressed

Power Transfer Characteristics MZM w/ Carrier



DR ~ 113 dB/Hz^{2/3}; Add EDFA w/ 1mA Detector ~ 129 dB/Hz^{2/3}
2nd Order Terms Are Suppressed

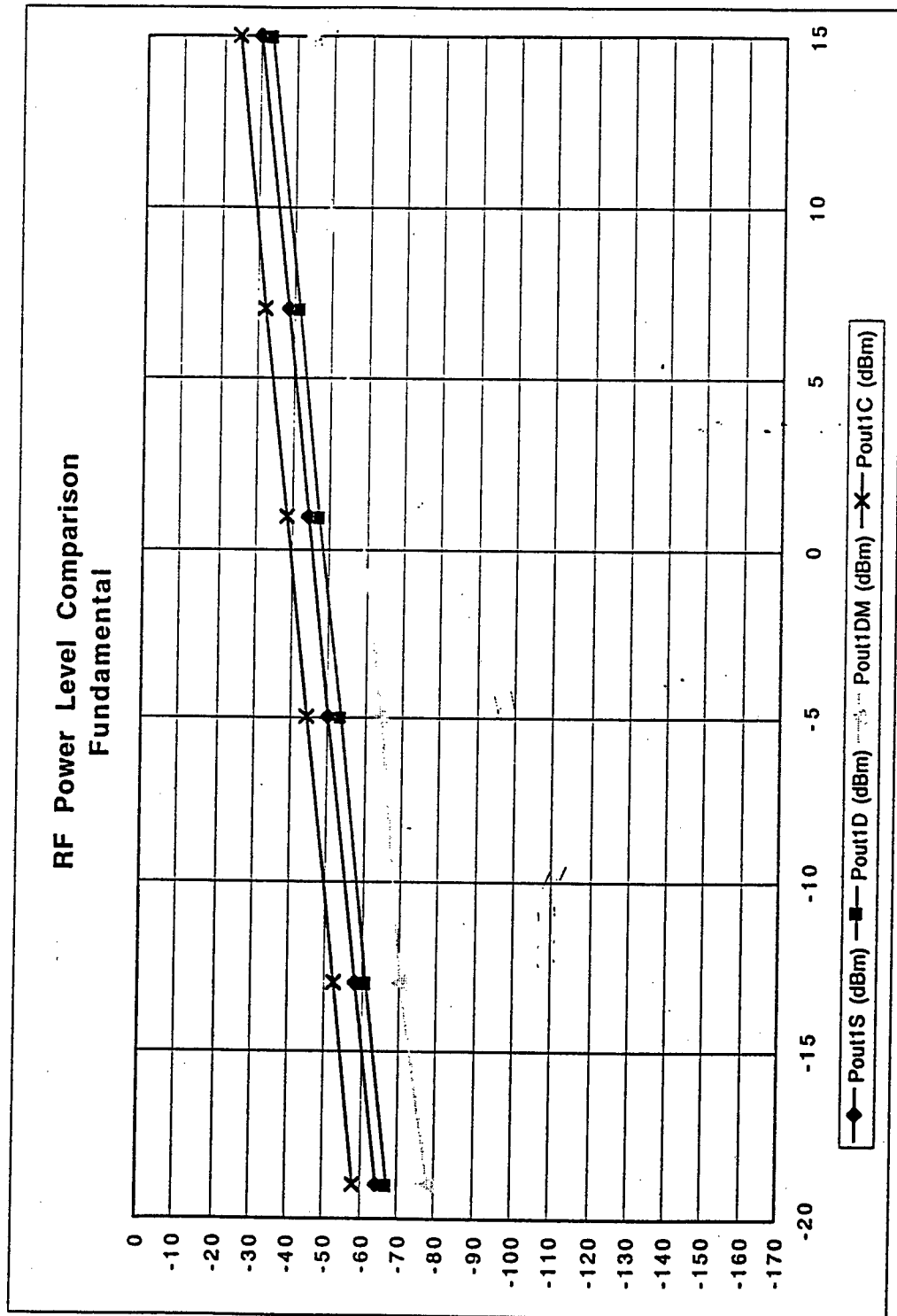
Power in DC Terms



EDFA Gain for 1 mA Detector Corresponds to a -13 dBm Pout

EDFA Gain for 10 mA Detector Corresponds to a 7 dBm Pout

Power in Fundamental



Performance Summary Chart

Modulator Configuration	Usable BW	DR* Hz ^{2/3}	Bias Simplicity	Norm Pwr of Fund	2nd Harmonic	3rd Harmonic	∂Pwr^{**} Fund/DC
DSSC	Octave	n/a***	Moderate	-9	High	Nullled	-11
Mod DSSC	Octave	128	Complex	-20	High	Suppressed	-3
Standard MZM	Wide	107	Simple	-6	Nullled	Moderate	-20
MZM w/ DC Injection	Wide	129	Simple	0	Nullled	Suppressed	-2

* Using an EDFA w/ a Detector That Saturates at 1 mA

** Measured When the Modulation Index is at 0.2; Mod Index = $\pi \cdot V_{dr} / V_{\pi}$

*** Measured on DSSC ~ 115 dB/Hz^{2/3}